Mississippi State University
Scholars Junction

Theses and Dissertations | Theses and Dissertations

8-6-2021

Novel considerations for lightning strike damage mitigation of Carbon Fiber Reinforced Polymer Matrix (CFRP) composite laminates

Kamran Yousefpour
kamran.yousefpour@gmail.com

Follow this and additional works at: https://scholarsjunction.msstate.edu/td

Recommended Citation
Yousefpour, Kamran, "Novel considerations for lightning strike damage mitigation of Carbon Fiber Reinforced Polymer Matrix (CFRP) composite laminates" (2021). *Theses and Dissertations*. 5223.
https://scholarsjunction.msstate.edu/td/5223

This Dissertation - Open Access is brought to you for free and open access by the Theses and Dissertations at Scholars Junction. It has been accepted for inclusion in Theses and Dissertations by an authorized administrator of Scholars Junction. For more information, please contact scholcomm@msstate.libanswers.com.

www.manaraa.com

Novel considerations for lightning strike damage mitigation of Carbon Fiber Reinforced Polymer Matrix (CFRP) composite laminates

By

Kamran Yousefpour

Approved by:

Chanyeop Park (Major Professor)
Yeqing Wang
John E. Ball
Masoud Karimi
Jenny Du (Graduate Coordinator)
Jason M. Keith (Dean, Bagley College of Engineering)

A Dissertation
Submitted to the Faculty of
Mississippi State University
in Partial Fulfillment of the Requirements
for the Degree of Doctor of Philosophy
in Electrical and Computer Engineering
in the Department of Electrical and Computer Engineering

Mississippi State, Mississippi

August 2021

www.manaraa.com

Copyright by

Kamran Yousefpour

2021

www.manaraa.com

Name: Kamran Yousefpour

Date of Degree: August 6, 2021

Institution: Mississippi State University

Major Field: Electrical and Computer Engineering

Major Professor: Chanyeop Park

Title of Study: Novel considerations for lightning strike damage mitigation of Carbon Fiber Reinforced Polymer Matrix (CFRP) composite laminates

Pages in Study: 140

Candidate for Degree of Doctor of Philosophy

Lightning current with high amplitude disseminates through the body of aircraft and causes physical damages including the delamination and puncture of materials. Also , such high-amplitude and high-frequency current could interfere with electronic devices through electromagnetic coupling with the conductive interfaces of an airplane. Hence, robust protection against lighting strike is essential in the aerospace industry. Carbon Fiber Reinforced Polymer (CFRP) Matrix Composites have become significant alternatives to conventional metal-base materials. Despite the superior physical and structural properties of CFRP composites, these materials are vulnerable to lightning strikes due to the low electrical conductivity compared to the metal counterpart. Many researchers have been working on the lightning strike damage mitigation of CFRP composites by increasing the electrical conductivity of materials.

Conventional methods are adding conductive layers such as metal foil and copper mesh to the composite structures. These layers are added to the composite structure during the manufacturing process and are placed at the top layer for the effective bypassing of lightning current to the ground. While adding the conductive layers reduces the lightning strike damage significantly, the industry is more interested in using conductive nanofillers to prevent the

www.manaraa.com

corrosion of metal layers in contact with carbon fibers and to avoid the higher weight of conductive layers than nanofillers. The lightning damage mitigation methods are studied by applying lightning strike current to the CFRP composites using an impulse current generator. Conventional lightning strike damage tolerance of CFRP composites are prone to misinterpretation. The risk of misinterpretation originates from the lack of standards clearly defining testbed design requirements including electrode size and ground electrode edge configuration.

In this dissertation, the effects of testbed configuration including discharge and ground electrode on lightning strike damage evaluation studies are demonstrated. Finite element analysis is applied to perform the simulations through the COMSOL Multiphysics to validate the experimental test results. Furthermore, after improving the testbed design, carbon black was added to the CFRP composites as a cost-effective additive for lightning strike damage mitigation performance. Correlations between lightning strike damage intensity and the added carbon black fillers as well as with other additive nanofillers are reported.

Keywords: Lightning, Aircraft, Carbon Fiber Reinforced Polymer, Impulse Current Generator, Carbon nanofiller, Ground Electrode, Discharge Electrode, , COMSOL Multiphysics, Plasma, Anode, Cathode, Temperature, Heat Flux, Joule Heating, Current Density, Hand lay-up, C-scanning, B-scanning.

www.manaraa.com

DEDICATION

To my beloved Family!

www.manaraa.com

ACKNOWLEDGEMENTS

I would like to express my deepest gratitude to my former advisor Dr. Joni Klüss, for giving me this opportunity to start working under his supervision. I am very grateful to my current advisor, Dr. Chanyeop Park, for his strong support in my Ph.D research study with his great source of knowledge and information. I am sincerely thankful for all the supports that I received from Dr. Yeqing Wang during my research at MSstate. I would also like to thank Dr. Masoud Karimi and Dr. John E. Ball for serving as my committee member.

My thanks also extend to Dr. David Wallace and Dr. Mojtaba Rostaghi for helping me while running my research and experiment in the High Voltage Lab. I would also like to thank all my friends and colleagues in Simrall: Saeed, Maziar, Pedram, Ali, Jason, Farhina, Tashfin, and Zeeshan for their precious supports. I am thankful to all members of the Iranian Student Association (IRSA) at Mississippi State University, who made my life in Starkville more pleasant. Special thanks to my best friends, from back home, who made my life much easier by their support, energy, and advice that never stopped since I was a little child. Lastly, I am very grateful to my dear parents, siblings, and brother in law who never stopped their love and support.

www.manaraa.com

TABLE OF CONTENTS

www.manaraa.com

www.manaraa.com

www.manaraa.com

LIST OF TABLES

www.manaraa.com

LIST OF FIGURES

www.manaraa.com

www.manaraa.com

www.manaraa.com

www.manaraa.com

www.manaraa.com

www.manaraa.com

CHAPTER I

PROBLEM STATEMENT

Traditionally, metals have been used as the main material for manufacturing aircraft body in the aerospace industry and wind turbine blades in the wind power industry. However, owing to several advantages over the metal-based panels, CFRP composites are recognized as promising alternatives in these industries. The main advantages of CFRP composites are light weight, structural stiffness, corrosion resistance, and high tensile strength that reduce operation and maintenance costs.

Although there are many advantages associated to using CFRP composites, the major challenge against the widespread use of CFRP composites is their low electrical conductivity originated from resins used in the fabrication process. The low electrical conductivity of resins causes enormous Joule heating at the moment of a lightning strike. Studies developing lightning strike damage reduction methods have been reported in the literature. However, these studies were mainly based on adding metal mesh layers, which increases the overall weight of the panels. When it comes to testbed design, the lack of a clear design guidelines for lightning strike experiments increases the chance of data misinterpretation. This thesis demonstrates ways of improving the testbed design by analyzing the impact of discharge electrode and ground electrode edge configuration. Base on the analyses, this study proposes novel methods for improving the lightning strike damage tolerance and the evaluation quality of CFRP composites.

www.manaraa.com

CHAPTER II

STATE OF THE ART

2.1 Carbon Fiber Reinforced Polymer (CFRP)

Various materials such as aluminum, steel, and composite have been used in the aerospace industry. CFRP composites have become significant alternatives to conventional metal-base materials in various applications. The composite material has the following advantages to the aircraft industry:

(a) Light Weight: The light weight of composites than metals is the most attractive feature because the reduction of aircraft weight provides better fuel economy and operating cost.

(b) Higher Strength to Weight Ratio: Stacking the layers of fiber with different weave angles makes the laminate isotropic and lead to having higher strength to weight ratio and a better weight distribution [1]. It means that at an identical thickness, CFRP composites can be stronger than aluminum while are 40% to 70% lighter [2]. Composite materials are anisotropic and their properties vary with different loads and orientations of the fiber directions.

(c) Flexibility: Composites have more flexibility to be made in various shapes thereby replacing parts consisted of many pieces made of other materials. So, the maintenance and lifetime cost of aircraft can be reduced [3]. Also, they can be formed into different shapes and complex structures. So, it reduces the use of fasteners and joints for assembling thereby reducing the assembly time

www.manaraa.com

and weak points of structural components. Due to these excellent advantages over metal, aerospace industry is replacing metal with composite in its structures.

2.1.1 Aerospace Application

In the past, only 1% of the structure of the Boeing 747 consists of composite materials, while, more that 50% of the total weight of a Boeing 787 is made of carbon fiber composites [4]. The usage of carbon fiber composites in the Boeing structure is shown in Figure 2.1.

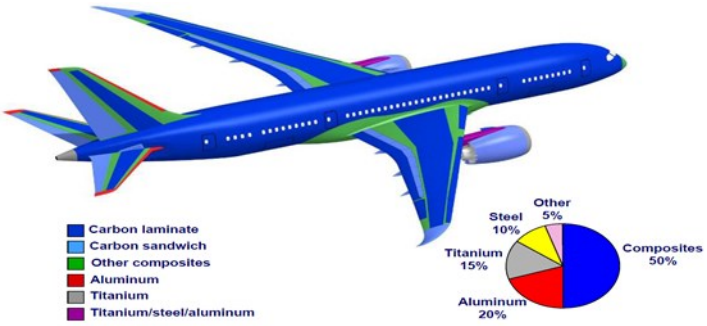

Figure 2.1 Composite material usage in the Boeing 787 [4]

2.1.2 Wind Turbine Application

CFRP composites is proven to be one of the most versatile material in manufacturing wind turbine blades. While fiberglass composites are utilized for manufacturing blades that are 40-50 meters in length, CFRP composites are more suitable for larger blades owing to their remarkable advantages such as better strength to weight ratio, stiffness, and cost which are critical for large scale wind blades. The incorporation of carbon fiber for manufacturing a 60 m wind turbine blades reduces the cost by 14% and decrease the mass by 38% in comparison to using fiberglass [5]. The other shortcoming of Glass Fiber Reinforced Polymer (GFRP) composites is that GFRP composites have lower modulus strength, which leads to fracture of the blades when imposed with

www.manaraa.com

sudden high stresses such as aerodynamic forces. The CFRP composites have low electrical conductivity that leads to slow dissipation of lightning strike current. This increases lightning strike damage because of the high temperature rise of the CFRP composites. The increasing in use of CFRP composites raises significant concerns over lightning strike impact and necessitates the improvement of their lightning strike damage tolerance.

2.2 Physics of Lightning

2.2.1 Thundercloud

Lightning phenomena have impacted humanity for a long time and were studied by various researchers. Lightning is a fast high-current discharge in the atmosphere which happens suddenly in any geographical area and can damage various equipment and objects such as buildings, antenna, transmission lines, and airplanes. Lightning occurs due to the breakdown of air and the thundercloud is the source. Thunderclouds are usually shaped due to the uprising of warm air with low density at low levels to the upstream cold air in atmosphere. In a research study [6], Marshall investigated the thunderstorm electric field and proposed that for inducing an electron avalanche, the thunderstorm electric field should exceed a critical value, known as the breakeven field. He measured the thunderstorm electrical field in different altitudes and showed that the cloud electrical field is hardly higher than the thunderstorm electrical field and lightning occurs when the field reaches the critical value. Solomon provided explanations for the resumption of lightning despite the low value of cloud electrical field in a thunderstorm [7]. The first reason is the increase of the electrical field caused by water droplet which leads to dielectric breakdown. Another reason is the enhancement of velocity of the high-energy electrons due to the cloud electrical field. Existing electrical charge in a cloud is due to the decomposition and collisions of ice particles and

www.manaraa.com

snow pellets. In Figure 2.2, Malan depicted the cloud charge distribution for a typical cumulonimbus (thundercloud) in South Africa [8].

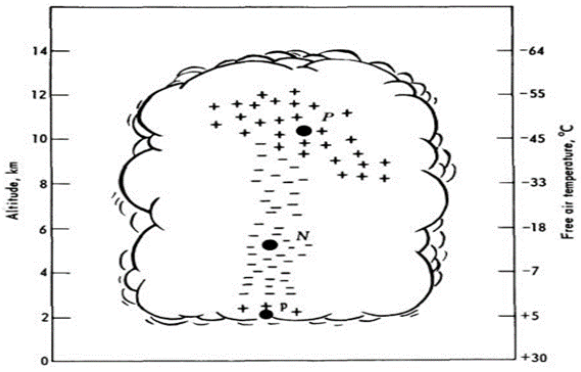

Figure 2.2 Cloud charge distribution for a typical cumulonimbus in South Africa [8]

The data of the charge distribution were obtained in adjacency of thunderclouds and as shown in Figure 2.2, P indicates positive zones and N indicates negative zones.

2.2.2 Types of Lightning

There are four kinds of thundercloud lightnings:

1- Intracloud or cloud discharges (IC): happens between different regions of a cloud.

2- Cloud to cloud discharge (CC): Occurs between clouds in the vicinity of each other.

3- Negative ground lightning (-CG): cloud to ground discharge in which the electrical discharge transport from cloud to the ground comes from negative region of the cloud.

4- Positive ground lightning (+CG): cloud to ground discharge in which the electrical discharge transport from cloud to the ground comes from positive region of the cloud.

www.manaraa.com

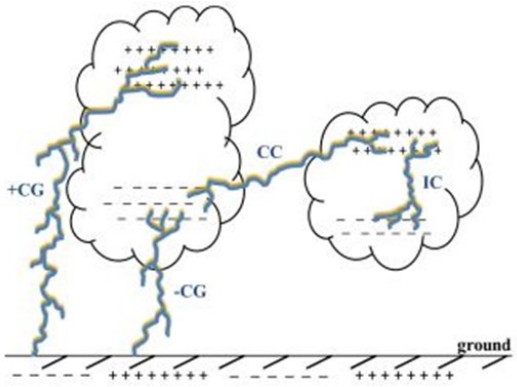

Figure 2.3 Four types of thundercloud lightning [9]

Figure 2.3 shows the four different types of thundercloud lightning. The cloud to ground lightning discharge has been brought to attention more than other types of thundercloud lightnings because it causes damage to the human life [9]. While about 90% lightning strikes to the ground are negative ground lightning (-CG), +CG is more dangerous because the electrical field correlated to the + CG is stronger because it burns more air for reaching the ground. Also, +CG has just one return strike with a continuous current with a longer continuity and the amount of charge transferred is about 10 times greater than -CG which is about 300 kA [10].

2.2.3 Lightning Channel

Positive discharges are usually developed due to the upward leaders which initiates by skyscrapers or tall trees. The discharge channel of electrons from cloud toward the ground is called stepped leader and the electrical field of the ground increases as the stepped leader gets close to it. When the electrical field exceeds the breakeven field, the upward leaders, known as streamers, go up toward the stepped leader and the return strike occurs as they encounter [11]. The lightning channel diameter ranges from several centimeters to several meters. The measurement of lightning diameter has been performed by investigating objects struck by lightning and by photography.

www.manaraa.com

When lightning strikes an object such as tree or rock, burned paths caused by lightning represent lightning channel diameter [12]. In [13], Uman used a fiberglass screen on a lightning rod and measured the hole diameter created by lightning discharge current. Some researchers have investigated the dimeter of lightning channels by using the photography data. Mitchell Krog took photos of lightning strikes in South Africa to estimate the size of lightning channel. In both lightning strikes shown in Figure 2.4 there are telegraph poles that were used as scales for estimating the size of lightning channel, which is around 12 m.

Figure 2.4 Lightning strike channel taken by Mitchell Krog in Pretoria, South Africa [14]

2.3 Lightning Strike on Aircraft

2.3.1 Initiation of Aircraft Lightning Strike

A lightning strike to an aircraft can either happen due to the presence of the aircraft in a strong electric field, which is known as aircraft triggered lightning, or due to a naturally occurring leader. Although aircraft triggered lightning has a lower current amplitude than most of cloud to ground lightning, it is the most frequent type of lightning strike to the aircraft, and accounts for about 90% of the events. Reports show that the probability of lightning strike to an aircraft is one

www.manaraa.com

strike per 1,000 - 20,000 flight hours which depends on various factors such as climate, flight profile, type of aircraft, etc [15]–[17]. The lightning channel is stationary and aircraft move a distance in lightning channel due to the aircraft's high speed and continuity of lightning channel existence. As aircraft moves forward while being struck by lightning, current sweeps back to the surface and restrikes the aircraft at various other locations as shown in Figure 2.5. This is called a swept channel and the damage it produces depends on the features of aircraft material [18].

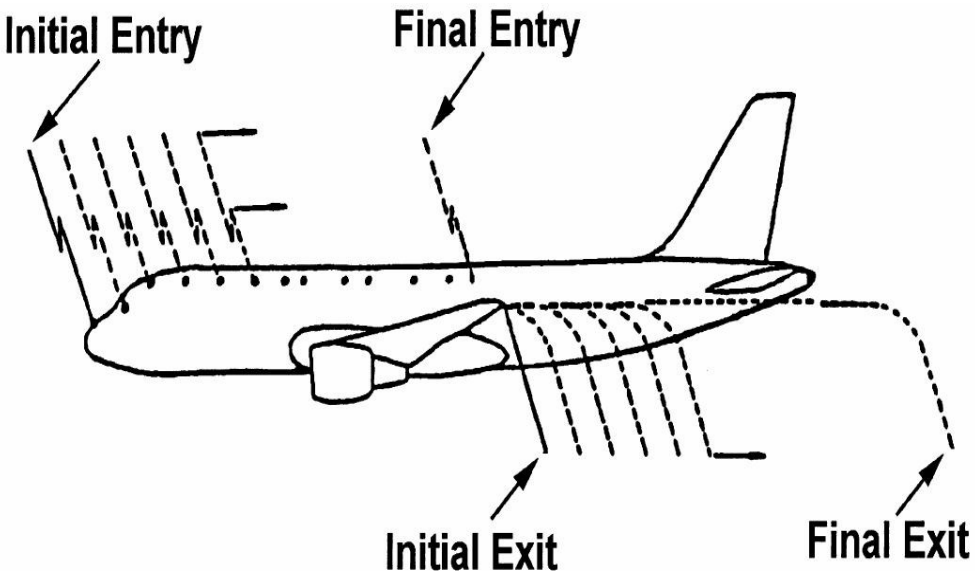

Figure 2.5 Swept Channel [18]

2.3.2 Lightning Strike Zones of Aircraft

Lightning current flows through aircraft surface between the entry and exit point. As shown in Figure 2.6, different areas of the aircraft are likely to be subjected to various types of lightning strike components. Different zones are introduced for the body of an aircraft to provide an efficient protection against lightning strike. Each zone is shown in the Figure 2.6 and explained below.

www.manaraa.com

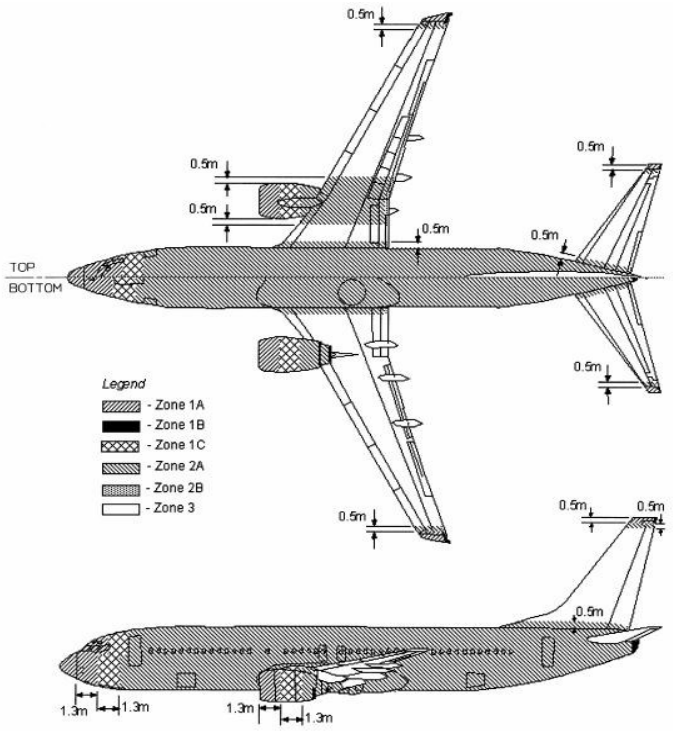

Figure 2.6 Lightning zoning diagram for a typical large commercial transport per SAE 5414 [18]

Following are the definitions of zones in an aircraft body [18]:

Zone 1A: This is the first return strike zone and includes all areas of aircraft's body, on which the first return strike is more likely to happen and the duration is likely to be shorter.

Zone 2A: Swept Strike Zone: All areas of an aircraft surface, on which the lightning channel is swept strike with a low expectation of flash continuing. It leads to a series of consecutive strikes due to the lightning flash sweeping across the aircraft due to the movement of the aircraft.

Zone 1B: This is the first return strike zone with long flash continuous that includes areas of aircraft surface where the first return strike with a lower amplitude is likely to occur and the flash over will hang on.

www.manaraa.com

Zone 2B: Swept Strike Zone with long flash continuing: All the areas of aircraft surface, on which the lightning channel is swept strike and flash hanging on.

Zone 1C: Transition zone for first return strike: The areas on aircraft where the first return strike of reduced amplitude is likely during the lightning strike with low probability of flash continuing.

Zone 3: Any zone that are not in zones 1A, 1B, 1C, 2A, or 2B, where the lightning is unlikely to strike and the zones which are beneath or between other zones.

2.4 Standard Lightning Waveform

According to the SAE 5412 standard [19], lightning current waveform consists of four components A, B, C, and D as shown in Figure 2.7.

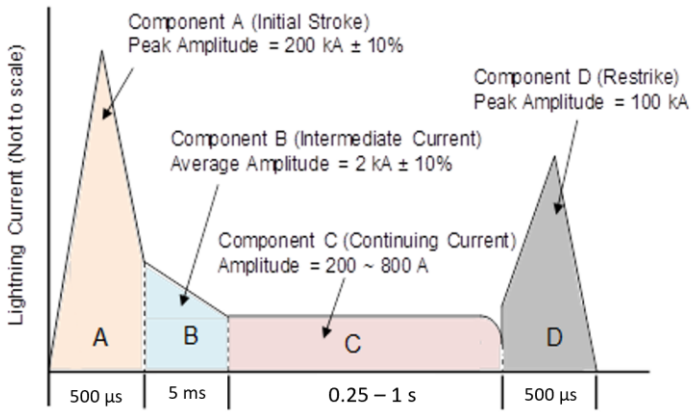

Figure 2.7 Standard lightning current waveform [19], [20]

The component characteristics of Lightning waveform are as below:

Component A: This is the initial current of a lightning that has a peak amplitude up to 200 kA and a time duration equal to or less than 500 µs. It usually strikes the aircraft flying at a lower

www.manaraa.com

altitude and the formula for demonstrating the Component A mathematically is double exponential:

$$I(t) = I_0(e^{-\alpha t}-e^{-\beta t}) \quad (2.1)$$

where, $\alpha = 11354s^{-1}$, $\beta = {}^{647265-1}$, $I_0 = 218810A$

Component B: This component is the intermediate current of a lightning waveform with a long hang-on that consists of some negative return strikes with the average amplitude of 2 kA and a time duration equal to or less than 5 ms. It can be represented by the double exponential formula that is described in equation (1), in which $\beta=2000s^{-1}$, $I_0=11300A$, and $\alpha= 700s^{-1}$.

Component C: This is a the continuous current of a lightning that contains some positive and negative restrike currents with an amplitude of 200 – 800 A and a time duration of 0.25 – 1 s. Component C with Component B act as a connection between first and second return strike. Also, as shown in figure 7, the component C waveform is rectangular.

Component D: This is a subsequent current strike with a peak amplitude of 100 kA and a time duration equal to or less than 500 μs. It is shown by the double exponential formula that is described in equation (1), in which $\beta=1294530s^{-1}$, $I_0=109405A$, and $\alpha= 22708s^{-1}$.

Conducting lightning strike experiments requires these lightning current components. The selection of the standard waveform component for lightning strike evaluation is limited by the type of available impulse current generator and the goal of a study.

2.5 Testbeds for Lightning Strike Damage Studies of CFRP Composites

With the aerospace industry replacing metal structures with CFRP matrix composite laminates, the lightning strike damage tolerance of these composite laminates has become increasingly important. Despite superior physical and structural properties, such as corrosion resistivity, light weight, and high specific strength and stiffness [21], these materials are vulnerable

www.manaraa.com

to lightning strikes due to their low electrical conductivity compared to the metal counterpart. The electrical conductivity of copper is 5.96×10^{7} S/m, whereas the electrical conductivity of carbon fiber sheet is generally about 6×10^{4} S/m, and epoxy resin, a widely used polymer matrix in aerospace applications, is substantially lower in electrical conductivity (10^{-9} S/m) than the two and generally assumed as an insulating material. The electrical conductivity of the CFRP composites is different in thickness and in-plane direction. While the in-plane conductivity is in the range of thousand, it is less than 10 S/m in thickness for the resin without conductive nano-filler. When the electrically resistive epoxy resin is infused into the carbon fiber preform, the resin partially separates the adjacent fibers which leads to further lowering the electrical conductivity of the CFRP matrix composite laminate in both transverse and through-the-thickness directions. When a CFRP matrix composite laminate is struck by lightning, extremely high current density flows through the material and causes substantial Joule heating due to the low electrical conductivity of the material. The temperature of the laminate quickly rises, which results in resin decomposition, delamination, matrix cracking, fiber breakage and pullout, fiber vaporization, and burning. In addition to these direct effects, lightning-impulse-induced electromagnetic waves also interfere with electronic devices through electromagnetic field coupling via the conductive interfaces of aircraft, which is also known as an indirect lightning strike effect [22].

The lightning strike tests of aerospace structures consists of high voltage and high current tests due to SAE ARP 5416.

2.5.1 High Voltage Test

The purpose of high voltage test is finding the puncture location on non-conductive surface, flashover over the non-conductive surface, and performance of the protection components such as segmented diverter. Figure 2.8 shows the test set-up recommended by the standard for high voltage

www.manaraa.com

tests [23]. The test electrode has a diameter no greater that 50 mm to apply the high voltage discharge to the test object. The test object is grounded through the fasteners or edges of the sample.

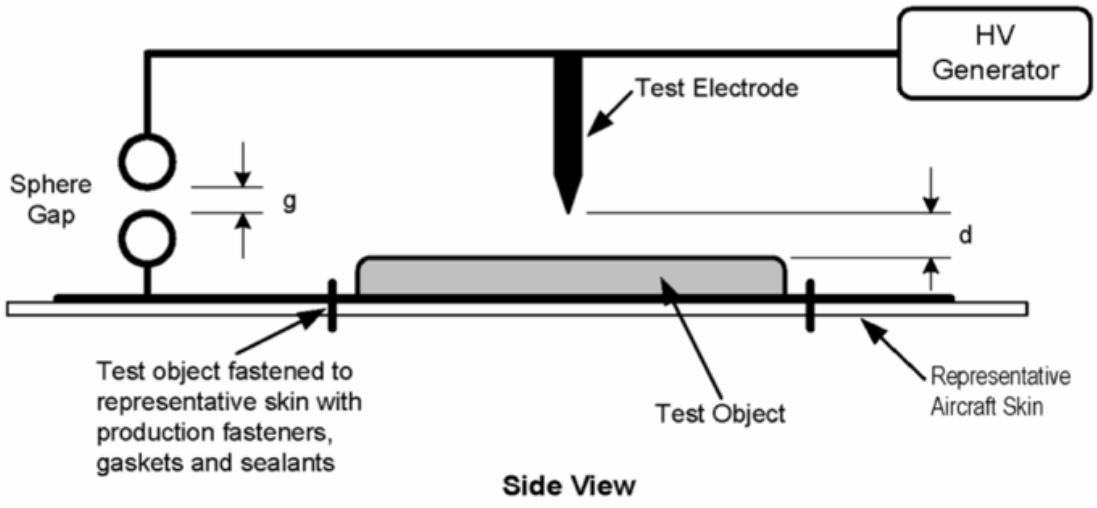

Figure 2.8 High Voltage lightning test set-up from SAE ARP 5416 [23]

High voltage tests with low current amplitude break downs the insulation and determines the attachment point.

2.5.2 High Current Test

After lightning attaches to the test objects, current flows to the sample and leads to the damage. Components A, B, C, and D are applied to the test object together or separately depending on the zoning of the aircraft's sample or the goal of the test. In order to simulate the effect of high current dissemination through the test samples, high current waveform in accordance with the lightning waveform shown in Figure 2.7 have to be applied to the samples. Figure 2.9 represents the High Current lightning test set-up from SAE ARP 5416 [23]. As it is shown, a jet diverter

www.manaraa.com

which is an insulation ball is used to eliminate the shockwave effect. An initiation wire with diameter of 0.1 mm is used to initiate the lightning channel. The gap distance is considered 50 mm when using the jet diverter. If the blast or shock effect is not an issue, a round electrode with diameter of 50 mm or greater can be used and the gap distance is depending on the insulation and conductivity of the test object and the goal of the test.

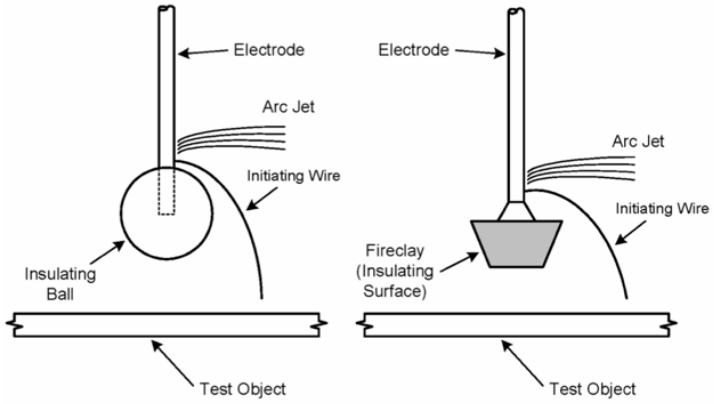

Figure 2.9 High Current lightning test set-up from SAE ARP 5416 [23]

High voltage and high current lightning tests are not considered to be performed simultaneously because generators are not capable of producing the high voltage and high current tests' standard waveforms. If a lightning impulse generator is capable generating both high voltage and high current together, the tests can be performed simultaneously.

Lightning strike experiments of CFRP matrix composite laminates are designed such that the discharge current hits the center of a panel and propagates radially to the ground electrode. Ground electrodes are made of flat pieces of metal conductors typically forming a square window at the center. The edges of composite panel samples are electrically coupled to the ground electrode edges such that impulse current flows through the sample radially. Based on such testbed designs,

www.manaraa.com

the mechanisms of lightning strike damage on composite laminates have been investigated in many experimental and simulation studies [24]–[31]. The physical parameters, including thickness, radius, and electron density of lightning arc have been reported in reference [32]. The study investigated the dynamics and shapes of lightning arcs captured by high-speed cameras to obtain the inductance and resistance of the measured arc. In references [11], [33], the lightning strike damage characteristics of composite laminates with copper mesh protection, pitch carbon fiber paper, and pultruded rod stitched efficient unitized structure (PRSEUS) were investigated. The researchers reported that the delamination of the composite laminate samples increases with the increasing energy of lightning discharge. The testbed they used consists of a big size electrode, PRSEUS panel, carbon/epoxy composite laminate sample, and aluminum strips that forms ground connections as shown in Figure 2.10 (a). In reference [34], Hirano et al. conducted simulated lightning strike tests and reported that the size and thickness of CFRP matrix composite laminates do not have substantial influence over lightning strike damage tolerance. The testbed they used for their simulated lightning strike tests consists of an 8 mm diameter discharge probe, ground plate, and a specimen as shown in Figure 2.10 (b). The specimen is placed between the discharge probe and the copper sheet connected to the ground. In addition, Ogasawara et al. [35] performed a coupled electric-thermal analysis to study the lightning strike experiments using the testbed configuration shown in Figure 2.10 (c). He reported that increasing the voltage increases the peak current amplitude and Joule heating that resulted in damaging the inner layers of the CFRP matrix composite laminates. Moreover, in reference [36], Kumar et al. discharged lightning impulse current to investigate the effect of adding multi-walled carbon nanotubes (MWCNT) to CFRP matrix composite laminates to improve lightning damage tolerance. In his lightning strike test experiments, samples were connected to a copper jig as shown in Figure 2.10 (d). A similar

www.manaraa.com

lightning strike testbed was used by the researchers of reference [37] as shown in Figure 2.10 (e). Furthermore, a testbed shown in Figure 2.10 (f) was used in reference [38] for studying the effect of adding polyaniline (PANI) to CFRP on lightning strike damage tolerance. In the study, a wire was used to help initiate the electric arc discharge with lightning impulse current from the indirect electrode that strikes samples placed on top of a ground plate. Furthermore, Figure 2.10 (g) presents the experimental setup of study [39], which was used to investigate the damage of CFRP caused by lightning impulse currents up to 50 kA. As shown in the figure, their test sample was grounded on two sides while the remaining two sides were ungrounded. Additionally, some researchers used a metallic wire connected to a spherical tip as recommended by the SAE 5416 standard to initiate the arc at a desired location as presented in Figure 2.10 (h) and Figure 2.10 (i) [40], [41]. Conductive wires were applied at the four edges of the samples to form an equipotential boundary around the ground electrode. Besides, a testbed similar to those of Figure 2.10 (b) and Figure 2.10 (f) is shown in Figure 2.10 (j), which was used by Li et al. [42]. Although the testbed shown in Figure 2.10 (j) is similar to those of Figure 2.10 (b) and Figure 2.10 (f), the size and shape of the electrodes are different which may have influenced the results. Lastly, a similar testbed shown in Figure 2.10 (k) and (l) was used by Sonehara et al. [43] to compare the effect of using a jet diverting electrode to using a rod electrode. The study concluded that the jet diverting electrode disperses electric charge over a wider area and reduces the damage of the CFRP matrix composite laminates compared to the rod electrode. In [44], [45], Kumar et al. used 3D polymeric and Polyaniline (PANI)-filled thermoset composite layers as a conductive layer on the top of CFRP structure to mitigate the lightning strike damage. The testbed used in the study is shown in Figure 2.10 (m). The specimen is placed on a wooden structure and the edges of the specimens are

www.manaraa.com

grounded by braided aluminum. Also, a conductive thread attached to a spherical electrical jet divertor is placed on the top of the specimen to initiate and discharge lightning current.

As summarized in in Figure 2.10, various lightning impulse current testbeds of unique features have been reported in the literature. However, a common design feature that is shared among all testbeds is the lack of electrical insulation covering the ground electrode edges. As clearly demonstrated in Figure 2.10 (e), without the electrically insulated ground electrode edges, portions of lightning discharge current are likely to directly hit the ground electrode edges without interacting with the samples. That is, the lightning strike damage tolerance assessments of CFRP matrix composite laminates using such testbeds are prone to misinterpretations without the use of electrically insulated ground electrode edges. As introduced, numerous research and experiments have been conducted to investigate the lightning strike damage of CFRP matrix composite laminates, but neither the effect of lightning discharge diameter, which is relevant to the various sizes of lightning, nor the possibility of data misinterpretation caused by the ground electrode configuration has been reported. In fact, current standards lack detailed guidelines regarding lightning testbed design for composite laminate panels, which is potentially problematic for generating consistent assessments of the panels. More specifically, standards for lightning strike analysis such as the SAE, IEC-60060-1, and MIL-STD-464 [23], [46], [47] do not specify electrode size even though it is necessary for representing lightning channel diameter, which ranges from several centimeters to several meters [9], [14], [48]. The standards also do not specify the design of sample holders including the design of ground electrodes.

www.manaraa.com

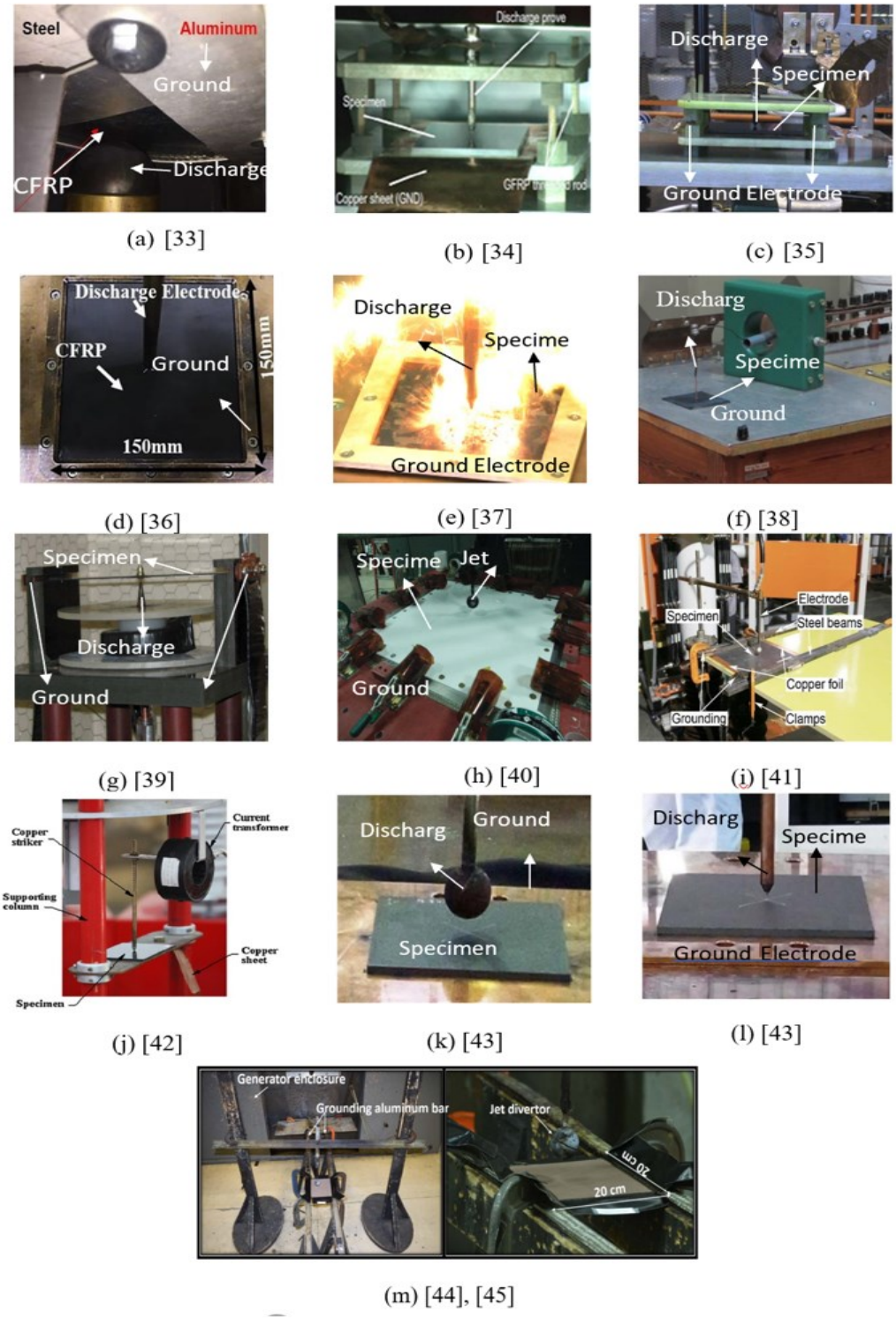

Figure 2.10 Various configurations of lightning strike testbeds used for CFRP lightning strike damage tolerance assessment

www.manaraa.com

2.6 Simulation and Analysis of Lightning Strike Damage of CFRP Composites

To understand and model the mechanism of the lightning strike, it is required to conduct the numerical and theoretical analysis of an electric arc. The lightning strike analysis is investigated by researchers using Finite Element Analysis (FEA) [29], [49]–[53]. COMSOL, ABAQUS, and ANSYS are commercial software being used for performing FEA Analysis for solving lightning problems [54]. The mathematical modeling of lightning strike is complicated especially for components A and B due to the high current amplitude. The fast increase in a short duration of time requires small time increment, which require fine mesh size to keep the heat equation stable [55]. The magneto-hydrodynamic (MHD) framework is a common method among researchers used to simulate the complex model of the arc channel [56]–[58], [59, p.]. MHD method needs coupled heat transfer and Maxell formula along with the Navier-strokes equation. Solving the combination of several nonlinear equations in one coupled model is intricate and iterative methods can be implemented by solving each formula at a time [60]. Solving the plasma without the MHD method is very complicated because the temperature and energy of each particle need to be calculated. To model the arc incorporating MHD approach requires assumption of plasma in the Local Thermodynamic Equilibrium (LTE) condition which accelerates the numerical calculation of the material transport property including viscosity, electrical conductivity, thermal conductivity, and heat capacity. Simulation of an arc plasma was studied by Freton et al. [54]. The thermal plasma was considered in LTE condition to simplify the model. To validate the model and confirm the results, the simulation results were compared with the experimental tests. The plasma transport properties can be considered and calculated as a function of temperature by using the LTE assumption. While the arc assumed as thermal plasma under the LTE condition, the areas close to the cathode and anode cannot be assumed to be in the LTE condition. The NLTE transition

www.manaraa.com

zone is an ohmic conductor and certifies the transition between cathode and the plasms [56]. Figure 2.11 shows an example of thermal model conditions in which the electrical conductivity at the surfaces near cathode and anode area in the air domain is different.

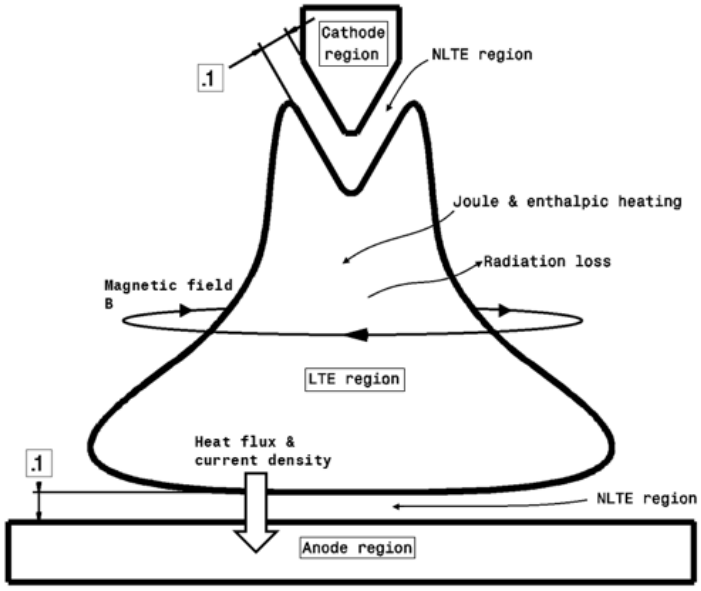

Figure 2.11 Thermal plasma model condition [60]

So, a non-LTE (NLTE) should be considered around cathode and anode. Some researchers modeled the cathode and the plasma separately to obtain the electric potential, current density, and the temperature distribution at cathode regions [51], [52]. Benilove et al. [61] observed that by modeling the plasma and cathode separately, the electrical potential drop around the NLTE region is identical all over the cathode area. To model the plasma and cathode concurrently, a fixed temperature boundary is required at the cathode and anode areas as Hsu et al. [62] imposed a 300 K temperature boundary at cathode and anode regions. Tanakara proposed 1-D model for obtaining

www.manaraa.com

the heat flux to regulate the temperature to estimate the NLTE condition [63]. He also suggested applying coarser mesh elements around the cathode and anode regions to reduce the temperature drop at those surfaces. This approach consists of using a small surface of plasma domain with thickness of 0.1 mm at the anode and cathode regions. The property of the region is the same as the plasma with a different electrical conductivity which has the value of electrode's conductivity. Studies done by Refs. [64]–[66] presented that the lightning strike can be analyzed using isotropic fluid domain with MHD numerical approach. So, the plasma domain is modeled and the material evaporation is obtained by the electrode temperature. Lightning model of SAE standard is simulated in many studies.

Researchers in [65], [67], [68], simulated the component C of the standard lightning strike with 200 A and 400 A DC current amplitude. The simulated waveform produces high material heating because of the 0.5 s time duration of component C of lightning strike. Other studies tried to simulate other components of lightning waveform. Abdelal et al. [56] used a large scale windows cluster consisting of a single node (16 cores , 3GHz) with a 64 GB RAM to simulate component B of the lightning strike current with amplitude of 11 kA and 1 ms time duration. The results showed the plasma temperature and magnetic field leads to 0.1 MPa pressure shock to the composite. The pressure shock and temperature from component B of lightning strike are too small to have significant effect on the composite because of the low time duration and the temperature that stayed at the range of 300K. On the contrary, component C simulation leads to significant material heating due to higher time duration, but the pressure is lower than one from component B simulation. Haidar et al. investigated the effect of the cathode's shape and purity on the temperature profile of the cathode's tip [53]. At the same conditions of arc simulating, the ionic parameter of the lightning arc is higher for a pure tungsten cathode than the cathode has been tested

www.manaraa.com

several times. Also, it has been observed that the maximum temperature profile at the cone's with sharper angles.

In [50], Liu et al. established a study on experimental and simulation of lightning strike damages. In experimental lightning tests, lightning strike with amplitude of 200 kA, 8 kA, 400 A, and 100 kA were applied to the Aluminum test samples. It was concluded that the lightning strike damage is a function of current amplitude and the charge transfer which has a direct relation with the damage depth and temperature rise. Liu et al simulated the lightning in another study and studied the effect of the current amplitude on the temperature rise by modeling the plasma [49]. The researcher used two-dimensional axisymmetric model to obtain the temperature distribution in regions as shown in Figure 2.12. The model geometry, dimensions, and mesh are shown in Figure 2.12 (b). All regions are presented in the model to simulate the plasma that represents the lightning. Different sizes of meshes are used in each domain to enable proper convergence of the simulation model. The element size is chosen in a way to prevent aggregation of the mesh elements in the regions, specially at the corners of the model. In the plasma region, maximum and minimum mesh element size of 0.8 mm and 0.003 mm are used, respectively. For cathode, element sizes of 2.88 mm and 0.012 mm are applied for maximum and minimum mesh element size. In the anode domain, the maximum size for the elements away from the arc is 0.4 mm and the minimum size near the arc is 8e-4 mm. Furthermore, 0.35 mm size is considered for both maximum and minimum element sizes of NLTE layers.

www.manaraa.com

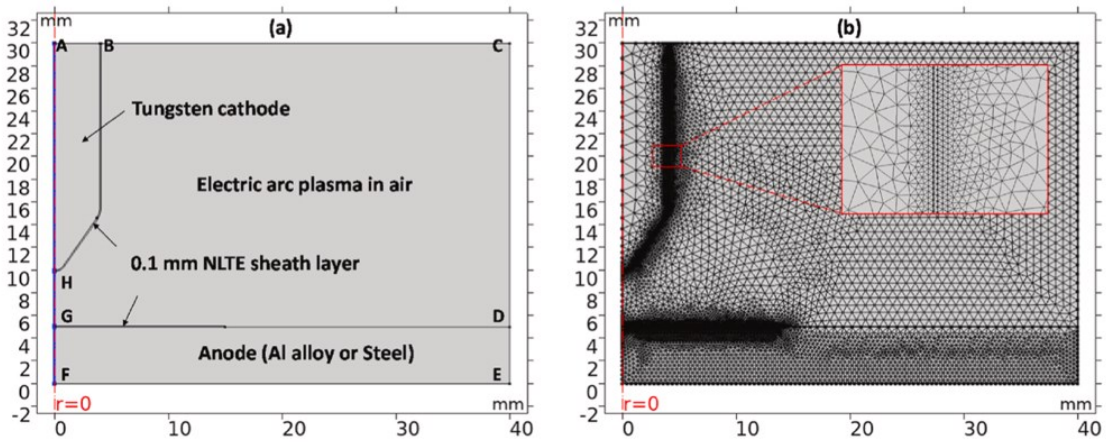

(a) (b)

Figure 2.12 Geometry of the model (b) Meshing of the domains [49]

Magnetic fields, heat transfer, and electric current modules are used in electrode and plasma domains to solve electric current, heat transfer, and magnetic field equations. The laminar flow is used to solve the Navier-Stokes equation in plasma region, which is a continuity equation. In addition, Multiphysics module is applied to perform the data exchange between the physic modules. Figure 2.13 shows the model simulated by Liu [49]. Liu simulated component C of the lightning strike and obtained the temperature distribution of anode, plasma, and cathode regions. The results from the method used by Liu et al. are shown in Figure 2.13. The air plasma temperature due to 404 A current amplitude reaches 2.92×10^4 K at the highest point in the plasma domain. The anode and cathode temperature are also calculated and are 3.32×10^3 K and 4.79×10^3 K, respectively.

www.manaraa.com

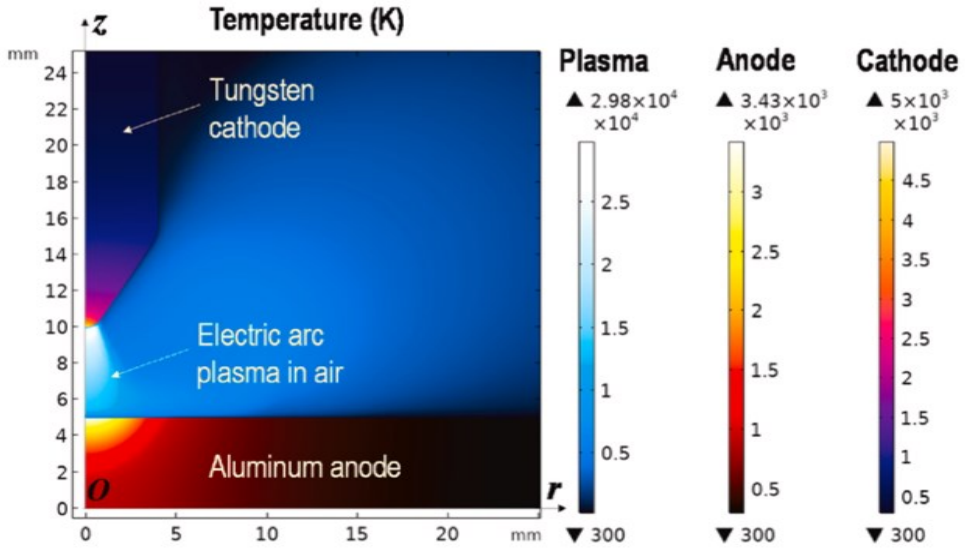

Figure 2.13 Temperature distribution of Plasma, Cathode, and Anode for 404 A continuing current [49].

Figure 2.14 represents the temperature distribution at plasma region due to different amplitudes of current. The results show that increasing the current results in the increase of temperature. It is shown that the plasma temperature goes up near the cathode because of acceleration of the electrons due to the strong electric field from cathode.

www.manaraa.com

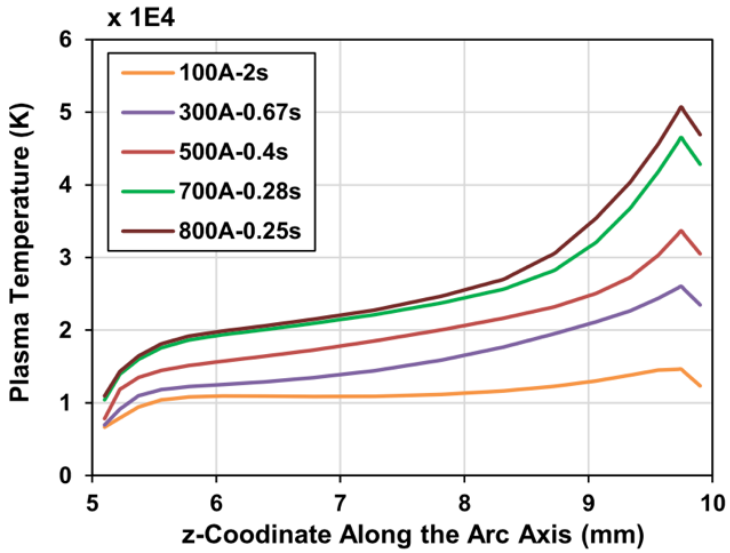

Figure 2.14 Plasma temperature distribution at different current amplitude [49].

2.7 Methods of Lightning Strike Damage Mitigation

The Joule heating produced by lightning strike current and heat of plasma channel are the primary causes of CFRP damage. The main lightning strike damage is the evaporation of the resin at the top layer. Although carbon fiber is electrically conductive, embedded resin decreases its electrical conductivity which leads to high Joule heating since the lightning current cannot propagate through the composite fast [31], [69]. Therefore, the primary approach for enhancing the lightning strike damage on composites is increasing the electrical conductivity. The damage detection of CFRP composites by measuring the electrical resistance was done by Abry et al. [70]. The electrodes' location was changed when measuring the electrical resistivity to find the conducting paths in the specimens and then flexural tests were performed. It was shown that the electrical conduction occurred at both along and opposite direction of the fiber due to the contacts

www.manaraa.com

of the adjacent fibers and plies. The electrical resistance in the longitudinal direction depends on the number of the fibers, while it depends on the length in traverse direction.

Lois et al presented an experimental investigation on the electrical resistivity of the CFRP composites in through-thickness direction. Prepregs carbon fibers with the thickness of 0.2 mm were used to fabricate the composite laminates [71]. The laminates were manufactured with curing process, where a thin layer of resin covers the laminates' surface after laminate preparation. The resin was polished to remove non-conductive path and a layer of conductive paint was applied to the polished area to create a uniform current density on the surface of composite laminates. The through thickness conductivity of the laminates were conducted using four-point method as shown in the Figure 2.15. A HP 3245A current source and a HP 3458A multimeter were used for applying current and measuring the voltage to obtain the resistivity.

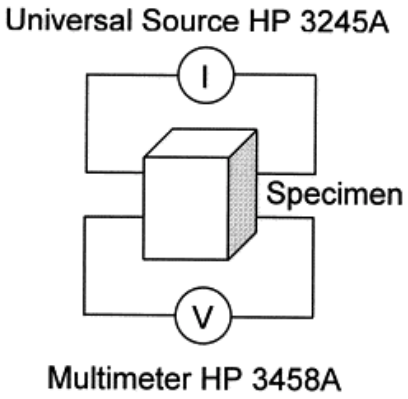

Figure 2.15 Four-point method for through-thickness electrical conductivity measurement [71]

It was seen that a uniform current density was achieved by increasing the thickness of the electrode that was used for applying the current. In addition, a noticeable difference in specific resistivity is observed between partially cured and fully cured CFRP composite laminates.

www.manaraa.com

Furthermore, it was concluded that the through-thickness specific resistivity increases when the angle between adjacent plies increases.

2.7.1 Adding Conductive Layers

Metal-base protection technique uses supplementary materials such as metal foil, metal fabrics, and metal mesh. Studies [40], [72], [73] used metal protection coating to the CFRP panels to enhance the surface electrical conductivity. The metal protections have extremely higher electrical conductivity than CFRP panels that disseminate the current easier. The main issue in using this technique is the corrosion of metal lightning strike protection (LSP) system due to the contact with carbon fiber [72]. Some other studies used non-metallic conductive layers to improve the electrical conductivity of the panels. Han et al. [74] used carbon nanotube paper, known as buckypaper (BP), with an insulating adhesive layer. The insulating adhesive layer can be punctured by a strong lightning current and lead to more damage to the composite panel. Although a stronger adhesive layer may prevent the breakdown, but higher voltage amplitude leads to the breakdown of insulation and propagation of the current through the composite.

Applying carbon nanofiber layers for lightning strike protection of composite structures is studied in [26]. The carbon nanofiber paper fabricated from carbon nanofiber fillers and nickel nano-strands through the manufacturing process. One layer of carbon nanofiber was added to the eight layers of carbon fiber with orientation of 0^0, -45^0, 90^0, $+45^0$, 0^0, -45^0, 90^0, and 45^0. The resin epoxy is added to the layers in a mold and left in room temperature overnight to cure and in oven for post-curing at 120^0 C. Three different samples are fabricated including CNFP-1, CNFP-2, AND CNFP-3. CNFP-1 consists of mono-layer, which prepared by adding carbon nanofillers and nickel nano-strands, and an sprayed latex binder layer for improving the handling strength. CNFP-2 consists of bi-layer, which consists of a pure carbon nanofiber at the base layer and a top layer

www.manaraa.com

with mixture of higher amount of carbon nanofibers and nickel nano-strands than CNFP-1, with latex binder layer. CNFP-3 consists of mono-layer, with the same amount of carbon nanofibers and nickel nano-strands as CFNP-2, without latex binder layer. The panels were subjected to 100 kA lightning strike and it was seen that the lightning strike damage decreased with increasement of carbon nanofibers and nickel nano-strands at the carbon nanofiber layer. Such an attribute is due to increasing of electrical conductivity. Also, the latex binder leaded to the damage reduction at the panel CFNP-3.

Duongthipthewa et al. [75], investigated the effect of the fuzzy fiber, a carbon-base lightning protection layer, on the thermal damage response of the CFRP composites. The CFRP composites were made through wet lay-up method after curing for 4 hours at 50^0 C and post curing at 15^0 C for 3 hours. The composite laminates have dimension of 1500x100x3.52 mm and consist of 16 layers of carbon layers laid up with the sequence of 0/90. The lightning protection layer in this study is a fuzzy fiber fabric that incorporated multi-walled nanotubes. For experimental test, component A of the standard lightning with amplitude of 20 kA and time duration over a 100-µs was applied to the composite panels with and without the lightning protection layer. The FF protection layer on the top of CFRP composites reduced the lightning strike damage drastically in compare with the unprotected CFRP composites. The damage and delamination affected five layers of CFRP composites without FF layer, whereas it reduced to 3 layers by applying FF protection layer. Kumar et al. [76] proposed polyaniline (PANI) base adhesive layer to the CFRP composites as an LSP layer for 100 kA lightning strike current. He reported that although the electrical conductivity of the PANI is less than BP, the PANI reduced the lightning damage more. Despite the effectiveness of metal-based protection layers, the industry is interested in adding

www.manaraa.com

conductive nanofillers to increase the conductivity since it reduces the total weight of aircraft than additive layers and accordingly reduce the operation cost of aircraft.

2.7.2 Adding Conductive Fillers

In [77], the researcher established a solution for polymer composite structure for increasing the electrical conductivity and improving the mechanical strength. Camphorsulfonic (CSA)-doped polyaniline is used a conductive filler for development of fully organic conductive composites for protection against the lightning strike. The PANI fillers have conductivity at the same level as semiconductors and are suitable to be considered as a conductive additive to composite structures. To solve the inhomogeneous problem of the mix, 16g of CSA (10%) is introduced to the fillers. CSA addition increases the electrical conductivity by making the mixture homogeneous. Due to poor mechanical property of the PANI, a proper amount of PANI should be added to the insulating resin. In this study, 30% PANI is added to the epoxy resin. The samples were tested using impulse current and impulse voltage generator separately. For impulse voltage test, 32 kV impulse voltage test with T1/T2 equal to 1.2/50 us was applied to the samples. For achieving this goal, the generator was charged to 15.5 kV and the resulting current was 1062A. The high current component of the lightning is the main reason for delamination and damage of the composites. High voltage test leads to the breakdown of the insulation and finding the injection point for high current test. 8.04 kA high current was applied to the composite laminates, charging the impulse current generator to 11.1kV. High current tests on the samples without conductive filler show led to delamination and damage of the composite panels, while the composite with CSA-doped polyaniline successfully carry the lightning high current with low damage.

Different kinds of nanoparticles applied to the composites to fabricate fire protected nanocomposites while keeping their functionality and mechanical properties [78], [79]. Zhao et al.

www.manaraa.com

[80] applied fabricated carbon nanofiller hybrid sheets to the CFRP composites. The sheets were added to the composite during the fabrication process using vacuum molding infusion method. The fire retardancy was tested by cone calorimetry, a polymer fire behavior test which is measures the decreasing oxygen concentration from the sample combustion gases after subjecting heat flux to the samples. It was concluded that the carbon nanofiller hybrid sheets reduce the heat released of the composites by 60%. Also, Gilma et al [81] studied reduction of flammability of polymer layered nanocomposites. Different range of polypropylene (PP) and polystyrene (PS) layered silicate nanocomposites were examined in the structures on the flammability properties. In this study, montmorillonite (MMT) clay was intercalated to prepare the composites. The fire retardancy was tested by cone calorimetry and the remainders from the combustion were investigated using Transmission Electron Microscopy (TEM). It was seen that the heat release rate (HRR) is reduced by 70 and 50 percent for PP and PS nanocomposites, respectively.

The configuration and electrical conductivity of the carbon nanotube network in polymer nanocomposites was studied in [82] by Du et al. Single-walled carbon-nanotube (SWNT) where prepared with coagulation method, which is a process of dispersion based on agglomerating colloidal particles using chemical materials. The alignment and dispersion of the nanotubes was tested by SEM, X-ray imaging, and optical microscopy. Also, electrical conductivity was obtained using two probe method. It was observed that the threshold of nanotubes amount for the polymer relaxation dynamics is 0.12 wt.% (weight percent), whereas the threshold for electrical conductivity improvement is 0.39%. The dispersion quality and alignment of the nanotubes have a significant effect on the properties of the nanocomposites. Longer polymer chains and better dispersion of the nanotubes result to a better electrical conductivity. Carbon based nano-materials including carbon nanotube (CNT), graphene, carbon black (CB), and carbon nanofibers are the

www.manaraa.com

most popular conductive additives used by researchers. A lot of researchers are improving the electrical conductivity of the resin by using carbon nanofillers. The critical issue on adding the carbon nanofillers is keeping or improving the mechanical property of the composite panels. Kumar et al. [83] added multiwall carbon nanotubes (MWCNT) to the matrix and investigated the mechanical strength with adding different percentage of MWCNT. It was observed that although increasing the MWCNT up to 0.5 % improves the electrical conductivity continuously, the mechanical strength decreases when the percentage of additive goes up to 0.2 %. In another work by Zhang et al. [84] CNTs were inserted to the CFRP composites to mitigate the lightning strike damage. To find the effectiveness of CNTs, it is compared with lightning strike protection with the silver coating. He conducted lightning strike tests on composite laminates to study the effect of a developed carbon nanotubes on the lightning strike damage. The damage of CFRP composites due to the lightning includes delamination and ablation which depends on the electrical conductivity of the specimen. Zhang applied a damped sinusoidal current component D waveform with amplitude of 200 kA and time duration of the 200us on three different specimens including a pristine CFRP composite specimen, CFRP composite with carbon nanotube, and CFRP composite with conventional silver coating. It was observed that lightning strike damage of the specimens with carbon nanotubes reduced by 68% and 77.6% in depth and area, respectively. Whereas, the lightning strike damage of the specimens with silver coating improved by 92% and 66.1% in depth and area, respectively. The additive carbon nanotube fillers improve the lightning current and energy conduction along both depth and in-plane direction of the specimen, while, incorporating surface silver coating conduct the energy and lightning current mainly along in-plane direction.

The electromagnetic issue in the electronic devices and cables are important that should be considered on lightning strike assessments. It has been reported that carbon nanotubes have

www.manaraa.com

significance influence on microwave absorption and reducing the electromagnetic interference too [85]. 0.5%, 1.1%, 1.25%, and 3% of CNTs were added to the composite structure to investigate the electrical conductivity improvement and electromagnetic interference reduction. The electrical conductivity is measured using four-probe method and increased by addition of conductive nano-fillers. The conductivity enhances from 150 S/cm to 400 S/cm as the amount of nanofillers increases from 0 to 3%. The electromagnetic shielding is investigated by calculating the reflection and absorption losses which depend on the parameters such as skin depth, frequency, relative permeability, and total conductivity. It was concluded that the electromagnetic interference enhanced from the -29.4 dB to -51.1 dB by adding the carbon nanotubes. In [30], the correlation between CNT and lightning strike protection was inspected. It was presented that despite the improper testbed that led to different results compared to other researches, the presence of CNT was effective in increasing of the electrical conductivity and mitigating the lightning strike damages. Kandare et al. [86] explored the mechanical and electrical conductivity features of Carbon Fiber-Reinforced Epoxy laminates incorporating the graphene nanoplatelet matrix filling by three nano-sized conductive fillers which are silver nanoparticles (SnPs), silver nanowires (SnWs), and graphene sheets (GnPs). The objective was finding the best combination of nano-inclusions that has better through-thickness thermal and electrical conductivity without degrading the mechanical strength such as compression, flexural, and tension. The results suggested that the silver nano-inclusions which increases the thermal and electrical conductivity, has a little or no adverse mechanical effect on the laminate.

In [87], Yang and co-workers achieved 23% increase in thermal conductivity of epoxy by adding 0.5% graphene nano-layers. They reported the adversary effect of higher amount of graphene additive due to agglomeration of the nano-particles. The agglomeration of the nano-

www.manaraa.com

particles lead reduces the surface area contact between the resin and additive nano particles which reduces the thermal conductivity. Also, Multi Walled Carbon Nanotubes (MWCNs) was added in addition to graphene and it was observed that MWCNs increases the performance of the graphene. Introducing MWCNs decreases the interfacial resistance incredibly by improving the contact surface area. A conducting composite material was proposed for lightning strike damage mitigation in [88]. The conducting material allows conducting the lightning current while maintaining the mechanical properties of a polymeric composite. The study proposed applying conductive polymers as additive instead of carbon nanostructures to increase the electrical conductivity of the composite structure. The four-probe approach was used in this study for electrical conductivity measurement. In four probe approach, as it is shown in Figure 2.16, a constant current is applied between two outer probes and the voltage drop between two inner probes is measured.

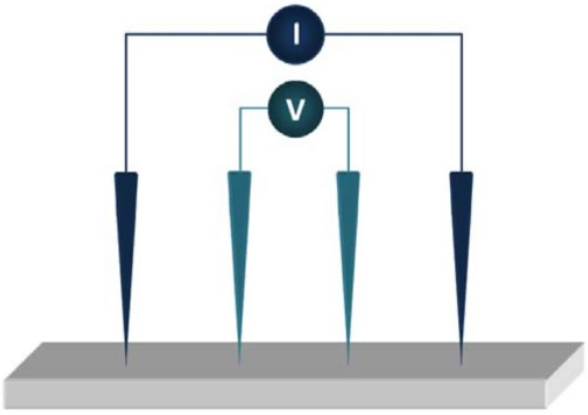

Figure 2.16 Four-point method for surface electrical conductivity measurement [88]

The conductive polymers have conductivity close to metals and the solution has an electrical conductivity more than the solution with carbon nanostructures. The only concern

www.manaraa.com

regarding adding the conductive polymer additive is the reduction of mechanical strength. To address this problem, the insulation polymers where used to achieve both electrical conductivity increasement and maintaining mechanical properties at the same time. Han et al. [89] conducted research on improving the through thickness thermal conductivity and compressive modulus of CFRP composites by introducing CB to the epoxy resin. Ethylene glycol monoethyl ether (EGME) was added to the epoxy for adding CB. EGME evaporates before fabrication. Carbon black has several features that makes it a better additive in compare to carbon fiber and CNTs. CB has a better compress-ability property which improves the comfortability of the structures. In addition, CB is less textured than two other carbon materials and there is no need for alignment accordingly. Furthermore, CB is less expensive than other nanotube materials which makes it an economic solution for increasing the thermal conductivity and compressive modulus of CFRP composites. The CB used in this study has a particle size of 30 nm and density of 1.7-1.9 g/cm^3. The dispersion quality of the CB in the epoxy resin is done by Scanning Electron Microscope (SEM) and it is shown in Figure 2.17. It can be seen that the dispersion in uniform and there is no agglomeration.

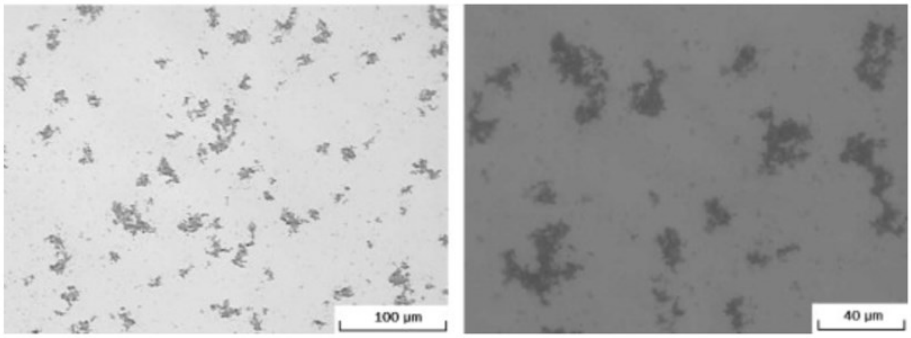

Figure 2.17 SEM image of epoxy resin with 0.8 wt% additive CB [89]

www.manaraa.com

For thermal conductivity measurement, two copper blocks were used at two plates located at longitudinal sides of the CFRP composite laminate. Thermometers are used before and after the laminated in the direction of the thermal flow at the plates to measure he temperature and obtain the thermal conductivity. Also, the compressive modulus, the ratio of the applies stress for resulting strain, is obtained using a testing machine with maximum load of 1000 lb between its two plates. It was concluded that applying CB with EGME to the epoxy resin increases the thermal conductivity and compressive modulus by 210% and 14%, respectively. In [90] the researcher investigated the incorporating CB and copper chloride (CC) to the epoxy matrix to improve the electrical conductivity of the composite laminate. Base on the experimental results, incorporating CB and CC can greatly enhance the electrical conductivity the epoxy matrix as shown in Figure 2.18.

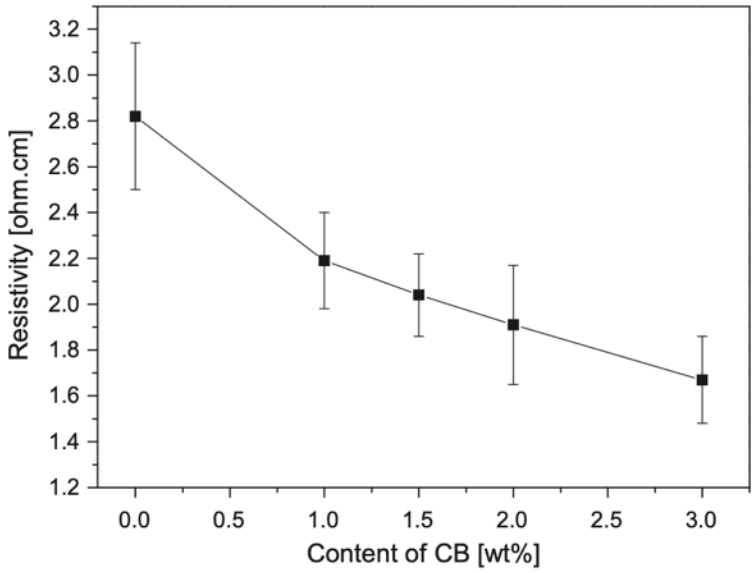

Figure 2.18 Resistivity of the composite panel at different ratio of the CB [90]

www.manaraa.com

Also, the mechanical property is enhanced due to the presence of the CB. Adding CC creates more cluster in the epoxy with CB which forms a better bridge-link and a network of Carbon nanofillers that reduces the electrical resistivity, which leads to the reduction of electrical resistivity. 3.0 wt% of CB, and 14.4% and 12.5% of CC used in this research study. Yang added carbon CB to the polypropylene/carbon fiber (PP/CF) to enhance the thermal stability, electrical conductivity, and flame retardancy. According to Yang, CB has two significant advantages. First, CB is very cheap with very high and permanent electrical conductivity. Second, CB has specific feature that block degradation of other materials, specially polymers, that leads to forming a crosslinking structures [91]. The carbon black had a 17 nm diameter and purity of more than 99%. For the preparation of the mixture, PP with PPMA of 10% and specific amount of CB or CF is mixed with a Haak batch intensive mixer at 100 rpm and 1,800 C for 10 minutes. It was shown that the dispersion of the one-dimensional CF in the PP matrix attributes to the creation of a 3-D network structure leads to a better conductive pathway. It has been shown that using CB as a filler to PP/CF composites improves the electrical conductivity dramatically, as it can be seen in Figure 2.19. First, zero-dimensional CB and one-dimensional CF leads to a 3D network. Second, it traps radicals (group of atoms which behave as a unit) at high temperatures. Also, CB does not reduce the mechanical strength.

www.manaraa.com

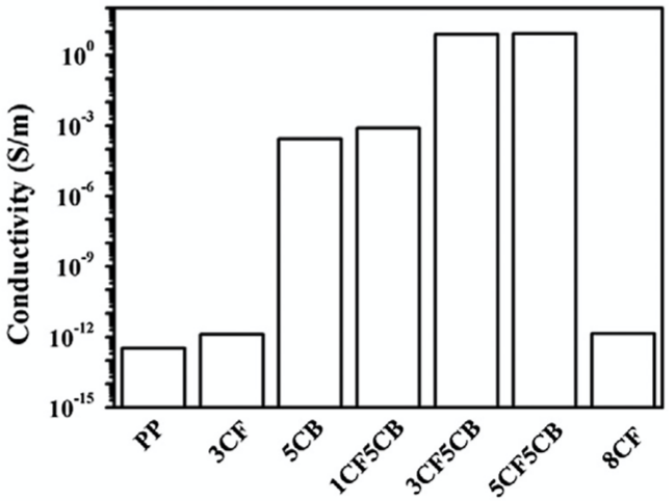

Figure 2.19 Electrical conductivity of the composite panel at different combination of the CB [91]

Numerous studies investigated the effect of the amount of dispersed carbon nanofillers on lightning strike damage mitigation, electrical resistivity improvement, and mechanical strength enhancement of composite materials, but the effect of CB on lightning strike damage mitigation has not been reported yet. A thorough investigation on the amount and type of dispersed carbon nanofiller material is essential for reducing the lightning strike damage of the composite laminates while maintaining the mechanical properties and reducing induced lightning strike damage.

www.manaraa.com

CHAPTER III

RESEARCH OBJECTIVES

The goal of this research is improving the electrical conductivity of the resin and thereby reducing the lightning strike damage of the CFRP composites. However, improving the electrical conductivity of CFRP composites can only be achieved given a reliable testbed is available. Many of the testbeds used and reported in the literature are prone to data misinterpretation, which is in part caused by the lack of clear testbed design guidelines.

The primary objectives of this dissertation are:

- Investigating effect of electrode diameter on lightning strike damage of CFRP composites. The standards have not considered a specific size of electrode and researchers use electrode with various sizes for lightning strike tests of composite samples which leads to probable result misinterpretation in the reports and studies. To demonstrate the impact of lightning discharge diameter on the damage tolerance of CFRP matrix composite laminates, various sizes of electrodes were used to produce lightning discharge with various diameters while the magnitude of the discharge current is kept constant. For validation of the lightning channel experiment results, a numerical analysis of electric arc is performed. COMSOL Multiphysics is used, which is based on Finite Element Analysis (FEA) for simulating plasma-anode interaction. The goal is to find out how the plasma temperature, anode temperature, and the current density differs as the electrode's size changes.

www.manaraa.com

- Providing a suitable ground electrode configuration for lightning strike test of CFRP composites. Grounding configurations used in the reported studies are inconsistent due to the lack of guidance provided by the standards. It has been observed that lightning strike testbeds not using electrically insulated ground electrode edges are prone to generating misleading test results. Although it is difficult to visually identify lightning discharge current bypassing a sample and directly hitting ground electrode edges, the results of our study clearly suggest that fractions of discharge current jump directly to the ground electrode instead of propagating through the CFRP matrix composite laminates in cases where conventional ground electrodes without electrically insulated edges are used. To demonstrate the importance of ground configuration two types of insulation are incorporated for the ground to prevent the lightning discharge hitting the ground. Two sizes of electrode with and without ground insulation are used while the magnitude of the discharge current is kept constant. The level of damage is inspected by visually inspecting the area of surface material removal and by performing c-scan to detect the severity of internal delamination. For validating the ground configuration experiment results, a numerical analysis of electric arc is performed by COMSOL Multiphysics for simulating plasma-anode interaction. COMSOL Multiphysics and FEA method is used for simulating plasma-anode interaction and showing the inherit effect of ground. Applying ground insulation makes the path between electrode and ground longer. So, in the simulation different length of ground domain are applied which changes the distance between cathode and ground. It is observed that how much the anode, cathode, and plasma temperature, and the current density changes as the ground get close to the cathode.

www.manaraa.com

- Studying effect of CB on lightning strike damage mitigation. There are many methods for increasing the electrical conductivity of the composite panels to dissipate the lightning strike induced Joule heating faster and accordingly to reduce the induced damage. But, effect of CB as an additive to the composite panels for improving the lightning strike damage tolerance is not studied yet. This research investigates the application of CB for lightning strike damage mitigation since it can be more economic to the industry in comparison to other additive materials. Also, its combination with CNT is investigated to find a suitable amount and type of dispersed carbon nanofillers to the CFRP composites to reduce the lightning strike damage. Adding the conductive nanofillers decreases the resistivity of the samples. The nanofillers are added to the CFRP composites during the manufacturing process and then the resistivity of the samples is measured. The CFRP composites with different percentage of nanofillers is subjected to the identical lightning strike and surface material loss and delamination size due to the lightning strike is observed.

The findings of this research suggest the suitable electrode size and ground electrode configuration for lightning strike experiments. Also, the effect of CB as an amount of dispersed nanofillers on lightning strike damage mitigation is inspected.

www.manaraa.com

CHAPTER IV

LIGHTNING STRIKE EXPERIMENT

4.1 Motivation

There has been a rising trend in using impulse current generators to investigate the lightning strike protection performance of materials including aluminum and composites in structures such as wind turbine blade and aircraft body. The focus of this chapter is to present the impulse current generator built in the High Voltage Lab at Mississippi State University. The generator is capable of producing component A and D of natural lightning discharges in accordance with the Society of Automotive Engineers (SAE) standard, which is widely used in the aerospace industry. The generator can supply lightning impulse energy up to 400 kJ with the capability of producing impulse currents with magnitudes greater than 200 kA. The electrical circuit and physical components of an improved impulse current generator are described and several lightning strike waveforms with different amplitudes are presented to compare with the standard waveform. The results of this chapter contribute to the fundamental understanding the functionality of the impulse current generators.

4.2 Standard Lightning Waveform

Wind energy and aerospace industries are interested in simulating lightning to increase the reliability and protection of equipment and structures that are prone to lightning strike. Society of

www.manaraa.com

Automotive Engineers (SAE) ARP 5412 standard suggests the use of lightning waveform that resembles those of the natural lightning phenomena for lightning experiments. The standard lightning waveform consists of four components including A, B, C, and D which have different current amplitudes and duration. Conducting lightning strike experiments requires these lightning current components. The selection of the standard waveform component for lightning strike evaluation is limited by the type of available impulse current generator and the goal of a study.

To perform the lightning strike study on aircraft structures, it is necessary to simulate at least one of the components from the standard. Impulse current generators are capable of producing lightning current in accordance with the SAE standard represented in Figure 4.1.

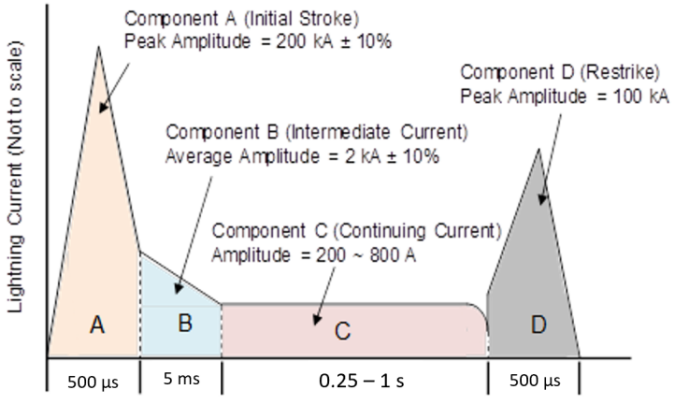

Figure 4.1 Standard Lightning waveform recommended by SAE [19], [20]

A comprehensive study is necessary for constructing the impulse current generator with accuracy in accordance with the standard and the mathematical equations while providing high-level safety. The functionality of the impulse current generators used and their construction and design for generating lightning current waveform have not been reported. In this chapter, the

www.manaraa.com

electrical circuit and physical components of the impulse current generator are described and several lightning strike waveforms with different amplitudes are presented.

4.3 Electrical Circuit of The Impulse Current Generator

The electrical circuit of an impulse current generator is identical to a series RLC circuit shown in Figure 4.2 [92], [93]. High voltage capacitors charged via a DC source up to U0 volt discharge suddenly discharge stored energy through a test sample. The inductance of circuit L includes the test circuit connection (could be adjustable), stray and test sample inductances, while the total resistance of circuit R consists of test circuit constant resistance and test sample resistances.

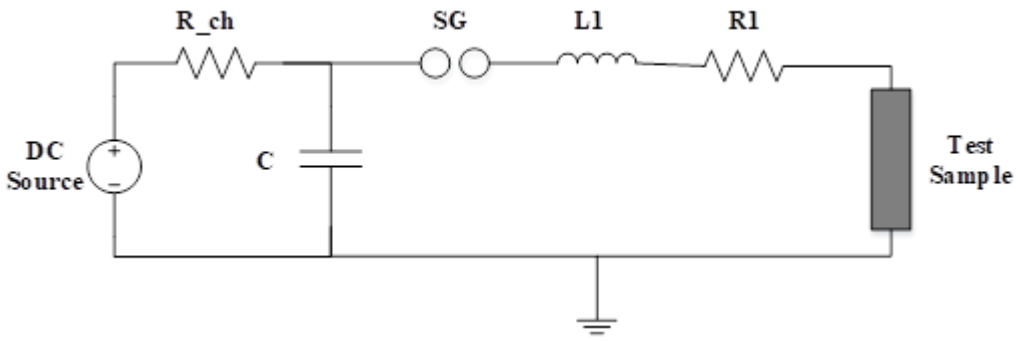

Figure 4.2 Equivalent circuit of impulse current generator

By triggering the spark gap, energy stored in capacitor C discharges through the total L and R. At this moment, current I(t) flowing through the circuit is calculated by solving the following equation.

$$I'' + \frac{R}{L}I' + \frac{1}{LC}I = U_0 \qquad (4.1)$$

Equation 4.1 is a second-order differential equation and its solution depends on the value of β.

www.manaraa.com

$$\beta = \sqrt{\frac{R^2}{4L^2} - \frac{1}{LC}} \tag{4.2}$$

Based on the test circuit parameters C, L and R, β could be:

$$\beta \begin{cases} > 0 & \text{Over\_damped} \\ = 0 & \text{Ciritical\_damped} \\ < 0 & \text{Under\_damped} \end{cases}$$

The lightning waveform can have three wave-shapes based on the β as shown in Figure 4.3.

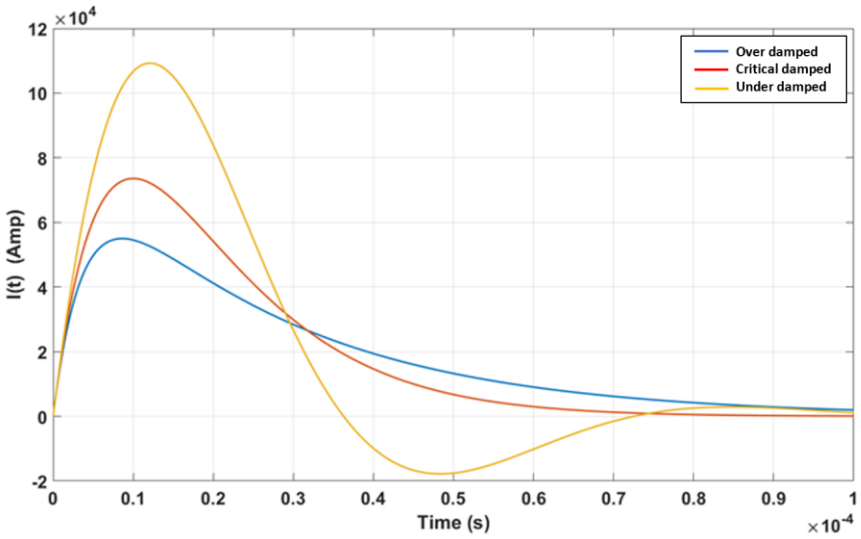

Figure 4.3 Three different waveforms of impulse current [46], [94]

In an overdamped condition ($\beta > 0$),

$$i_k(t) = \frac{U_0}{Z}\left(e^{\frac{R-Z}{2L}t} - e^{\frac{R+Z}{2L}t}\right) \tag{4.3}$$

The current waveform used for SAE standard is an over damped waveform with a double exponential driven equation as below:

$$I(t) = I_{max}(e^{-\alpha t} - e^{-\beta t}) \tag{4.4}$$

www.manaraa.com

The electrical circuit of a conventional impulse current generator at MSU-HVL is shown in Fig. 4. 4. In this setup, the capacitors are discharged by triggering the spark gap, and a discharged occurs through the 1Ω resistors to a test subject. When the capacitors are charged completely and the target voltage is obtained, the capacitor bank will be discharged by switching a triggered gap that applies the voltage of the charged capacitors to the gap between the test subject and the output electrode. The resulting electrical arc delivers the current stroke to the surface of the test article as it shown with red lines.

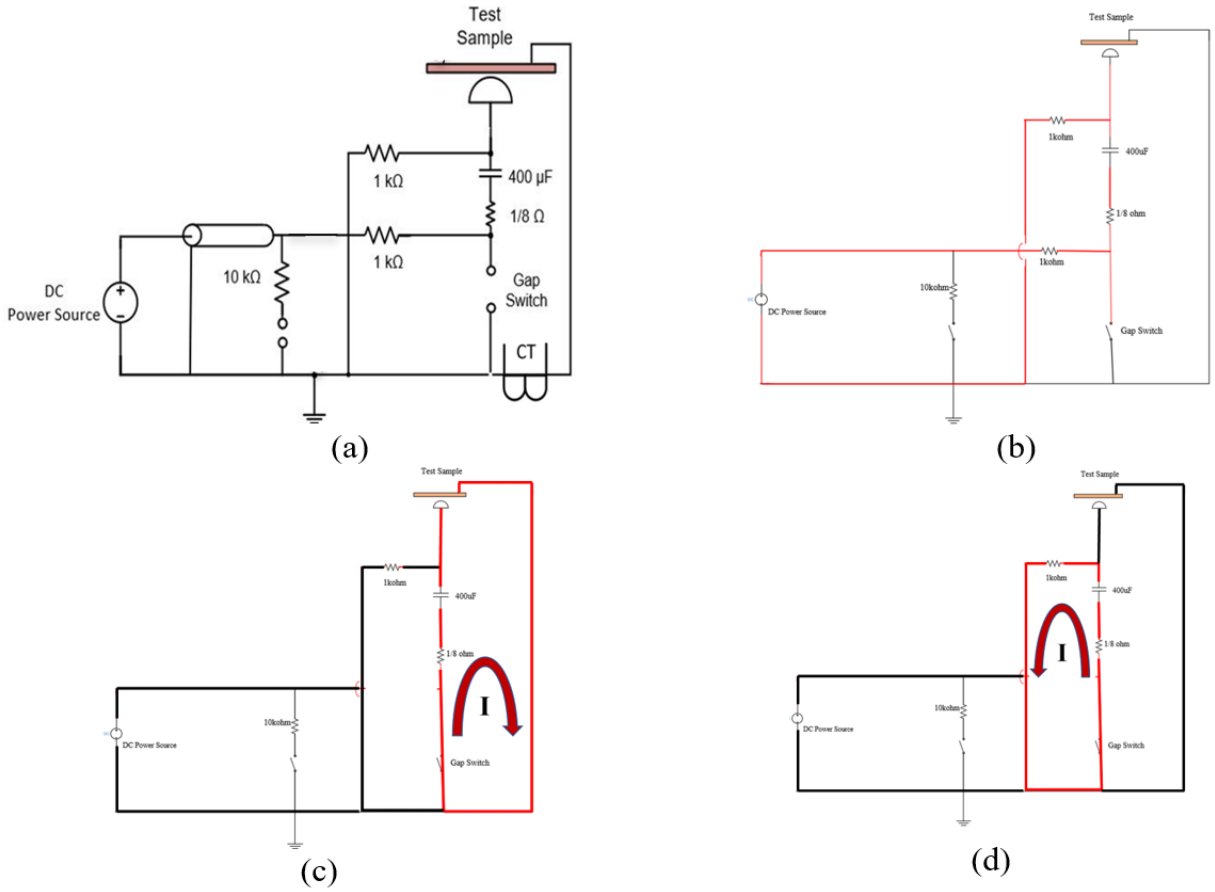

Figure 4.4 Equivalent circuit of impulse current generator: (a)Electrical circuit of components, (b) Charging circuit, (c) Discharge circuit, (d) Misfire circuit

www.manaraa.com

Figure 4.4 (a) is a RLC circuit as explained in Figure 4.2. The red line in Figure 4.4 (b), Figure 4.4 (c), and Figure 4.4 (d) shows the charging circuit, discharge circuit, and misfire circuit, respectively. The capacitors' energy does not discharge through the test subject if the resistance of the subject is large or the gap between the discharge electrode and the test subject is high. In this case, the discharge occurs through the misfire circuit where a 1kΩ resistor is installed. The inductance of the circuit is the inductance of the conductors. The two 1kΩ resistors are the charging and discharge resistors. Also, the 10 kΩ resistor is used for an alternative bypass switch to increase the safety and ground the circuit after discharge. The selection of the standard waveform component for lightning strike is limited by the type of available impulse current generator.

4.4 Impulse Current Generator

4.4.1 The Impulse Current Generator at MSU-HVL

The impulse current generator in this study is capable of producing lightning components A and D. The configuration and electrical components of the impulse current generator are shown in Figure 4.5. The impulse current generator has a total of eight 47 μF capacitors connected in parallel, each of which has a voltage rating of 44 kV. This provides total lightning impulse energy up to 400 kJ. Once the capacitors are charged to a targeted voltage, lightning current discharge is triggered by a pneumatically actuated gap that directs the voltage of the charged capacitors to the gap between the output electrode and the ground electrode. The lightning current flows from the output electrode, through a sample, and into the ground electrode.

www.manaraa.com

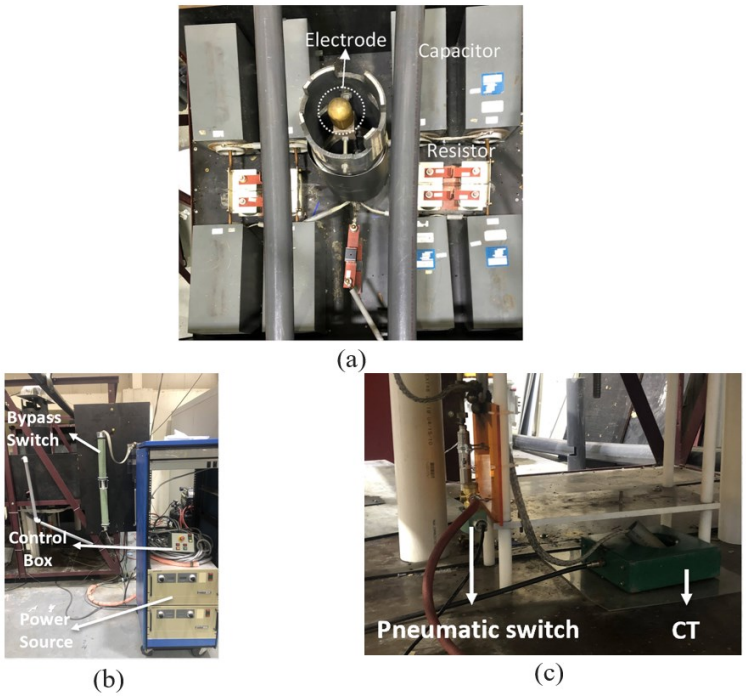

Figure 4.5 Impulse current generator at MSU-HVL: (a) Capacitors, (b) Power supply, (c) Pneumatic switch

It was not possible to get high currents due to the improper clearance of the generator. The capacitors could not be charged to the required voltage for high current lightning discharge because of the improper designed clearance, which caused uncontrolled self-ignition of the circuit before triggering the circuit. So, tests failed and led to the damage of generator as shown in Figure 4.6. In order to enhance the performance of the generator, different configurations were tested for the resistors and the connections. The optimized configuration for resistors and connections is shown in Figure 4.6 (c), in which the flexible braided wires were replaced with copper pipes for connection between the resistors and capacitors. Also, the resistors were rearranged.

www.manaraa.com

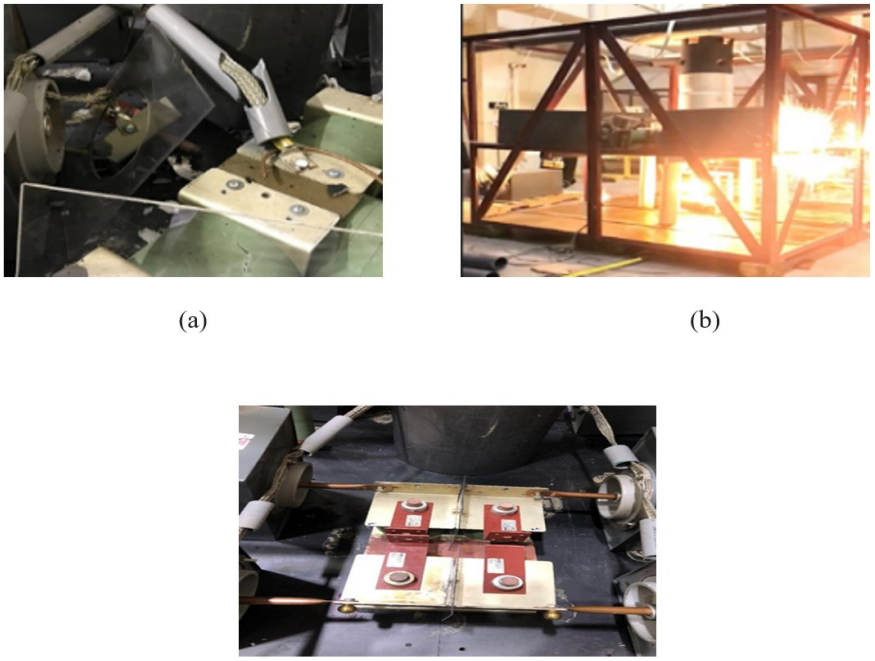

(a) (b)

(c)

Figure 4.6 Problems through the impulse current generator because of the improper clearance: (a) connectors breakdown, (b) self-ignition in the circuit, (c) new configuration

4.4.2 The Impulse Current Generator Parameters

Since all parameters of the generator such as capacitors, resistors, and inductance are adjustable, the magnitude of the lightning current can be controlled by either changing the voltage or the number of parallel connections of the capacitors. In order to find out the parameters of the generator, an Aluminum panel is used to perform the high current test and predict the inductance and resistance of the circuit. Six parallel capacitors were charged to 6.2 kV for injecting 50 kA impulse current to the panel. Figure 4.7 represents 50 kA impulse current which is a double exponential waveform with time duration less than 500 μs. Curve fitting analysis was performed

www.manaraa.com

on the output current of our impulse generator to find the circuit element parameters as shown in the Figure 4.7.

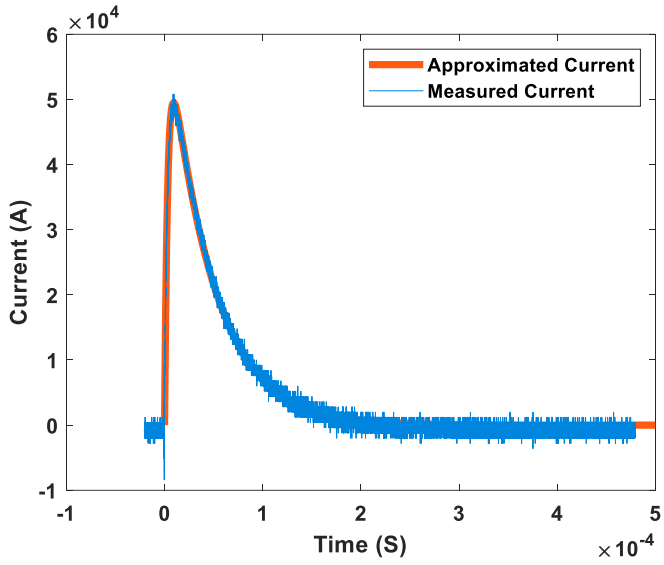

Figure 4.7 Curve fitting of measured current

$$a \times (e^{-bt} - e^{-ct}) \Longrightarrow \begin{cases} a = 6.560320 * 10^4 \\ b = 2.22221 * 10^4 \\ c = 30.52725 * 10^4 \end{cases}$$

By comparing the obtained values with the equation 4.3 and considering the total capacitance 6×47 µF and the voltage of 6.2 kV, the predicted resistance and inductance of existing impulse current test circuit are:

R= 0.108 Ω

L = 0.33 µH

4.4.3 The Impulse Current Generator Output

The energy of lightning discharge is a factor that damages materials. Six 50 µF capacitors connected in parallel are installed and charged to different levels of voltages to get the required

www.manaraa.com

lightning currents which are 50 kA, 100 kA, 150 kA, and 200 kA. Figure 4.8 represents the charged energy of the capacitors at different voltage levels.

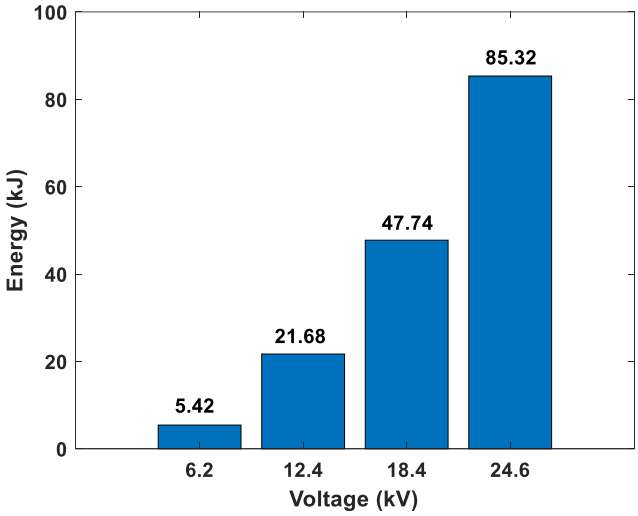

Figure 4.8 Energy of capacitors at different voltage levels

Component A of the lightning strike that has a peak amplitude lower than 200 kA and the time duration of equal or less than 500 μs is generated by our impulse current generator. A Pearson current transformer (CT) with the volt per amp ratio of 0.001 is placed on the current path and a Tektronix DPO 7104 digitizer is used to capture the lightning impulse waveform. The generator produced component A and D of lightning current waveforms with the current amplitudes of 50 kA, 100 kA, 150 kA, 200kA. The lightning current with different amplitudes are shown in Figure 4.9.

www.manaraa.com

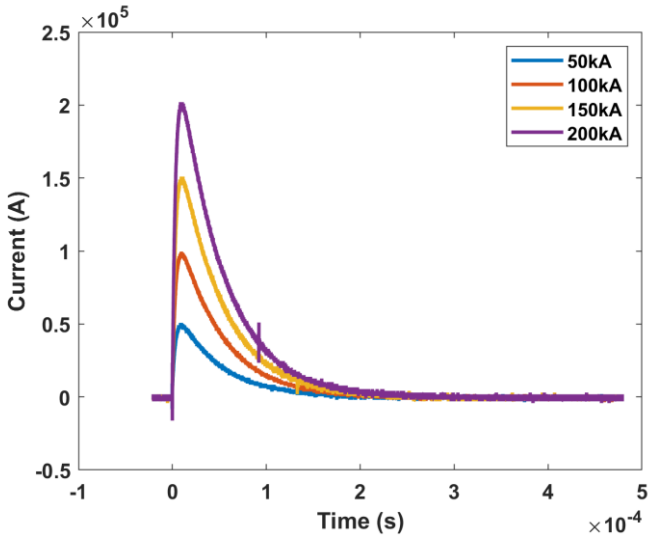

Figure 4.9 Impulse current waveforms generated by generator at HVL-MSU

Figure 4.10 shows the correlation between the voltage of capacitors and the produced maximum impulse current value. As shown, the correlation is linear which means a desired current amplitude can be obtained by changing the voltage.

www.manaraa.com

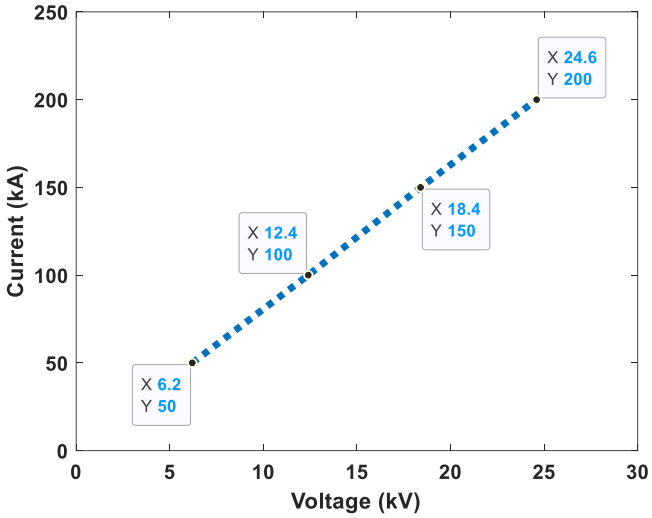

Figure 4.10 Linear correlation of voltage and current of generator

The linear correlation exists for testing samples with the same resistance. Figure 4.11 shows flames generated at a moment of a lightning current discharge.

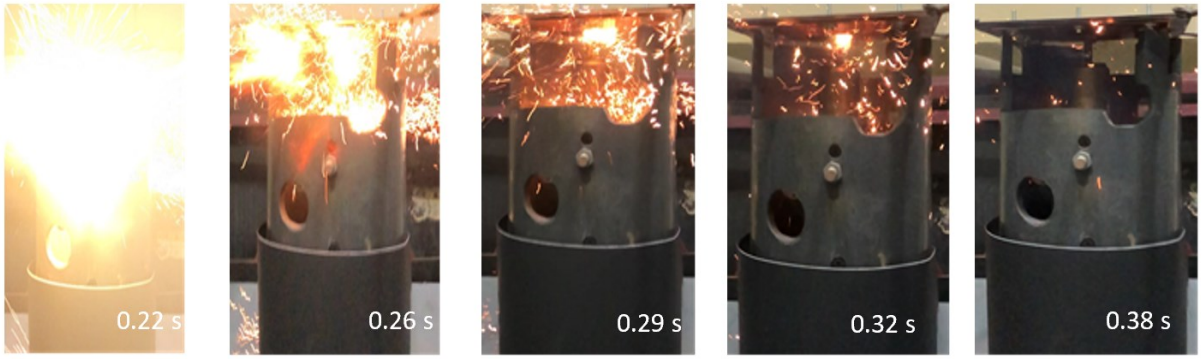

Figure 4.11 The moment of lightning strike of a CFRP matrix composite laminate sample

www.manaraa.com

4.4.4 New Impulse Current Generator

The problem of the old impulse current generator at MSU-HVL was the low flexibility. It was not possible to get high currents frequently due to the improper clearance of generator. It was not possible to charge the capacitors to the desired voltage and get the high current because of the improper clearance which caused uncontrolled ignition in the circuit before triggering the circuit. So, tests failed and led to the damage of the generator. Besides, it was hard and time consuming for mounting the samples on top of the discharge electrode in the past. In order to enhance the performance of the generator, a new impulse generator was constructed for lightning impulse tests. The configuration of the new impulse current generator at HVL-MSU is shown in Figure 4.12 (a). Figure 4.12 (b) represents the moments of lightning strike to a panel that got delaminated and decomposed.

www.manaraa.com

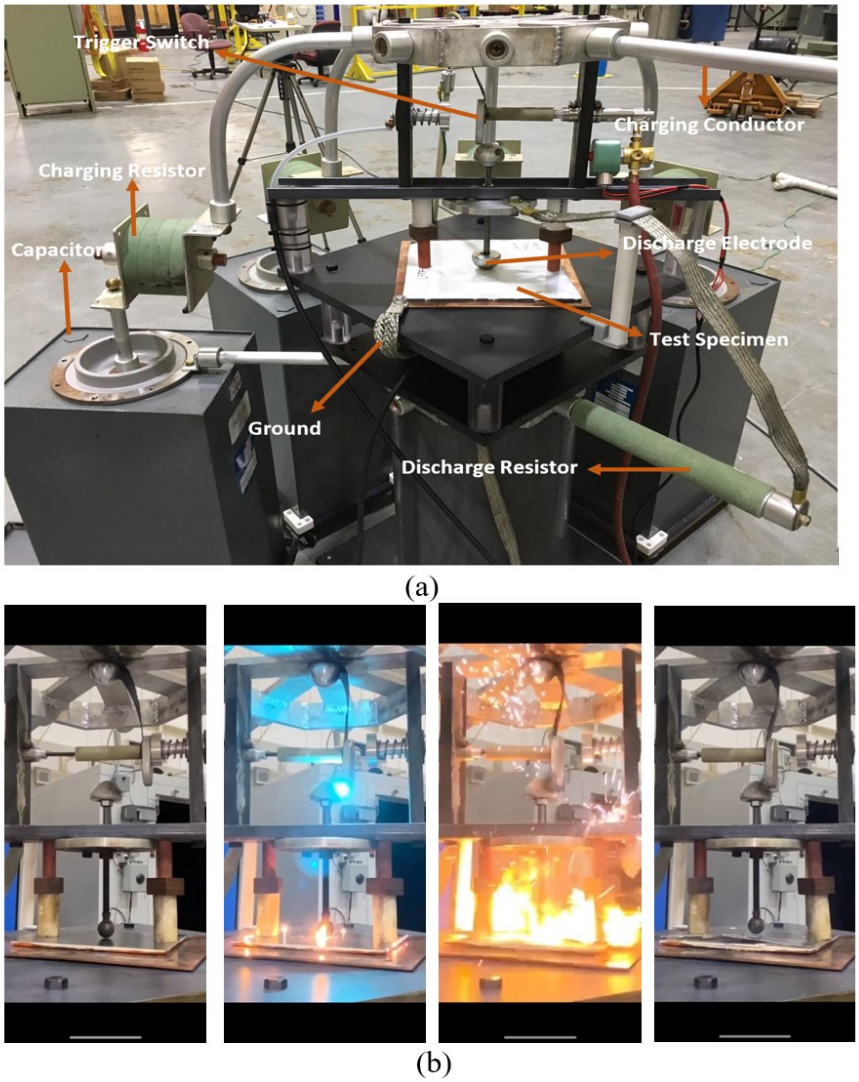

Figure 4.12 Impulse current generator: (a) New developed generator, (b)The moment of lightning strike of a CFRP matrix composite laminate sample

4.5 Summary

The configuration of the impulse current generators was described in this chapter and lightning strike waveform with different amplitudes was presented. The generator is a RLC circuit and capable of producing lightning impulse current with amplitudes greater than 200 kA. The waveform of the generator fulfills the SAE standard requirements for lightning strike test of aircraft structures. The lightning current can be controlled by changing the charging voltage of the

www.manaraa.com

capacitors. A preliminary test is required for each test sample to estimate the charging voltage of the capacitors to obtain a desired current amplitude. The charging voltage can be predicted from the extrapolation of the preliminary results. The results of this study validate the functionality of our impulse current generators in the High Voltage Lab at Mississippi State University based on the SAE standard requirement.

www.manaraa.com

CHAPTER V

EXPERIMENTAL FOUNDATION OF THE RESEARCH

5.1 Motivation

To investigate the research objectives, three components are required to be designed and manufactured for the test. First, CFRP composites are made of several materials. The performance and strength of the composite structures depend on the well-quality production processes. Two common manufacturing methods and the process of adding nano-fillers to the composites are described in this chapter. Second, to study the effect of discharge diameter of lightning, three hemisphere electrodes with various diameters are manufactured. Third, to prevent the misinterpretations in the lightning strike damage studies of CFRP composites, insulation is applied to the ground electrode.

5.2 Fabrication of CFRP Composites

5.2.1 Infusion Method

The vacuum assisted resin infusion process was used to fabricate the CFRP matrix composite laminate panel samples. The infusion method is commonly used by manufacturers in the aerospace industry including Mitsubishi and Boeing owing to its low-cost and short processing time. Figure 5.1 is the setup used for the vacuum infusion process. The CFRP matrix composite laminates used in this study consists of 8 layers of woven carbon fiber fabrics laid up with the

www.manaraa.com

orientation of [0/90/0/90] on a metal mold. Since the dry carbon fiber was used is a 2×2 twill weave, track of the warp direction of each layer of the fabric was kept. In other words, the angles shown in our laminate layup indicate the warp direction of the woven fabric. Such method of reporting the laminate layout for woven fabric was also used in [95]. Each laminate is fabricated using Adtech 820 epoxy resin with 824 hardener. Also, 3K Twill weave carbon fiber fabrics with the volume fraction of 73.5 % is used. A vacuum bag is used to enable the infusion process and to remove excess resin from the carbon fiber layers. A valve at the inlet is used for inserting resin while the other valve at the outlet is used for applying vacuum. Before injection of the resin, the inlet valve was closed and pulled vacuum until the mold interior pressure reached -27 in/hg (i.e., -91 kPa) with respect to atmospheric pressure (i.e., 101 kPa). Once the desired interior pressure is achieved, the resin is injected to the mold and the infused carbon fiber sheets are kept in room temperature for 24 hours to cure. After the curing process, the composite samples are trimmed to remove rough edges. To perform lightning strike experiments under various conditions, 9 identical CFRP matrix composite laminate samples are fabricated with the size of 22.86 cm by 22.86 cm. The average thickness of the samples is 1.9 mm with the standard deviation of 0.042 mm.

Figure 5.1 Infusion process of CFRP matrix composite laminate fabrication

www.manaraa.com

5.2.2 Hand Lay-up Method

5.2.2.1 Adding Nano-fillers

To achieve the goal of reducing lightning strike damage, carbon nanofillers are added to the composite structure during the fabrication process. Figure 5.2 illustrates the process of adding nanofillers to the composites. The nanofillers are dispersed in epoxy using sonicator that mix the carbon nanofillers to the resin for 72 minutes. Then, the mixture is hold in a bulk and degassed by vacuum pump for 45 minutes. After degassing, the hardener is added to the mixture manually and degassed again for 10 minutes. Finally, the epoxy resin mixed with nanofillers was used for making the CFRP composite laminates using hand-layup method. Figure 5.2 shows the outline of adding conductive nanofillers to the adhesive.

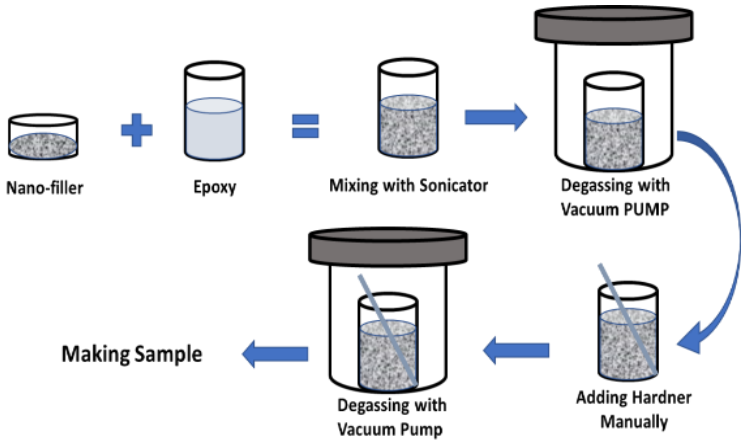

Figure 5.2 Outline of adding nano-fillers to the CFRP composites process

0.75% of nanofillers were added to the epoxy using an ultrasonic sonicator as it is shown in Figure 5.3. Ice cubes is used to reduce the temperature rise during the ultrasonic vibration. Three CFRP composites containing 0.75% of CB, CNT, and CNT+ CB were fabricated for our study.

www.manaraa.com

One sample was made without any additive nano-filler and three samples were made with nanofillers including CB, CNT, and CB+CNT to study the effect of carbon nanofillers on lightning strike damage mitigation of CFRP composites. CB is sphere shape with 150 nm diameter and CNT is Multi Walled Nanotubes with diameter of 20 nm.

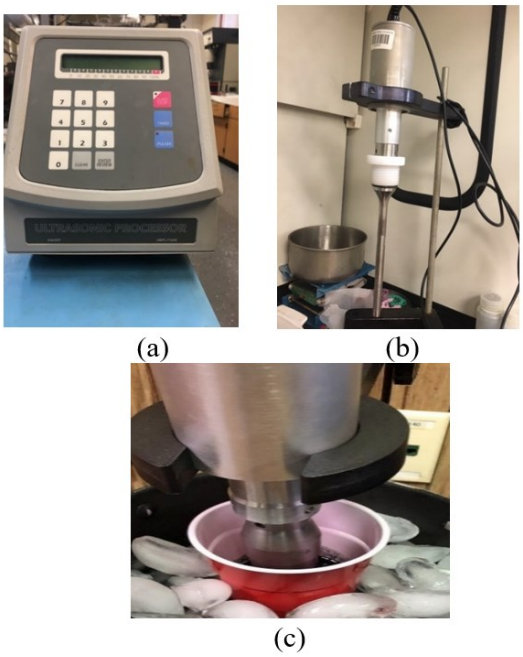

Figure 5.3 Ultrasonic processor for adding the nano-fillers to the resin: (a) Sonicator (b) Sonicator probe (c) Mixing set-up

5.2.2.2 Hand lay-up

The hand lay-up is a significant conventional process in manufacturing the composite laminates owing to such advantages as simplicity in processes and lower tool cost. Figure 5.4 shows the hand layup set-up for fabricating CFRP composite samples. Infusion method is not a good way for adding the resin with nano-fillers to the composite layers because the nano fillers stuck at the entry areas and does not distribute among the composite structures consistently. The hand lay-up method is an efficient method for making CFRP composites with nano-fillers.

www.manaraa.com

8 layers of carbon fibers were cut 30 cm × 30 cm and laid up one by one on a metal mold with $[0/90/0/90]_s$ direction. 200 g of Adtech 820 resin was mixed manually with 36 g Adtech 824 hardener to make a strong adhesive. The adhesive is added to each carbon fiber layers manually and by using a brush. A vacuum bag is used to seal the mold using a vacuum pump connecting to the mold. The vacuum pump makes the interior pressure -91,432.5 Pa lower than atmospheric pressure and draw out the air from the mold. The CFRP composite samples were ready after keeping them in the room temperature for 24 hours. After the curing process, the composite samples were trimmed to remove rough edges. Eleven 30 cm × 30 cm CFRP composites were made for this research study.

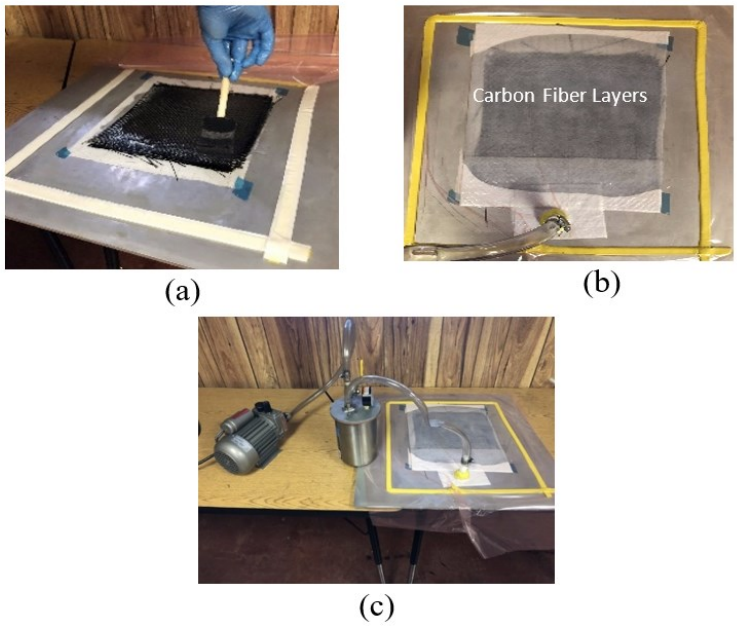

Figure 5.4 Hand layup method for CFRP fabrication: Adding the resin with brush (b) Vacuuming the mold, (c) Hand layup method set-up

The type and amount of nanofiller incorporated for manufacturing the samples are shown in Table 5.1. It was not possible to mix 1% of CB and CB+CNT due to high viscosity of the resin after adding the nano-fillers.

www.manaraa.com

Table 5.1 Type and amount of nanofiller

Type of Nano-filler	Percentage of Nano-filler			
	0.25%	0.5%	0.75%	1%
CB	✓	✓	✓	✓
CB + CNT	✓	✓	✓	×
CNT	✓	✓	✓	×

5.3 Electrodes of Various Sizes

In addition to current amplitude, lightning strike damage varies as a function of electrode size, which determines the diameter of lightning discharge. To study the effect of discharge diameter of lightning, three hemisphere electrodes with distinct diameters of 16 mm, 46 mm, and 98 mm were designed as shown in Figure 5.5.

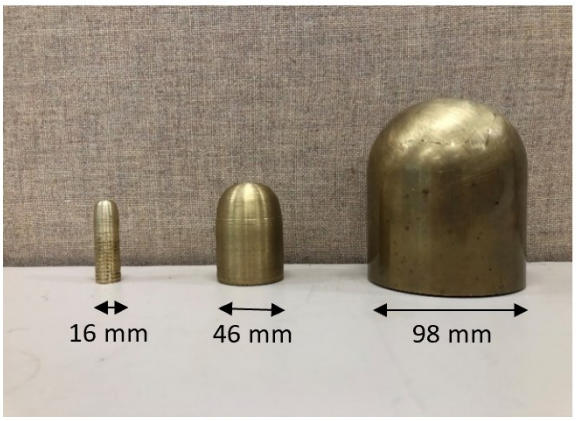

Figure 5.5 Three electrodes used for studying the impact of lightning discharge diameter

5.4 Ground Electrode Configuration

Ideally, in lightning strike tests, the entire lightning discharge should interact with composite laminate samples. However, depending on the ground electrode configuration, it is possible that the portions of the discharge current hit the ground electrode directly instead of propagating through the test samples. This results in the reduced damage of the CFRP samples, which can be misinterpreted as the sample resisting or tolerating the impact of lightning strike

www.manaraa.com

effectively. To prevent such misinterpretations, the entire lightning discharge current must be ensured to propagate through or at least interact with the samples. To address this issue, two different approaches of electrically insulating are applied to the ground electrode edges. As shown in Figure 5.6, two different insulation barriers are installed in the testbed. Figure 5.6 (b) shows a 3D printed dielectric frame that covers the edges of the ground electrode. The square dielectric frame has a width of 127 mm and a height of 25.4 mm that covers the edges of the ground electrode. To ensure that the height of the dielectric barrier does not influence the lightning experiment results, the second type of insulation is applied by covering the ground electrode edges with dielectric tape as shown in Figure 5.6 (c).

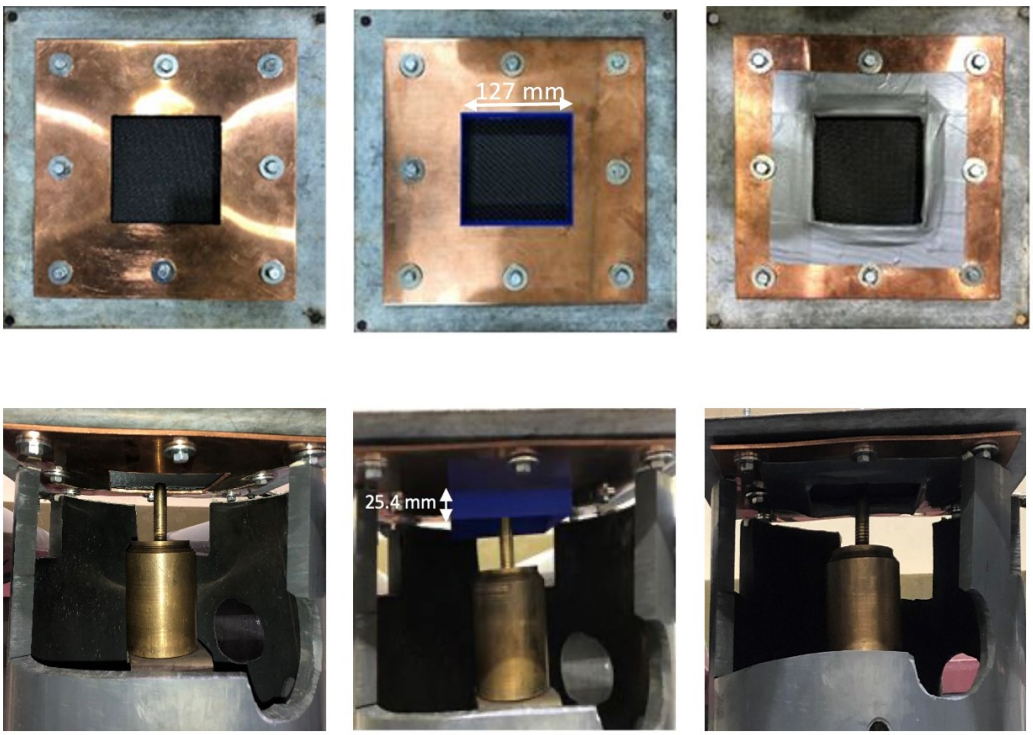

Figure 5.6 Ground configuration and testbed for lightning strike test: (a) Without ground edge insulation (b) With square frame insulation, (c) With insulation tape

www.manaraa.com

5.5 Summary

In other to study the effect of the testbed components such as ground electrode design and size of discharge electrode, nine CFRP composites were manufactured. The vacuum assisted resin infusion process was used to fabricate the samples. Three electrodes with different sizes are made to investigate the lightning strike damages at the same current level but different sizes of electrode.

To ensure that the height of the dielectric barrier does not influence the lightning experiment results two types of insulation are applied by covering the ground electrode edges with dielectric materials.

In addition, to achieve the goal of reducing lightning strike damage, carbon nanofillers are added to the composite structure during the fabrication process. The nanofillers are dispersed in epoxy using sonicator that mix the carbon nanofillers to the resin. Hand lay-up method is applied to make the composite samples with the conductive resin.

www.manaraa.com

CHAPTER VI

EFFECT OF ELECTRODE SIZE

6.1 Motivation

The effect of lightning channel diameter on lightning strike damage modes on the CFRP composites has not been reported. There is no specific value for the size of electrode for the lightning strike test in the SAE standard and this study provides insights into important characteristics and correlations between lightning strike damage of CFRP composites and lightning channel diameter. This study analyzes the effect of lightning channel diameter by applying different sizes of discharge electrodes to select a proper electrode for lightning strike tests [20], [96]. The results of the study will aid in the development of standards for lightning strike tests.

6.2 Effect of Electrode Size on Surface Material Loss

For all electrode sizes, the energy of lightning discharge is kept identical. Three different sizes of electrodes (see Figure 5.5) were used at the current amplitude of 47.2 kA without using electrical insulation for the ground electrode. The impulse current waveform applied to the samples is shown in Figure 6.1.

www.manaraa.com

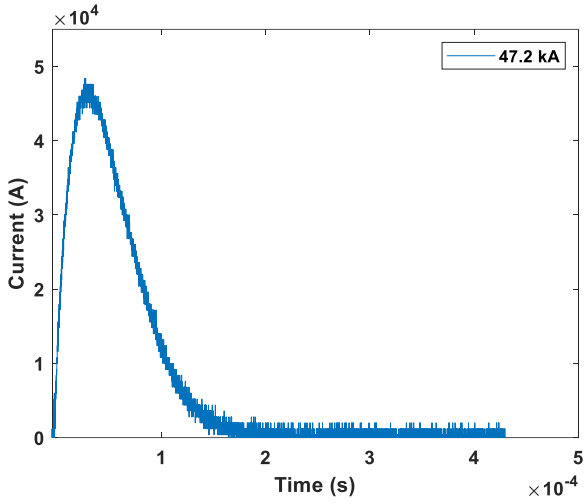

Figure 6.1 Impulse current waveform for electrode size study

The damages of CFRP matrix composite laminates caused by the lightning strikes are shown in Figure 6.2. The results show that considerable surface material loss occurs at the first two layers of the CFRP matrix composite laminates. Here, the surface material loss area refers to the area where the material experiences complete fiber and matrix vaporization with also fiber breakage and fiber pullout. The surface material loss area forms an approximate circular shape since the electrical and thermal conductivities in the longitudinal and transverse directions are identical for the woven carbon fiber composite. The corresponding damage diameter of surface material loss is measured. A clear trend of the increasing CFRP damage is observed as a function of electrode size. While there is no noticeable carbon fiber surface material loss caused by the big electrode with the diameter of 98 mm, the surface material loss diameter increases to 7.29 mm and 12.27 mm as the electrode size reduces to 46 mm and 16 mm, respectively. It is therefore evident that, for component D of lightning current waveform, the size of the electrode has a considerable influence on the lightning strike damage of CFRP matrix composite laminates.

www.manaraa.com

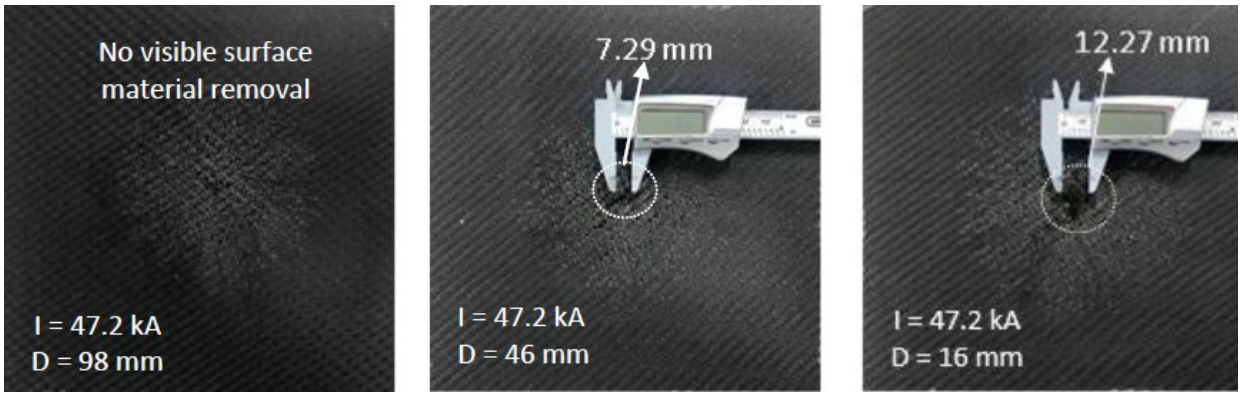

Figure 6.2 Lightning damage to CFRP matrix composite laminates: at 47.2 kA peak current and without insulation for ground electrode: (a) big electrode (b) medium electrode (c) small electrode

Figure 6.3 summarizes the surface material loss area as a function of electrode diameter. While there is no noticeable carbon fiber surface material loss area caused by the big electrode with the diameter of 98 mm, the surface material loss area increases to 0.42 cm^2 and 1.2 cm^2 as the electrode size reduces to 46 mm and 16 mm, respectively.

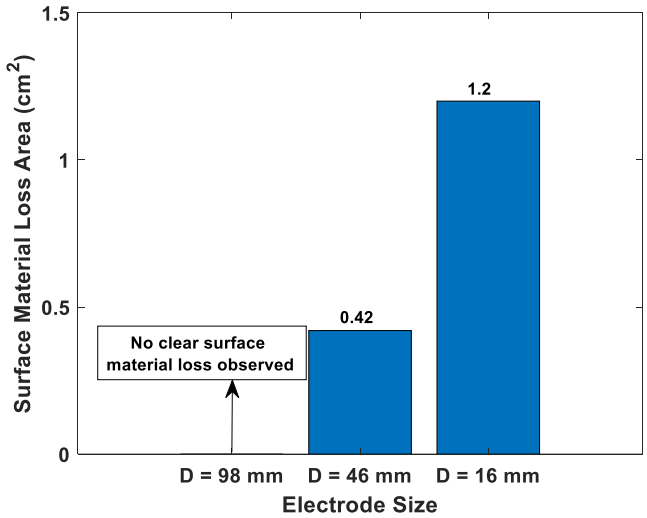

Figure 6.3 Electrode size vs. area of surface material loss. Note that there are no error bars in the data as one sample per experimental condition was used

www.manaraa.com

6.3 Effect of Electrode Size on Delamination

Reducing the size of electrode not only increases the degree of the surface material loss area, but also increases internal delamination of the CFRP composite material. To determine the delamination, ultrasonic inspection was performed using the OmniScan SX Flaw Detctor, which is a 16:64PR phased array unit. The obtained C-Scanned images are presented in Figure 6.4. C-scanning is the image that represents the data obtains from the ultrasonic inspection for showing the damage and it presents a plan view of the component. As one can see, the delamination area (i.e., light blue circular area) of the CFRP composites increases in diameter and severity with the decreasing electrode size. A trend of the increasing CFRP composites damage in the thickness direction is observed as a function of decreasing electrode size in the B-Scanned images. B-scanning images show the data from ultrasonic inspection in two-dimensional view. While the through thickness damage is mildest in the case of the big electrode with the diameter of 98 mm, the damage increases as the electrode size reduces to 46 mm and 16 mm, respectively. The results imply that more electric current may have penetrated into the inner layers and leads to more delamination of the CFRP matrix composites, as the size of the electrode reduces. It should be noted that the discharge energy of the lightning strikes was kept identical at 20.32 kJ for all electrode sizes.

www.manaraa.com

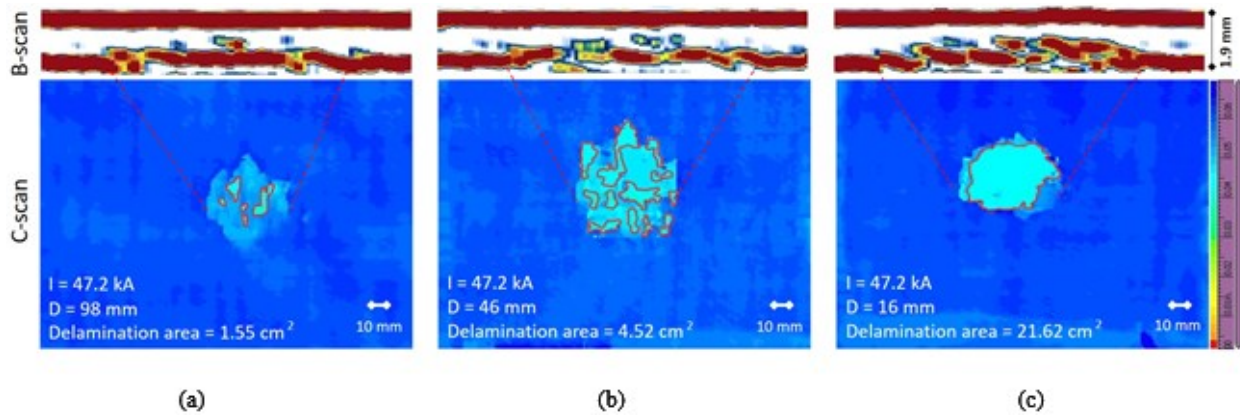

Figure 6.4 C-Scan and B-scan images showing the delamination of the CFRP composites after simulated lightning strike tests at 47.2 kA peak current without ground electrode edge insulation: (a) D = 98 mm (b) D = 46 mm (c) D = 16 mm. Note: the red contours indicate the areas of severe delamination (i.e., delamination of multiple layers)

The trend in influence of electrode size on the delaminated area of CFRP composites are clearly shown in Figure 6.5. The delaminated areas defined by the red contours of Figure 6.4, which represents the delamination of multiple layers, are calculated. For all three cases, 20 kJ energy and at 47.2 kA lightning impulse current were applied. The size of the delaminated area increased by 192 % and 1,294 % when the 46 mm and the 16 mm diameter electrode were used, respectively, compared to the case of the 98 mm diameter electrode.

www.manaraa.com

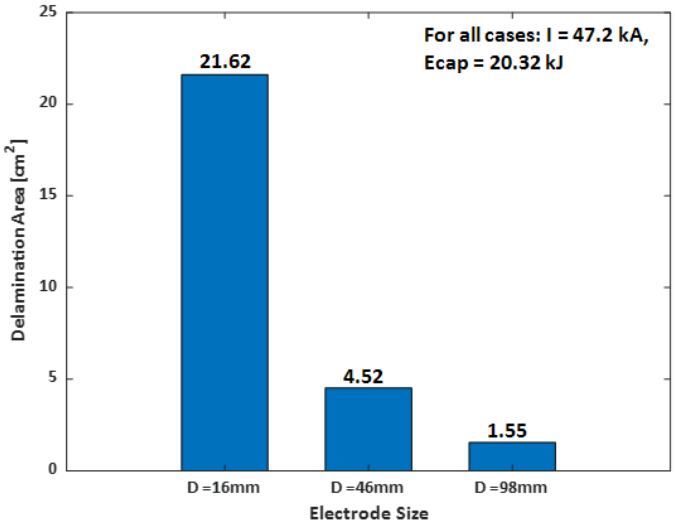

Figure 6.5 Electrode size vs. delamination area defined by the red contours of Figure 6.3. Note that there are no error bars in the data as one sample per experimental condition was used

6.4 Simulation Results

Numerous researchers are focusing on the modeling of lightning phenomena and its interaction with test samples. Finite Element Analysis (FEA) is a common method that is used by researchers to study the electric arc characteristics in welding and lightning strike applications. Various sizes of electrodes were used in the model to simulate the lightning arc plasma and to find the temperature distribution. The electrode is modeled with various sizes while a constant discharge current is applied to demonstrate the impact of lightning discharge diameter on the temperature distribution of plasma and the sample. Since the composite structures cannot be assumed to be axisymmetric, metal sample is used in this study and the granted understanding can provide insights to the lightning strike damage investigation of composite materials.

www.manaraa.com

6.4.1 Mathematical Equations of the Model

The physics that applied to the model include Magnetic Fields, Electric Current, Laminar Flow, Heat Transfer, and Multiphysics. To solve the electric current conservation, heat transfer, magnetic field equations in electrode and plasma regions, magnetic fields, heat transfer, electric current modules are applied. The laminar flow is used to solve the Navier-Stokes equations in the plasma region, which is a time dependent continuity equation. In addition, Multiphysics module is applied to perform the data exchange between the physic modules. Table 6.1 Summarizes the physics has been applied in each domain.

Table 6.1 Physics applied to each domain

Physics	**Domains**				
	Plasma	**Cathode**	**Anode**	**NLTE-Cathode**	**NLTE - Anode**
Electric Current	✓	✓	✓	✓	✓
Magnetic Fields	✓	✓	✓	✓	✓
Heat Transfer	✓	✓	✓	✓	✓
Laminar Flow	✓	×	×	✓	✓
Plasma	✓	×	×	✓	✓

6.4.1.1 Conservation of Electric Current

The current density and electric potential can be obtained using the conservation equation.

$$\nabla \cdot J = Q_{J,V} \tag{6.1}$$

where J is current density and $Q_{J,V}$ is the rate of change in electric current charge density respect to time. Since the current is constant, the $Q_{J,V}$ is equal to zero. The below formula can be used for obtaining the electric field.

www.manaraa.com

$$J = \sigma E + \frac{\partial D}{\partial t} + J_{e1} \tag{6.2}$$

where D is electric flux density and J_{e1} is magnetic field's induced current which can be used when the simulating current is time varying. Since the simulated component C current is constant, J_{e1} is negligible. So, the electric flux density is written as

$$D = \varepsilon_0 \varepsilon_r E \tag{6.3}$$

Also, the electric potential can be calculated by

$$E = -\nabla V \tag{6.4}$$

6.4.1.2 Magnetic Field Equations

The magnetic field equation is solved by Maxwell's equations.

$$\nabla \times \mathrm{H} = \mathrm{J} \tag{6.5}$$

$$B = \nabla \times A \tag{6.6}$$

$$J = \sigma E + \sigma v \times B + J_{e2} \tag{6.7}$$

$$E = -\frac{\partial A}{\partial t} \tag{6.8}$$

Where A, v, B, and H are magnetic potential, conductor velocity, magnetic flux density, and magnetic field intensity, respectively. Also, J_{e2} is the externally generated electric current and equals to: $J_{e2} = -\sigma \nabla V$.

6.4.1.3 Heat Transfer Equations

The heat equation is coupled with the current equations as below.

$$\rho C_p \frac{\partial T}{\partial t} + \rho C_p u \cdot \nabla T = \nabla \cdot (k \nabla T) + Q \tag{6.9}$$

www.manaraa.com

Where u, Cp, and ρ are velocity vector, specific heat capacity, and gas density, respectively. The formula for volumetric heat source (Q) that consists of, radiation loss, Joule heating, and enthalpic transport is:

$$Q = \frac{\partial}{\partial T}\left[\frac{5k_B T}{2e}\right](\nabla T \cdot J) + E \cdot J - 4\pi\varepsilon_N \quad (6.10)$$

where ε_N is the net emission coefficient of air at different temperatures that obtained from [97]. The net emission coefficient of the air is the approximation to radiative energy transport from the collision of free electrons with ions.

6.4.1.4 Fluid Flow Equations

The fluid flow is modeled as a laminar flow and consists of equations including continuity equation, conservation of momentum, and Lorentz force, as expressed as the following equations.

$$\frac{\partial \rho}{\partial t} + \nabla \cdot (\rho u) = 0 \quad (6.11)$$

$$\rho \frac{\partial \rho}{\partial t} + \rho(u \cdot \nabla)\, u = \nabla \cdot [-PI + \tau] + F \quad (6.12)$$

$$F = J \times B \quad (6.13)$$

where F is the volumetric force that refers specifically to the magnetic force.

6.4.2 Model Validation

To confirm the experimental results and show the effects of the size of discharge electrode on lightning strike damage, COMSOL Multiphysics is used to model arc plasmas. In this regard, I used the method used by Liu et al. [49] to perform the lightning plasma arc modeling. Liu simulated component C of the lightning strike and obtained the temperature distribution of anode, plasma, and cathode regions as was shown in Figure 2.13.

www.manaraa.com

6.4.2.1 Model Geometry

The electric arc model consists of three main domains including cathode, plasma, and anode. Cathode that represents the discharge electrode, is made of pure Tungsten. The plasma region consists of air with varying electrical conductivity as a function of temperature. The anode layer is the material that lightning current disseminates through and is assumed to be aluminum in this model. These three regions are modeled under the Local Thermodynamic Equilibrium (LTE) condition in simulations which means that the plasma temperature is equal to the heavier particles including positive and negative ions. This assumption facilitates calculating the properties of material such as electrical conductivity, heat capacity, and thermal conductivity. In a real plasma, the temperature drops at the areas close to the anode and cathode that is due to the voltage drop near those areas that is due to lower electrical resistance. So, the regions around these surfaces cannot be applied with the LTE assumption. Therefore, two thin layers around the cathode and anode are regarded non-LTE assumption. The regions with the non-LTE assumption have properties equivalent to air except for the electrical conductivity which is equal to the electrical conductivity of the region it is close to. Two-dimensional axisymmetric model is used in this study to validate the reference model and obtain the temperature distribution in regions as shown in Figure 6.6. All regions are presented in the model to simulate the plasma that represents the lightning. The z-coordinate arc axis refers to center of the arc axis between cathode ($r = 0, z = 10$ mm) and anode ($r = 0, z = 5$ mm).

www.manaraa.com

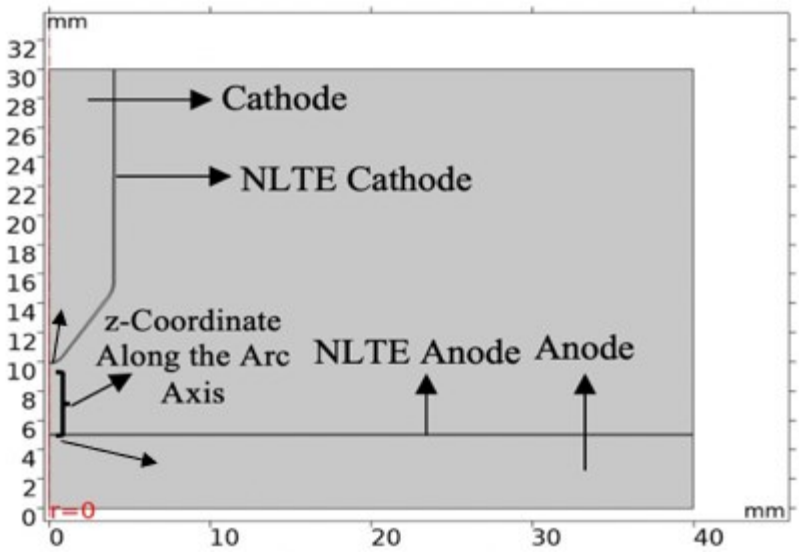

Figure 6.6 Model geometry and dimensions

6.4.2.2 Meshing and Boundary Conditions

It is better to divide the domains to small elements to solve the problems. For domains with smaller element size, the accuracy is guaranteed but the model needs more time and computational resources to solve the plasma problem. The size of the meshes at different regions is summarized in table 6.2.

Table 6.2 Size of meshes in different regions

Region	Size of Mesh (mm)	
	Maximum	Minimum
Anode	0.4	0.008
Cathode	2.88	0.012
Plasma	0.8	0.003
NLTE layers	0.35	0.35

www.manaraa.com

Different sizes of meshes are used in each domain to enable proper convergence of the simulation model as shown in figure 6.7. The element size is chosen in a way to prevent aggregation of the mesh elements in the regions, specially at the corners of the model.

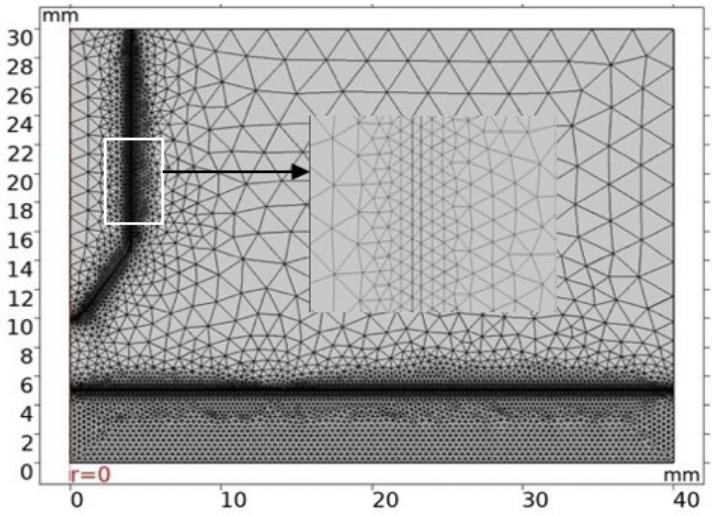

Figure 6.7 Typical mesh applied to the model

6.4.2.3 Assumptions and Boundary Conditions

The plasma simulation is very complicated because various chemical and atmospheric and physical components are involved. So, some assumptions and boundary conditions are considered for simplifying the model. The assumptions made in the model are as follows:

- Plasma is considered to be a fluid and the LTE condition is met.
- The arc is symmetric along the z-axis, so 2D symmetry is acceptable.
- The surface of the anode is flat and is not deformed during the simulation.
- The effect of gravity is not considered due to its low impact on the plasma.
- The lightning strikes of the experimental tests were up to 100 kA. However, the lightning current amplitude considered in the model is up to 404A. The plasma model is a nonlinear

www.manaraa.com

problem because of the temperature dependency of the material properties. So, simulating the plasma at the high current amplitudes requires massive computing power. In a research study [60], it took 70 days to simulate the lightning strike on a cluster (High Performance Computing). So, researchers use low current amplitude for lightning simulations.

- The anode is considered an axisymmetric material such as Aluminum and Copper. The CFRP composites are not axisymmetric, so the 2D axisymmetric space in COMSOL cannot be used for modeling CFRP composites. The 2D axisymmetric is only valid for homogeneous and axisymmetric materials such as metals. CFRP laminate is inhomogeneous and anisotropic, and it should not be assumed as a simple 2D axisymmetric problem. The CFRP composites should be modeled in 3D space. However, this would be extremely challenging due to the significant increase of complexity to get the model converged and the significant increase of the computational cost. Since the focus of the simulation in this study is not the material, axisymmetric materials such as Aluminum and Copper are used as anode in the models.

A summary of boundary condition considered for the model is illustrated in Table 6.3. Where, u is velocity, V is electrical potential, T is temperature, A is magnetic potential, and J is current density. The AB, BC, CD, DE, EF, DG, BH, and AF boundaries are taken from the model geometry in Figure 6.6.

www.manaraa.com

Table 6.3 Boundary conditions of the model [98]

	AB	BC	CD	DE	EF	DG	BH	AF
T	300K	300K	300K	300K	300K			$\frac{\delta A}{\delta r} = 0$
u	-	Open BC	Open BC	0	0	0	0	$\frac{\delta A}{\delta r} = 0$
J	J.n = - Jin	n.J=0	n.J=0	-	-	-	-	$\frac{\delta A}{\delta r} = 0$
V	-	-	-	0	0	-	-	$\frac{\delta A}{\delta r} = 0$
A	n.A=0	n.A=0	n.A=0	n.A=0	n.A=0	-	-	$\frac{\delta A}{\delta r} = 0$

6.4.2.4 Material Properties in the Model

In this research study, plasma is simulated in air. The air's property, which is considered ideal, is extracted from the COMSOL library. The relative permeability and relative permittivity are 1 and the ratio of the specific heats is 1.4. The reference pressure value is considered 1 [atm]. Other properties including electrical conductivity, density, heat capacity, dynamic viscosity, thermal conductivity, and ratio of the specific heats of the air are temperature dependent as shown in Figure 6.8. The air properties are derived from reference [99] and COMSOL library.

www.manaraa.com

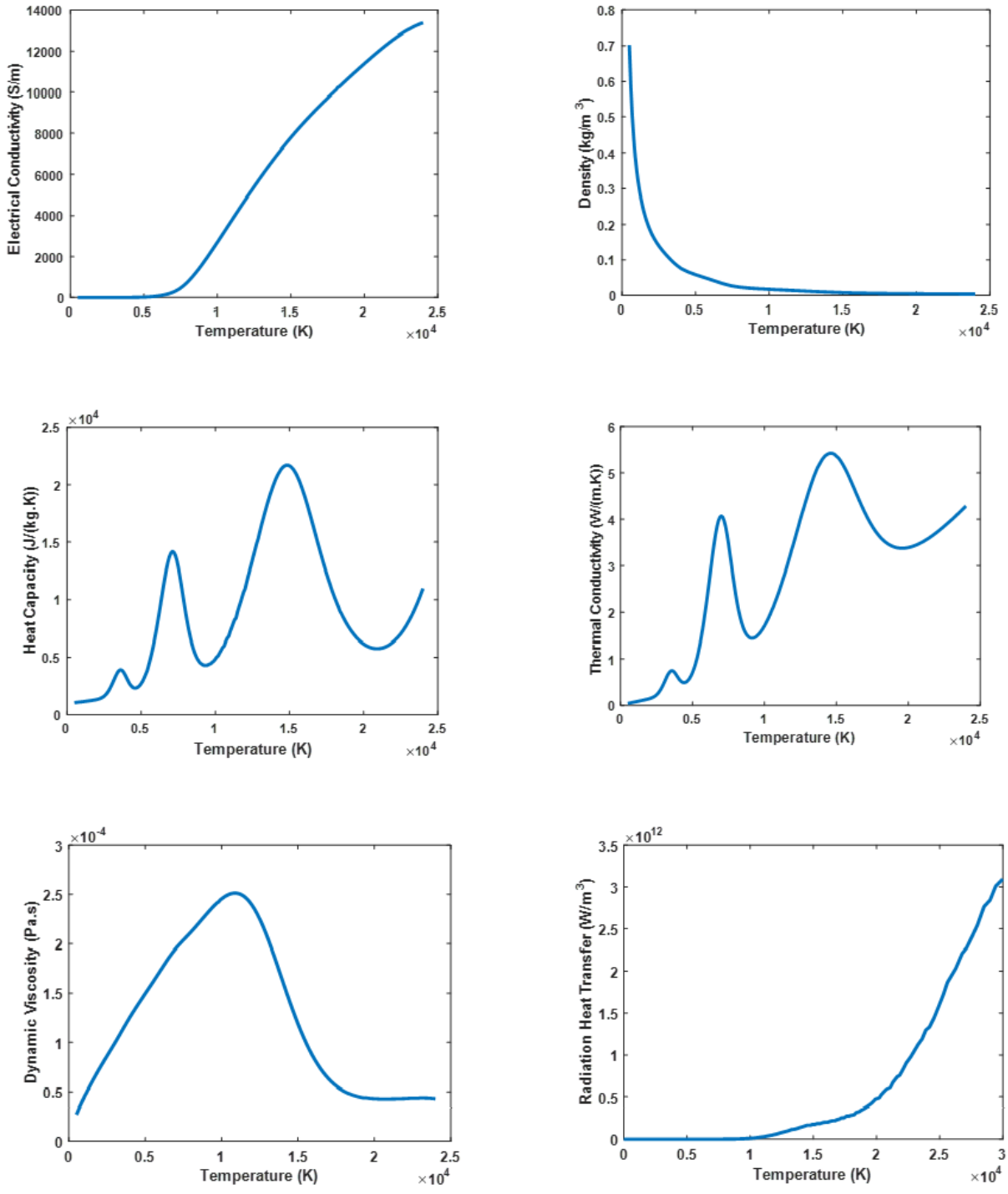

Figure 6.8 Temperature dependent properties of air

www.manaraa.com

The temperature dependent properties of the air in our model is shown in the Figure 6.8 and the ambient condition is not considered in this study. Chunlin et al. [100] has investigated the effect of the humidity and atmospheric pressure on the temperature dependent properties to simulate an accurate model for air plasma. Figure 6.9 presents the effect of the humidity on the properties of the air. For this purpose, the properties are achieved at different temperature base on different amount of H_2O. According to the results, there is just a little difference between the properties at different range of humidity. The electron temperature is considered equal to the plasma temperature in the plasma models.

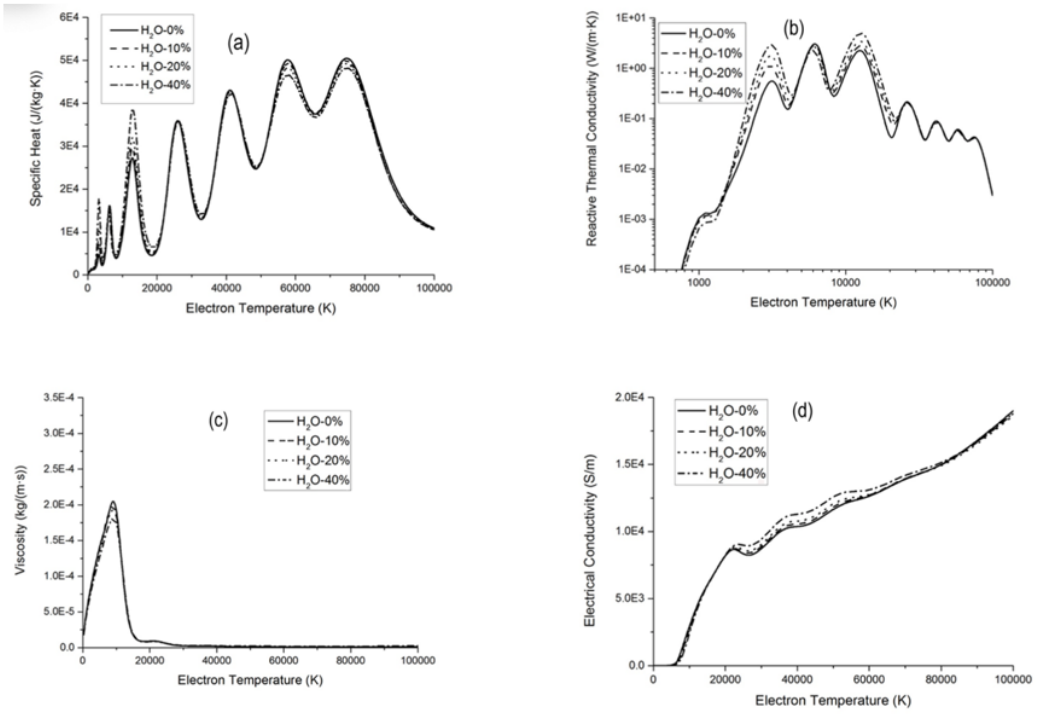

Figure 6.9 Temperature dependent properties of air [100]

www.manaraa.com

Figure 6.10 presents the effect of the atmosphere pressure on the properties of the air. For this purpose, the properties are achieved at different temperature base on different amplitude of the pressure. According to the results, the ionization reaction is shifted to a higher temperature due to Chatelier's principle.

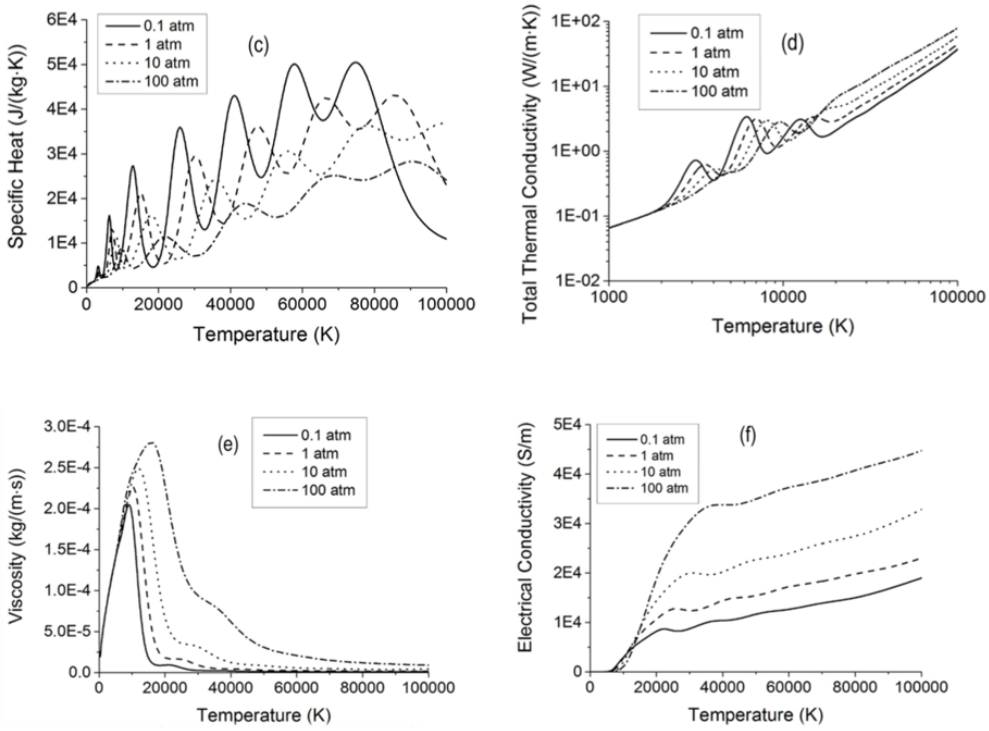

Figure 6.10 Temperature dependent properties of air [100]

This information can be applied to the models for simulating the plasma air more accurately. In this study, the properties of the air are derived from reference [99] and COMSOL library to make an acceptable comparison with the arc plasma modeled by Liu et al. [49]

www.manaraa.com

6.4.2.5 Validation Result

The time-dependent solver of the COMSOL with time increment of 1×10^{-13} seconds with an automatic time-stepping is used for this study. The model was solved using a 2.3 GHz dual core and 8 GB ram laptop in an approximate time of 3 hours and 30 minutes for each case. The results from the method used by Liu et al. are shown in Figure 6.11 (a). The air plasma temperature due to 404 A current amplitude reaches 2.98×10^{4} K at the highest point in the plasma domain. The anode and cathode temperature are also calculated and are 3.43×10^{3} K and 5×10^{3} K, respectively. Figure 6.11(b) shows the temperature distribution in different regions of the model by applying 404 A constant current. As shown in the results, the temperatures of plasma, cathode, and anode regions are close to the reference model. So, the model is validated and qualified to be used for further research in this research.

www.manaraa.com

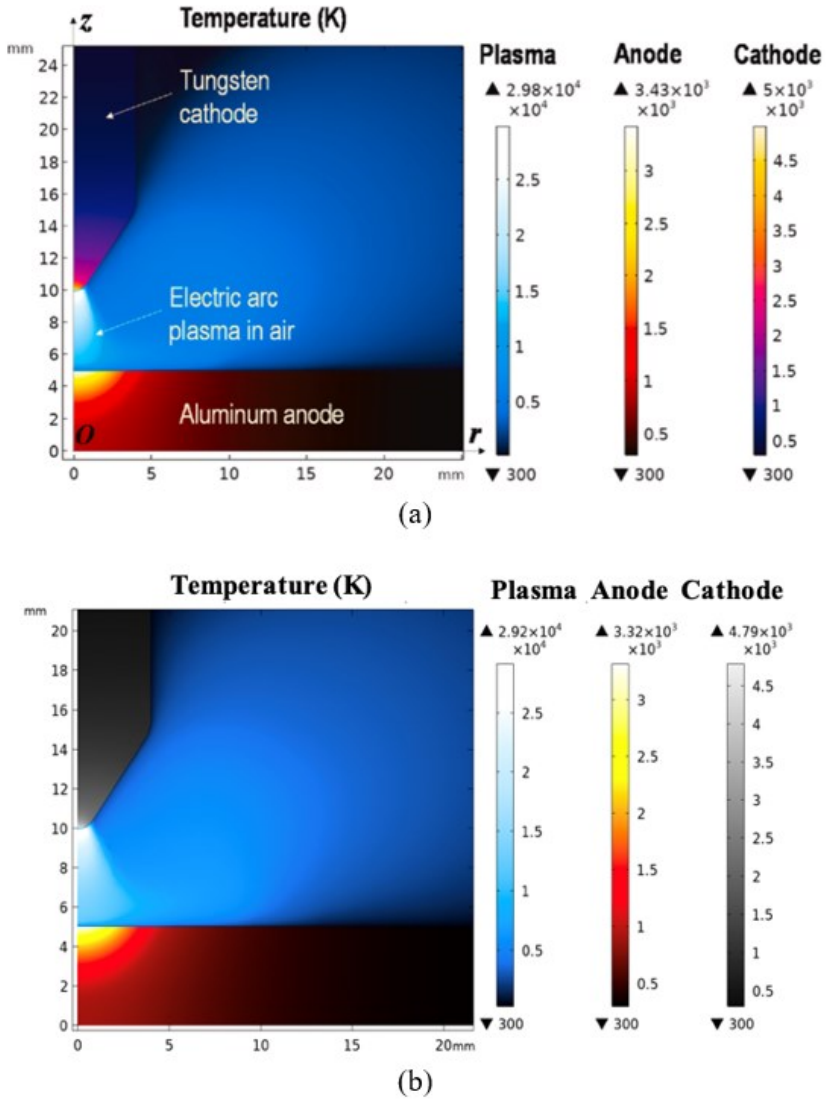

Figure 6.11 Temperature distribution within anode, plasma, and cathode regions at t = 0.52s from: (a) the reference model [49], (b) the model in this study

6.4.3 Simulating Effect of Cathode's Size

Three different sizes of cathode including 2mm, 4mm, and 6mm were used at a constant current amplitude of 404 A. Figure 6.12 shows the temperature distribution in different regions of model by applying 404 A at electrode with radius of 6mm. The air plasma temperature reaches

www.manaraa.com

2.82×10^4 K at the highest point in the plasma domain. The anode and cathode temperature are also calculated and are 3.02×10^3 K and 3.84×10^3 K, respectively.

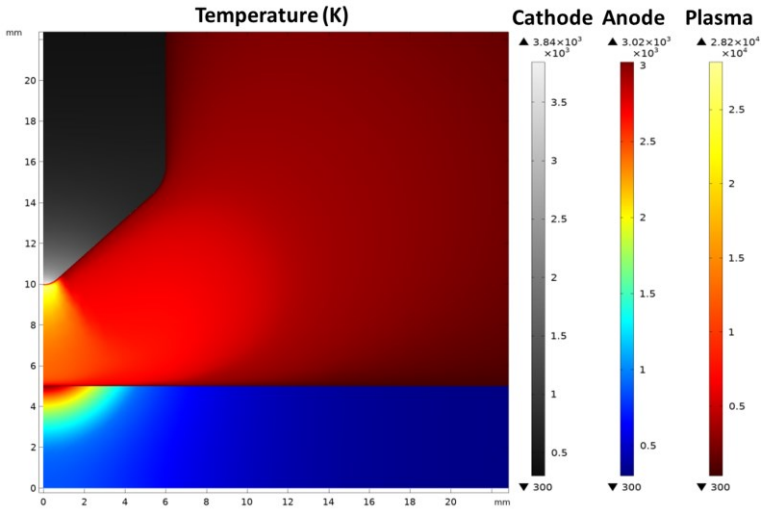

Figure 6.12 Temperature distribution within anode, plasma, and cathode regions with 6mm electrode at t = 0.52s

Figure 6.13 shows the temperature distribution in different regions of model by applying 404 A at electrode with radius of 4mm. The air plasma temperature reaches 2.92×10^4 K at the highest point in the plasma domain. The anode and cathode temperature are also calculated and are 3.32×10^3 K and 4.79×10^3 K, respectively.

www.manaraa.com

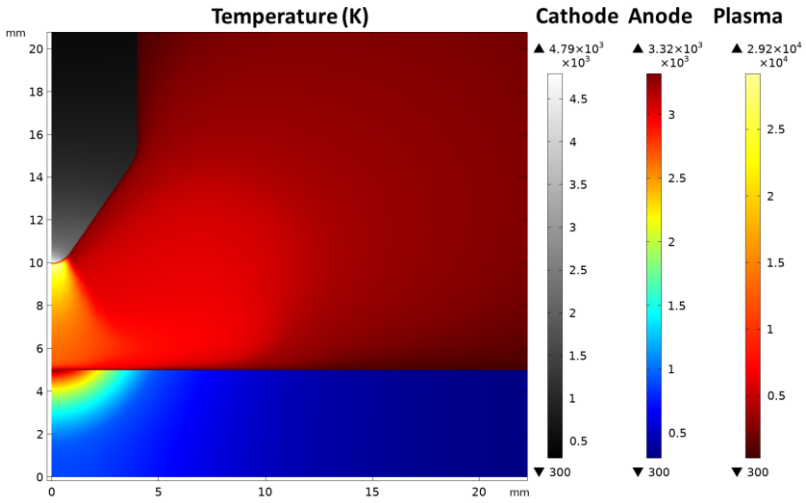

Figure 6.13 Temperature distribution within anode, plasma, and cathode regions with 4mm electrode at t = 0.52s

Figure 6.14 shows the temperature distribution in different regions of model by applying 404 A at electrode with radius of 4mm. The air plasma temperature reaches 3.47×10^4 K at the highest point in the plasma domain. The anode and cathode temperature are also calculated and are 3.51×10^3 K and 5.6×10^3 K, respectively.

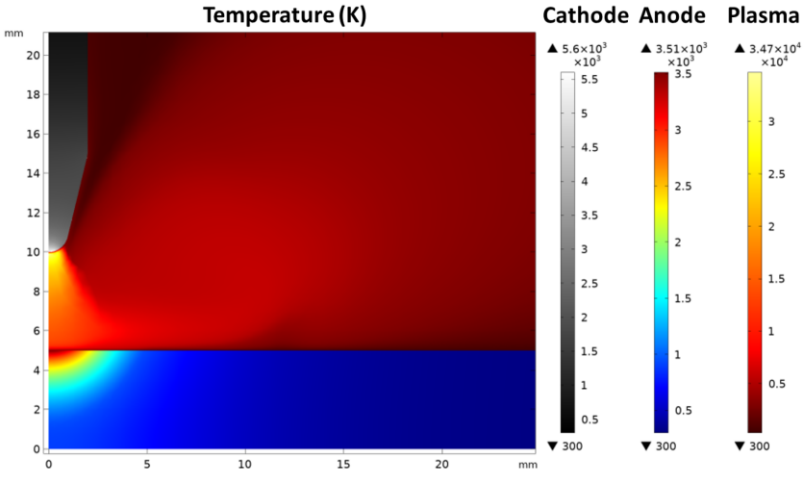

Figure 6.14 Temperature distribution within anode, plasma, and cathode regions with 2mm electrode at t = 0.52s

www.manaraa.com

Figure 6.15 summarizes the maximum temperature distribution in three regions due to different size of cathodes with radius of 2mm, 4mm, and 6mm. The results show that the decrease of the cathode size results in the increase of temperature at all regions.

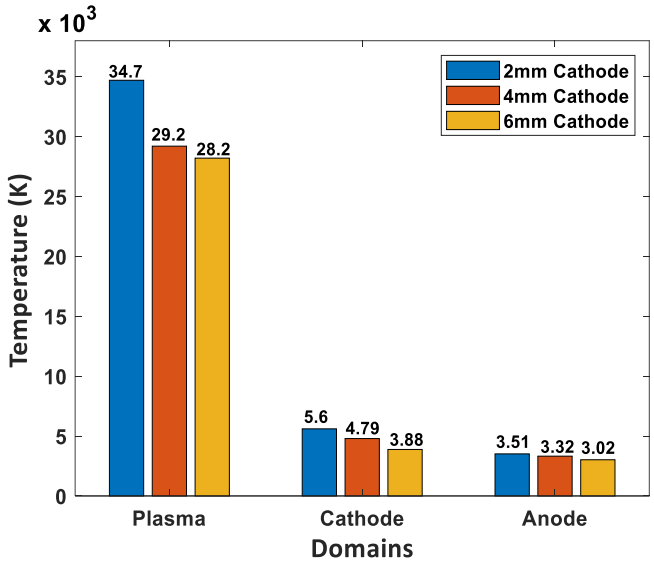

Figure 6.15 Maximum temperature within anode, plasma, and cathode regions with different sizes of cathode

Figure 6.16 shows the temperature along the arc axis. The injected heat from the plasma causes significant damage to the materials. The results show that the decrease of the cathode size results in the increase of temperature along the arc axis. The plasma reaches its peak around 9.7 mm along the arc axis that increases the electrical conductivity. This leads to faster movement of plasma near the cathode that reduces the electron density.

www.manaraa.com

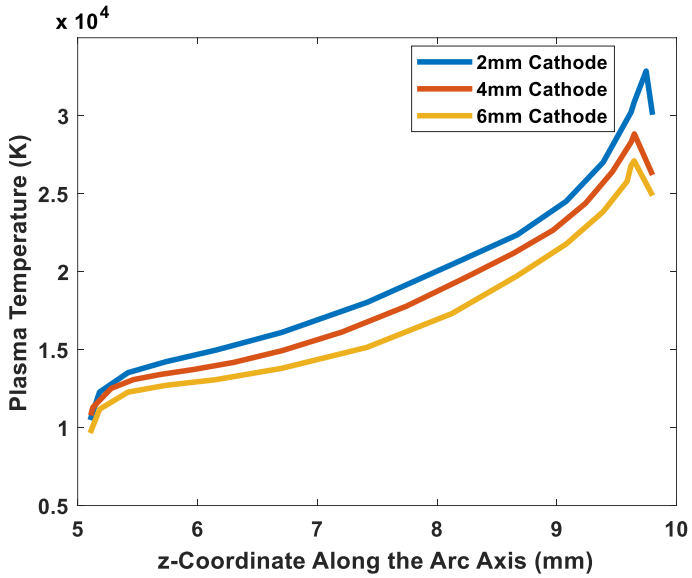

Figure 6.16 Temperature within the arc axis with different sizes of cathode (between cathode ($r = 0$, $z = 10$ mm) and anode ($r = 0$, $z = 5$ mm)

In the plasma temperature modeling, the plasma heating consists of several mechanism including Joule heating, radiative emission, and electronic enthalpic flux. In this section, each mechanism is investigated for the three electrodes.

6.4.3.1 Joule Heating

Joule heating is generated by current passing through a conductor. Joule heating along the plasma arc center is obtained by J^2/σ, where J is the current density and σ is the electrical conductivity of the plasma. Figure 6.16 shows how the electrical conductivity is modeled and how it changes with temperature. For the temperatures more than the highest temperature in Figure 6.16, a linear regression is used to find the desired electrical conductivity. Electrical conductivity of the air at different temperatures is shown Figure 6.17.

www.manaraa.com

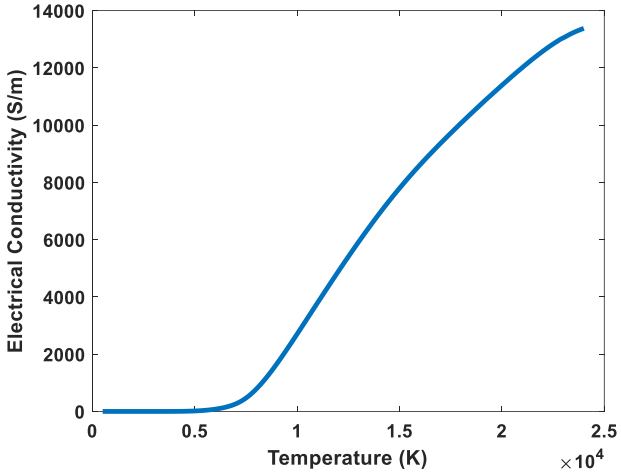

Figure 6.17 Conductivity of the air at different temperatures

Figure 6.18 shows the joule heating along the arc center. An increasing trend in the peak of joule heating can be seen with decreasing cathode size. As it is shown in Figure 6.18, the Joule heating increased by 60 % to 7.2×10^{12} after reducing the electrode's diameter from 6mm to 2mm.

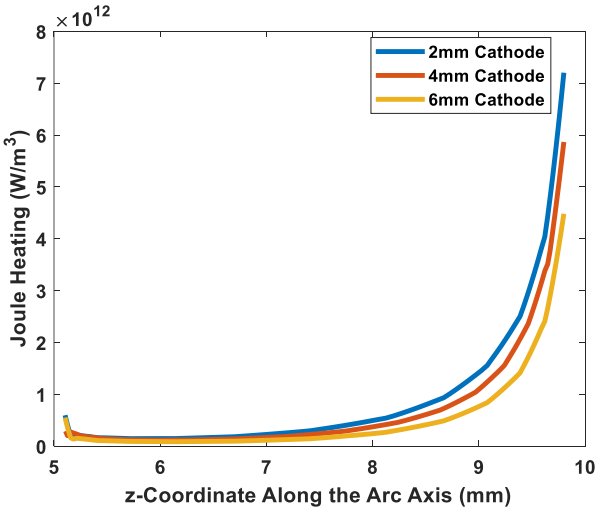

Figure 6.18 Joule Heating along the arc axis at different size of cathode (between cathode ($r = 0$, $z = 10$ mm) and anode)

www.manaraa.com

6.4.3.2 Enthalpic Heating

The enthalpy of electrons is the amount of energy released or absorbed by atoms when gaining the electrons. The enthalpic heating energy is captured by: $H = \frac{\partial}{\partial T}\left[\frac{5k_BT}{2e}\right](\nabla T \cdot J)$ W/m^3 in which k_B is the Boltzmann's constant that equals to 8.6173303×10^{-5} eV/K, ∇T is gradient of temperature with unit of K/m. Figure 6.19 shows the electronic enthalpic heating along the arc axis. As the cathode's size decreases, current density and plasma temperature increases. Figure 6.19 shows the electronic enthalpic heating along the arc axis. The enthalpic heating is a function of the temperature gradient and current polarity which is negative in this model. The negative and positive value of the enthalpy refers to the releasing and absorbing heat, respectively. There is a noticeable change from positive to negative in electronic enthalpic heating energy (W/m^3) at the highest temperature point (z=9.7 mm). The temperature gradient represents significant change at the highest temperature point is the reason for alteration in positive-negative. As shown in Figure 6.19, the enthalpic heating decreases along the arc axis from the cathode surface down to the z = 7.2 mm and then rebounds at z= 5.8 mm down to the anode surface. This can be concluded from assumption of NLTE layer near the cathode and anode that causes disturbance surface and the LTE condition in the plasma in which the enthalpic heating has a constant trend.

www.manaraa.com

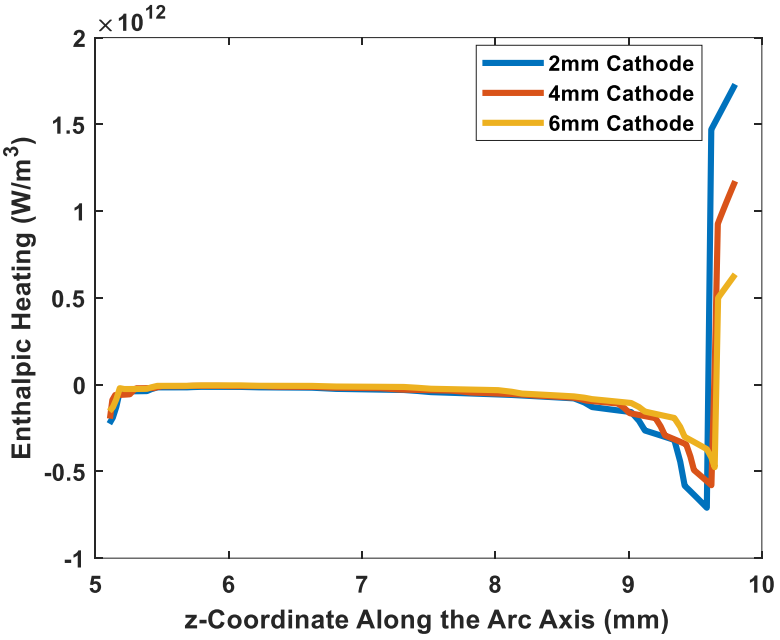

Figure 6.19 Electronic enthalpic along the arc axis (between cathode (r = 0, z = 10 mm) and anode (r = 0, z = 5 mm)

6.4.3.3 Emission Heating

The radiative emission from the collision of free electrons with ions depends on the net radiative coefficient and the content of the electrons. The emission heating is determined from the plasma heat source in the model from the volumetric heat source is formula 6.10 that consists of the radiation loss, Joule heating, and enthalpic transport. The emission heating is $4\pi\varepsilon_N$ in which ε_N is the net emission coefficient of the gas and derived from the COMSOL library. Figure 6.20 represents the emission heat loss along the arc axis (between cathode (r = 0, z = 10 mm) and anode (r = 0, z = 5 mm). It can be seen that the value of emission heating is higher close to the cathode and reduces along the arc axis down to the cathode. The emission heating peak is at the highest plasma temperature point where electrons are accelerated due to the strong field from the cathode.

www.manaraa.com

When the cathode's size reduces from 6mm to 2 mm, the emission heating increases for about 60% that is in accordance with the trend in plasma temperature in Figure 6.16.

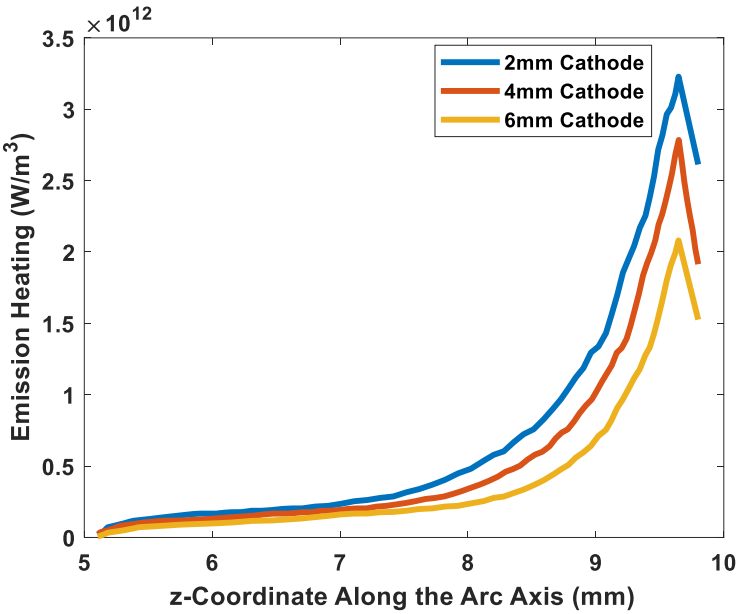

Figure 6.20 Emission heat loss along the arc axis (between cathode ($r = 0$, $z = 10$ mm) and anode ($r = 0$, $z = 5$ mm)

6.4.3.4 Heat Flux

The heat flux distribution has a significant effect on the damage of material surface and the injected heat from the plasma causes significant damage to materials. That is, the heat flux distribution has a significant effect on the damage of material surface. The heat flux is determined by $q = -k\nabla T$, where q is the heat flux density ($W.m^{-2}$), k is the materials conductivity ($W.m^{-1}.K^{-1}$), and ∇T is the temperature gradient ($K.m^{-1}$). Figure 6.21 shows the heat flux along the anode surface. An increasing trend in the peak of heat flux can be seen with decreasing cathode size. A significant change of heat flux along the radial distance from the arc center is observed which can be described by similar behavior of energies waveforms including joule heating and emission

www.manaraa.com

heating that increase with reducing the electrode size. Also, it is observed that the heat flux shows a steeper increase for lower size of cathodes. The sharper reduction of heat flux in cases with lower sizes of cathode is due to higher emission loss at higher current densities because of reducing the cathode's size.

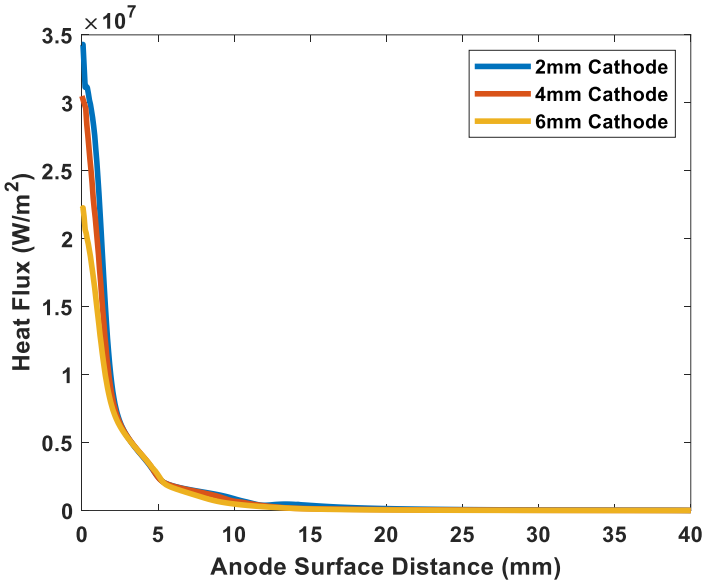

Figure 6.21 Heat Flux along the anode surface

6.5 Summary

The damage of CFRP matrix composite laminates clearly varies as a function of electrode size (i.e., lightning discharge diameter). According to the results, the affected area decreases with increasing electrode diameter. Such trend is likely contributed by the increasing discharge current density with decreasing cross section area of the discharge. Larger current density flowing through a smaller cross-sectional area of the sample would cause significantly larger Joule heating and greater damage because the smaller cross sectional area of discharge current contributes to the increase of the local electrical resistance of the samples (resistance = resistivity × length / cross

www.manaraa.com

section area). That is, at least the resistance of the top layer, where lighting current enters the CFRP composites, will show high resistance with decreasing discharge electrode diameter. However, the conductivity of CFRP composites is a function of temperature that generally increases with elevating temperature, which contributes to the decrease of the electrical resistance of the sample. Hence, the overall variation of the local resistance of the sample depends on the balance between the decrease in cross section area and the increase in electrical conductivity of the sample. The increase of delaminated areas suggests that deeper layers of the CFRP composites are impacted with the decrease of lightning discharge diameter which has a significant effect on plasma temperature.

www.manaraa.com

CHAPTER VII

GROUND ELECTRODE CONFIGURATION

7.1 Motivation

As discussed in chapter 2, researchers use different testbeds to perform lightning strike experiments on CFRP composites. In part, this is due to the lack of specific configuration guidelines for the lightning strike testbed. Inconsistencies in the experimental conditions not only make it difficult to compare results among research groups, but also introduces the risk of data misinterpretation. Here, insights into important characteristics of the testbed that affects the lightning strike damage of the CFRP composites are provided. Ideally, in lightning strike tests, the entire lightning discharge should interact with composite laminate samples. However, depending on the ground electrode configuration, it is possible that the portions of the discharge current hit the ground electrode directly instead of propagating through the test samples. This results in the reduced damage of the CFRP samples, which can be misinterpreted as the sample resisting or tolerating the impact of lightning strike effectively. To prevent such misinterpretations, the entire lightning discharge current must be ensured to propagate through or at least interact with the samples. This study analyzes the effect of ground electrode configuration by applying two different types of insulation for ground electrode to select a proper configuration for lightning strike tests [20]. The results of the study will aid in the development of standards for lightning strike tests.

www.manaraa.com

7.2 Effect of Ground Electrode Configuration on Surface Material Loss

For different types of ground insulation for ground electrode, the energy of lightning discharge is kept identical. Two different types of insulation for ground electrodes (see Figure 5.6) were used at the current amplitude of 100 kA with using identical size of discharge electrode. The impulse current waveform applied to the samples is shown in Figure 7.1.

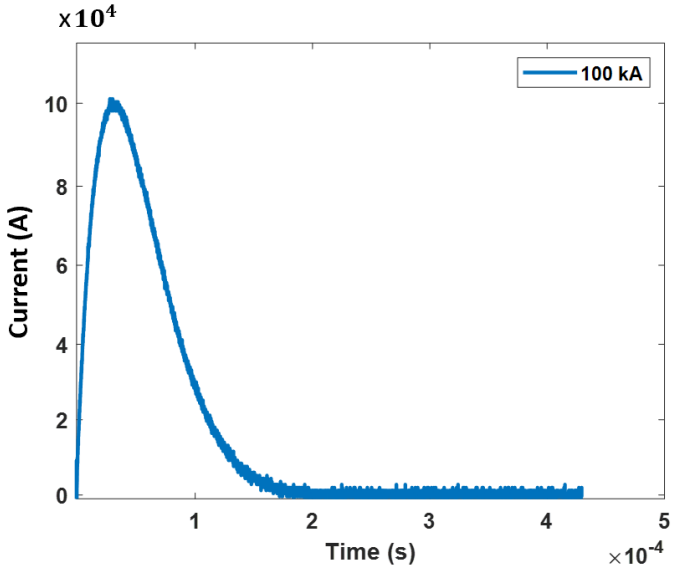

Figure 7.1 Impulse current waveform for ground electrode insulation study

For consistent and accurate lightning damage assessments of CFRP matrix composite laminates, it is essential that the entire lightning discharge current interacts with the CFRP samples. To ensure that all lightning discharge current interacts with the samples instead of directly jumping to the ground electrode, the edges of the ground electrode are electrically insulated by either installing a 3D printed dielectric barrier or applying insulation tape as shown in Figure 7.2. For this study, 6 CFRP matrix composite laminate samples are struke with the lightning impulse of 100 kA peak current amplitude. The samples were tested by two different electrode diameters of

www.manaraa.com

16 mm and 98 mm and by two different types of ground electrode edge insulations. The damages of samples obtained by lightning strike experiments are shown in Figure 7.2. The top row of the figure shows the results using the 16 mm diameter electrode while the bottom row shows those using the 98 mm diameter electrode. The three columns of Figure 7.2 represent the different types of ground electrode edge insulation. Specifically, Figure 7.2 (a) and (d), the first column of the figure, show the damage caused by 100 kA lightning impulse using the 16 mm diameter electrode and 98 mm diameter electrode, respectively, without ground electrode insulation. The surface material loss areas are also approximated using circular shapes. As shown, the surface material loss areas are 71.91 mm and 98 mm in diameter for the case using the 16 mm diameter electrode and 98 mm diameter electrode, respectively. In addition, Figure 7.2 (b) and (e), the second column of the figure, show the damage caused by 100 kA lightning impulse using the 16 mm diameter electrode and 98 mm diameter electrode, respectively, with the dielectric frame electrically insulating the ground electrode edges. The surface material loss area caused by the 16 mm diameter electrode is 77.07 mm in diameter while that caused by the 98 mm diameter electrode is 26.11 mm in diameter. Furthermore, Figure 7.2 (c) and (f), the third column of the figure, show the damage caused by 100 kA lightning impulse using the 16 mm diameter electrode and 98 mm diameter electrode, respectively, with insulation tape electrically insulating the ground electrode edges. The size of the surface material loss caused by the 16 mm diameter electrode is 77.11 mm in diameter while that caused by the 98 mm diameter electrode is 26.76 mm in diameter

The influence of the electrode edge grounding configuration can be clearly noticed in Figure 7.2. For all three cases of using the 16 mm diameter electrode (Figure 7.2 (a) - (c)), the size of the surface material loss area increased by 12.19% and 12.7% when the 3D printed dielectric frame and the insulation tape were used, respectively, compared to the case without ground

www.manaraa.com

electrode edge insulation. In addition, for all other three cases of using the 98 mm diameter electrode (Figure 7.2 (d) - (f)), the surface material loss area increased by 120% and 140% when the 3D printed dielectric frame and the insulation tape were used, respectively, compared to the case without using ground electrode edge insulation. Our results suggest that the effect of the ground electrode edge configuration becomes more pronounced when an electrode with a larger size is used. The results are as expected since the use of larger discharge electrodes decreases the distance between the discharge electrode and the ground electrode edges, which causes more lightning discharge current to bypass the samples and directly hit the ground electrode edges. However, with the electrical insulation in place, regardless of the distance, lightning discharge current is prevented from directly hitting the ground electrode edges, which results in a substantially higher level of sample damage.

www.manaraa.com

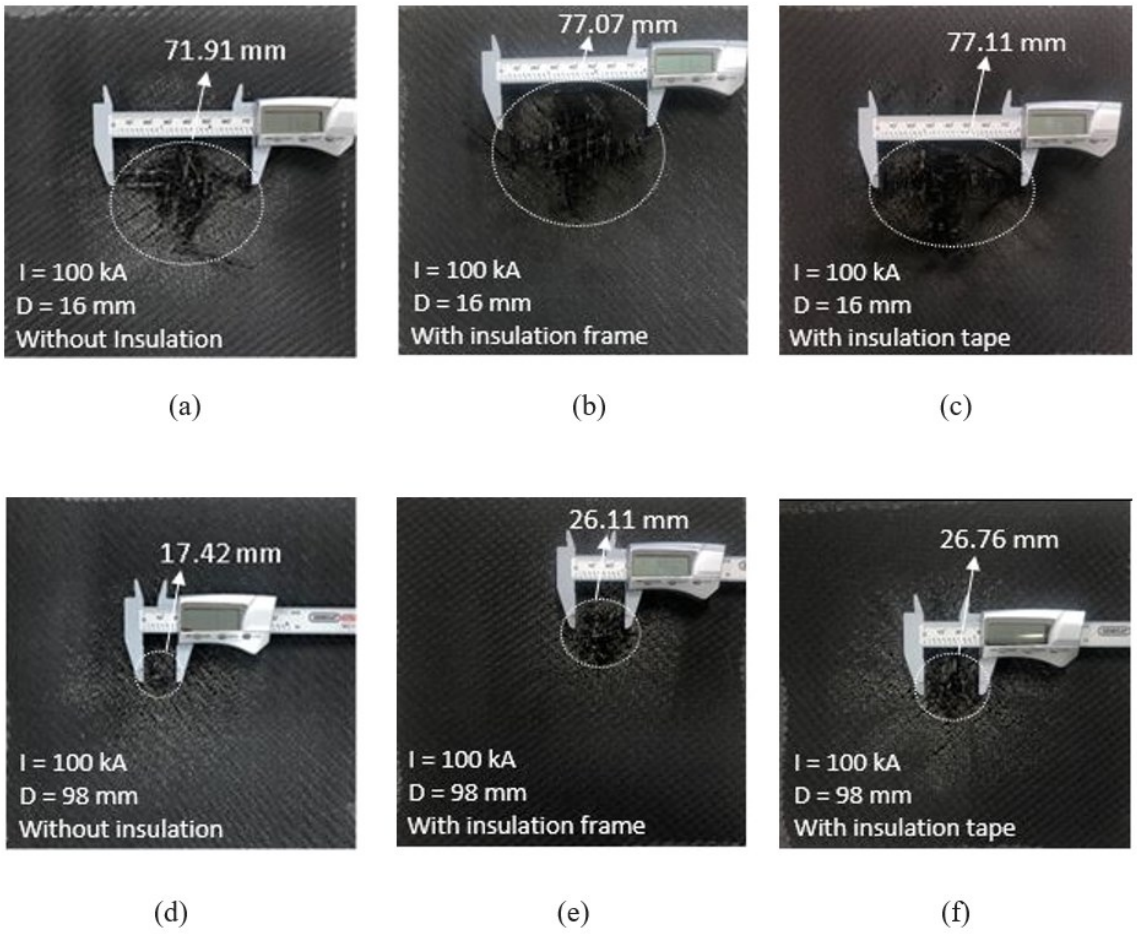

Figure 7.2 Lightning strike damage on CFRP matrix composite laminates by using ground insulation at 100 kA lightning current and 96.80 kJ energy: (a) Using small electrode without insulation, (b) Using small electrode with insulation frame (c) using small electrode with insulation tape, (d) using big electrode without insulation, (e) using big electrode with insulation frame, (f) using big electrode with insulation tape

Figure 7.3 compares the possible discharge current paths of testbeds without and with ground electrode edge insulation. In both cases, ground electrodes are electrically connected firmly to the sample through copper braids. The electrical contact enables discharge current to flow from the sample to the ground electrode even with the insulated edge as shown in Figure 7.3 (b). Also,

www.manaraa.com

no spark occurs on the specimen edges to the ground since the two are electrically connected and are at the same electrical potential. Figure 7.3 (b) depicts the effects of using the ground electrode with electrically insulated edges. In this case, lightning discharge current is directed to flow through the sample as the insulated edge impedes discharge current from directly hitting the ground electrode by jumping or flashing over the sample surface. In both cases, as depicted by the dashed line, small amount of current flows through the CFRP sample to the grounded aluminum plate due to the comparatively high resistance of the vertical discharge path.

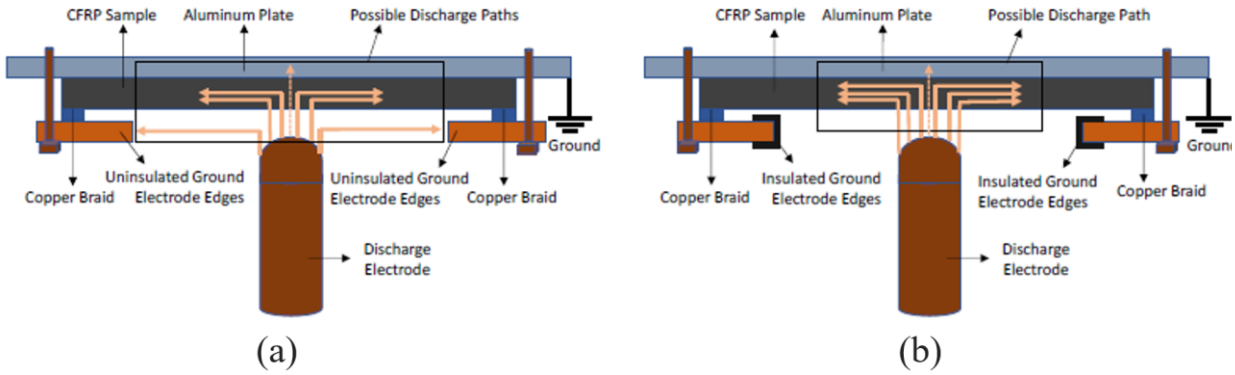

Figure 7.3 Various paths of lightning discharge current. (a) Without electrically insulated ground electrode edges, (b) With electrically insulated ground electrode edges

Figure 7.4 summarizes the correlation between the surface material loss area of the CFRP composites and the ground configurations, respectively, under the same level of lightning impulse energy. The surface material loss area of CFRP composites increases with the electrical insulation installed in the ground electrode of the testbed. The increase of the surface material loss area occurs as all discharge current flows through the CFRP composites with the use of electrically insulated ground electrode edges.

www.manaraa.com

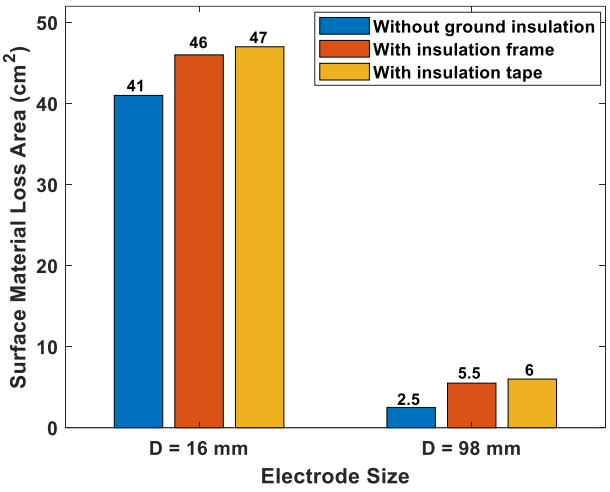

Figure 7.4 Ground electrode edge configuration vs. area of surface material loss

7.3 Effect of Ground Electrode Configuration on Delamination

Figure 7.5 shows the C-Scan images of the corresponding lightning strike damaged CFRP composites (see Figure 7.5). The more greenish color represents greater delamination of the composite sample. As one can see, the c-scan images are in close agreement with the visual observations shown in Figure 7.5. The delaminated area clearly increases with the adoption of the electrical insulation around the ground electrode edges. Also, the delamination propagates into much deeper layers of the composite laminates in the case where electrodes with smaller diameters are used. The B-scan images of Figure 7.5 show delamination occurring in deeper CFRP layers with the use of electrically insulated ground electrode edges. The figure also shows that the delamination propagates into deeper layers of the composite laminates in the case of the 16 mm electrode (Figure 7.5 (a), (b), (c)) compared to the case of 98 mm electrode (Figure 7.5 (d), (e), (f)).

www.manaraa.com

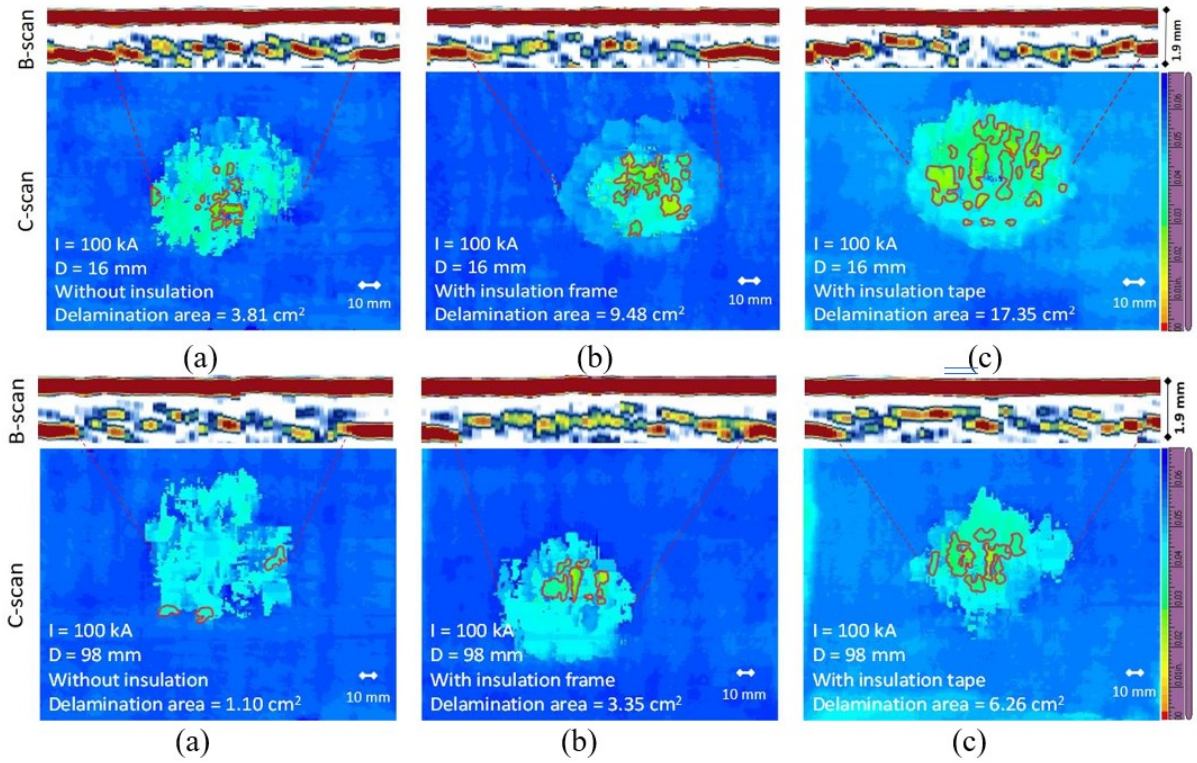

Figure 7.5 B-scan and C-scan images of delamination caused by 100 kA lightning current and 96.80 kJ energy: (a) Using small electrode without insulation, (b) using small electrode with insulation frame, (c) using small electrode with insulation tape, (d) using big electrode without insulation, (e) using big electrode with insulation frame, (f) using big electrode with insulation tape. Note: the red contours indicate the areas of severe delamination (i.e., delamination of multiple layers).

The influence of the ground electrode edge configuration on the severity of the delamination is clearly summarized in Figure 7.6. Here, severe delamination is defined as areas where delamination occurred on multiple layers. For all three cases using the 16 mm diameter electrode, the size of the delamination area increased by 149 % and 356 % when the 3D printed dielectric frame and the insulation tape were used, respectively, compared to the case without ground electrode edge insulation. In addition, for the other three cases of using the 98 mm diameter electrode, the delamination area increased by 206 % and 471 % when the 3D printed dielectric

www.manaraa.com

frame and the insulation tape were used, respectively, compared to the case without using ground electrode edge insulation. Our results suggest that the effect of the ground electrode edge configuration is more pronounced in the case where large electrode is used. This also indicates that larger portions of lightning discharge current bypass the samples when large electrodes are used without the electrically insulated ground electrode edges. However, with the electrically insulated ground electrode edges in place, the bypassing of discharge current is significantly reduced, which results in increased surface material loss and multiple layer delamination.

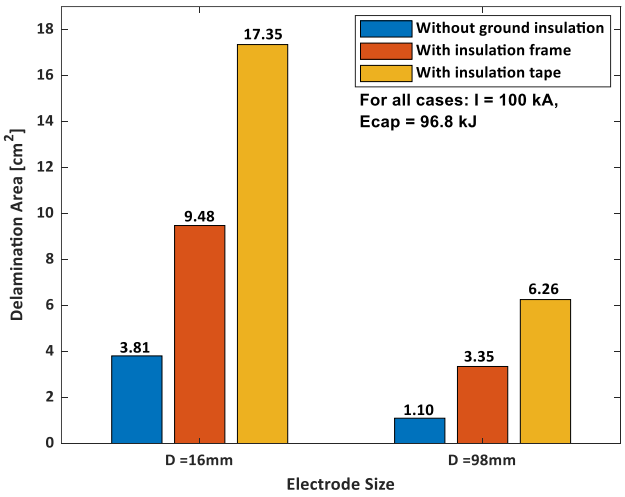

Figure 7.6 Ground electrode edge configuration vs. delamination area

The lightning induced damage modes of CFRP matrix composite laminates include the matrix decomposition and delamination of carbon fibers caused by Joule heating and mechanical stress. Joule heating from the high current density of lightning discharge causes melting, fiber vaporization, and delamination of CFRP matrix composite laminates. The mechanical stress originating from the overpressure of the explosion that produces a shock wave also contributes to the delamination, fiber breakage, pullout, and matrix cracking of the samples [101].

www.manaraa.com

7.4 Simulation Results

Finite Element Analysis (FEA) is used to find the effect of ground electrode in the model and the lightning arc plasma simulated. A constant discharge current is applied to demonstrate the impact of lightning discharge diameter on the temperature distribution of plasma and the sample. Since the composite structures cannot be assumed to be axisymmetric, metal sample is used in this study and the understanding obtained can provide insight into lightning strike damage investigation of composite materials as well. The COMSOL model from previous chapter is used to find the effect of the ground electrode in the simulation model.

7.4.1 Model Geometry

Two-dimensional axisymmetric model used in this research study to investigate the effect of ground electrode and obtain the temperature distribution in regions is shown in Figure 7.7 (a). The model geometry, dimensions, and mesh are shown in Figure 7.7 (b). Finer meshing is used to prevent aggregation of the mesh elements in the regions, specially at the corners of the model. All regions are presented in the model to simulate the plasma that represents the lightning.

www.manaraa.com

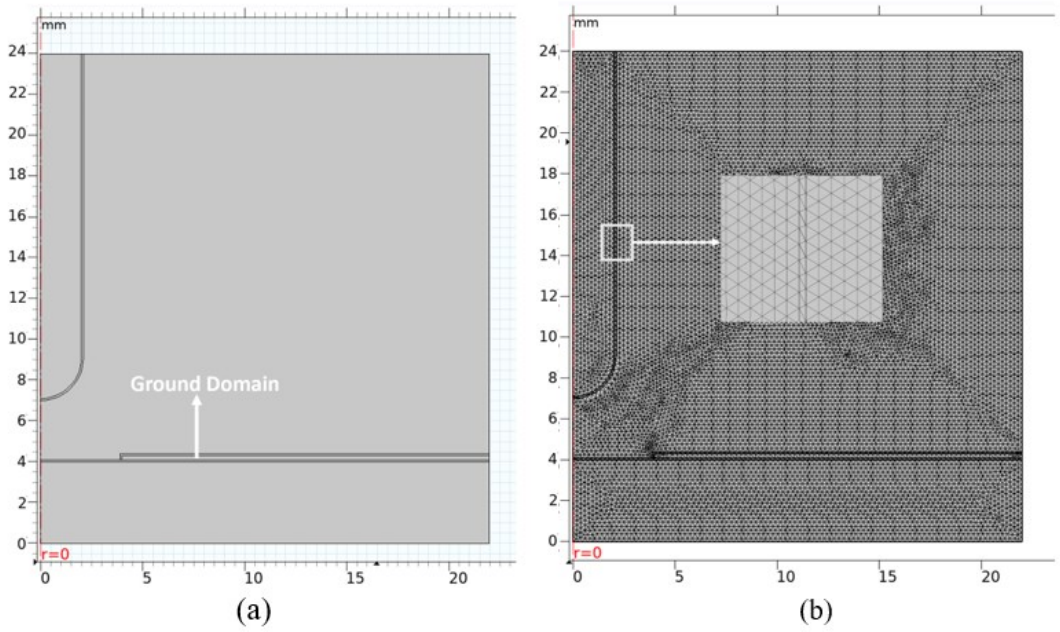

Figure 7.7 COMSOL model: (a) Model geometry (b) Typical mesh

As in can be seen from the model, a domain is added to the model as the ground domain which is representative of the ground electrode and is made up of copper. Also, Anode is made of aluminum with low electrical conductivity (about 100 S/m). This assumption is made to represent the experimental test set-up conditions and make the model easier because CFRP laminate is inhomogeneous and anisotropic and should never be assumed as a simple 2D axisymmetric problem. The ground domain is 4mm far from the arc center. In ground electrode effect study, the anode is made of copper. The cathode is made up of pure tungsten and has a semi-spherical shape which is similar to the electrode shape is used in this study.

www.manaraa.com

7.4.2 Simulation Result

7.4.2.1 Temperature Distribution

Figure 7.8 shows the temperature distribution in different regions of our model by applying 200 A constant current. As it is shown from the results on the model with ground electrode 4 mm far from the arc center, the burning air temperature reaches to $1.69*10^4$ K at highest point in the plasma domain. The anode, cathode, and ground domains' temperature are 379 K, $4.6*10^3$ K, and $2.9*10^3$ K, respectively.

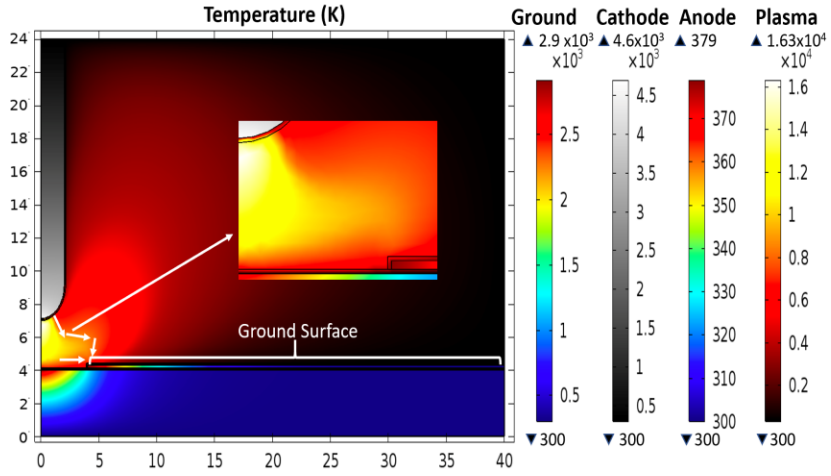

Figure 7.8 Temperature distribution within anode, plasma, cathode, and ground regions at t = 0.5s – with ground electrode at 4mm.

Figure 7.9 shows the 2D plot for current density with ground domain at 4mm distance from the arc axis by applying 200A constant current. As it is clearly represented, parts of plasma current discharges through the ground directly without disseminating through the anode.

www.manaraa.com

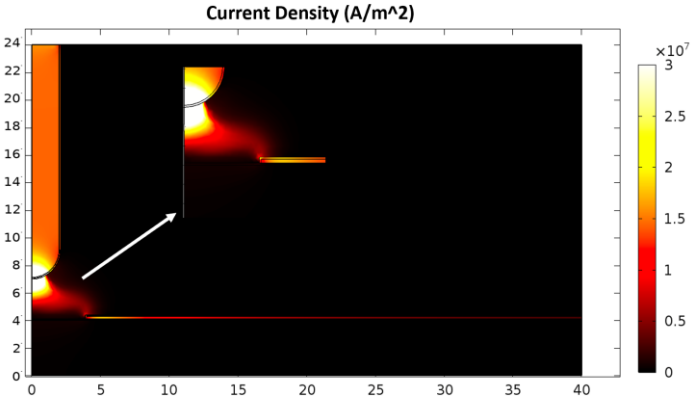

Figure 7.9 2D plot for current density with ground domain at 4mm distance from the arc axis

Figure 7.10 shows the temperature distribution in different regions of our model by applying 200 A constant current. As it is shown from the results on the model with ground electrode 6 mm far from the arc center, the burning air temperature reaches to $1.94*10^4$ K at highest point in the plasma domain. The anode, cathode, and ground domains' temperature are 383 K, $4.62*10^3$ K, and $2.46*10^3$ K, respectively.

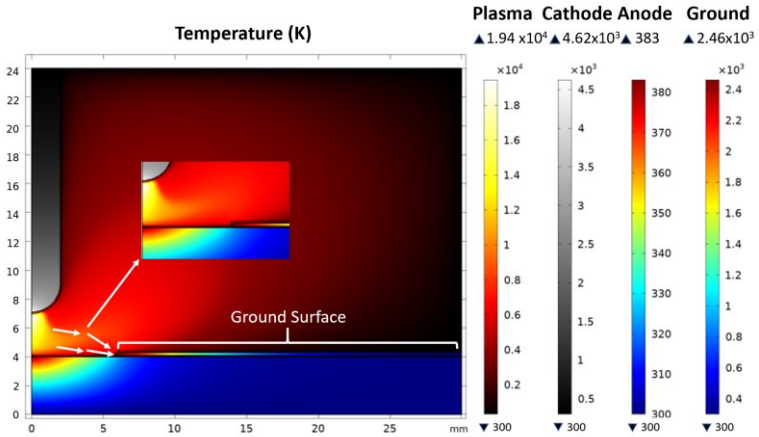

Figure 7.10 Temperature distribution within anode, plasma, cathode, and ground regions at t = 0.5s – with ground electrode at 6mm distance from the arc axis

www.manaraa.com

Figure 7.11 shows the 2D plot for current density with ground domain at 4mm distance from the arc axis by applying 200A constant current. As it is clearly represented, parts of plasma current discharges through the ground directly without disseminating through the anode.

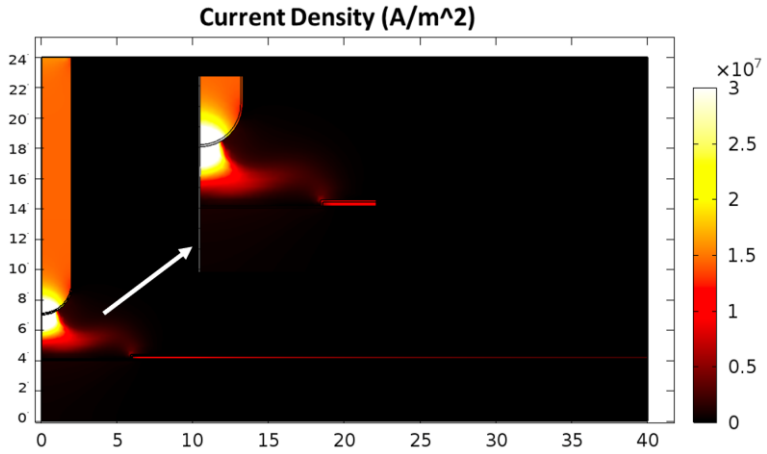

Figure 7.11 2D plot for current density with ground domain at 6mm distance from the arc axis

Figure 7.12 shows the temperature distribution in different regions of our model by applying 200 A constant current without ground electrode. As it is shown from the results on the model without ground electrode far, the burning air temperature reaches to $2.3*10^4$ K at highest point in the plasma domain. The anode and ground domains' temperature are 440 K and $4.7*10^3$ K, respectively. The results show that the absence of ground electrode results in the increase of temperature in all regions.

www.manaraa.com

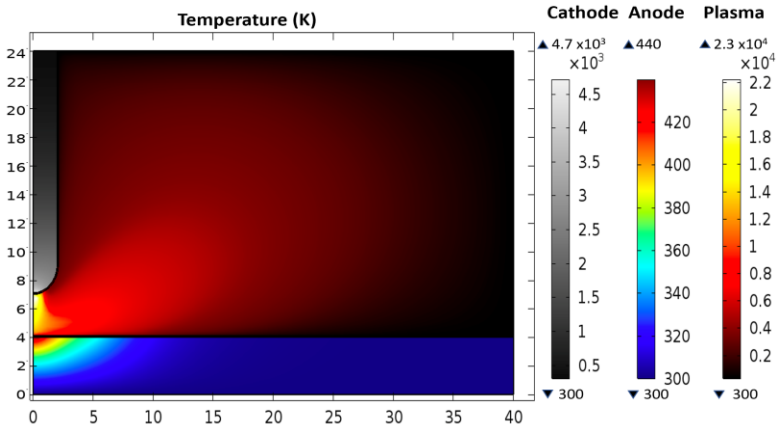

Figure 7.12 Temperature distribution within anode, plasma, cathode, and ground regions at t = 0.5s – without ground.

Figure 7.13 shows the 2D plot for current density without ground domain by applying 200A constant current. As it is clearly represented, all plasma current disseminates through the anode.

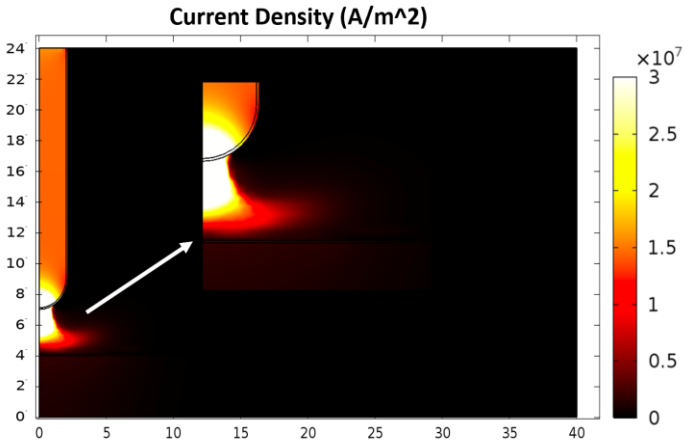

Figure 7.13 2D plot for current density without ground domain

Figure 7.14 shows the temperature along the arc axis. The injected heat from the plasma causes significant damage to the materials. The results show that the locating the ground domain

www.manaraa.com

far from the arc center or eliminating the ground domain results in the increase of temperature along the arc axis. The plasma reaches its peak around 6.7 mm along the arc axis that increases the electrical conductivity. This leads to faster movement of plasma near the cathode that reduces the electron density.

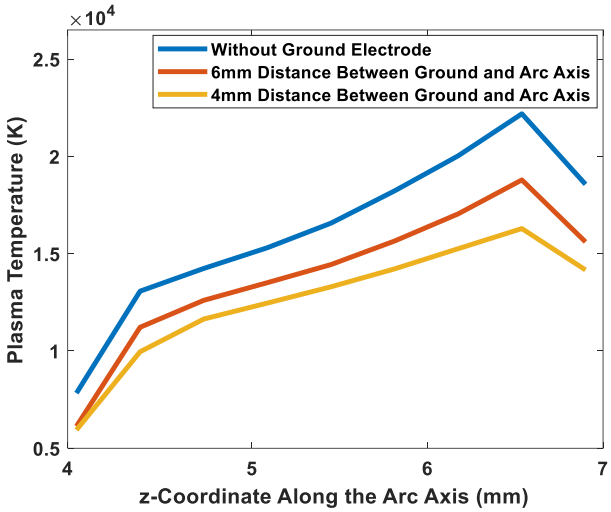

Figure 7.14 Temperature within the arc axis with different distances of ground from the arc axis

In the plasma temperature modeling, the plasma heating consists of several mechanism including Joule heating, radiative emission, and electronic enthalpic flux. In this section, each mechanism is investigated for three size of electrodes.

7.4.2.2 Joule Heating

Joule heating is the thermal energy generates by current passing through a conductor. Joule heating along the plasma arc center is obtained by J^2/σ, where J is the current density and σ is the electrical conductivity of the plasma. Figure 7.15 shows the joule heating along the arc center. A

www.manaraa.com

decreasing trend in the peak of joule heating can be seen with locating the ground close to the arc axis. As it is shown in Figure 7.15, the Joule heating increased by 100 % to 2.4×10^{12} after adding the cathode at 4mm distance from the arc axis.

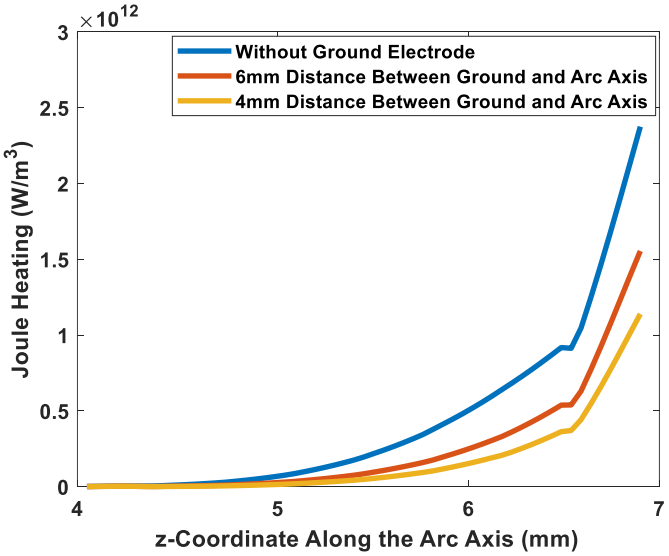

Figure 7.15 Joule Heating along the arc axis at different distances of ground from the arc axis

7.4.2.3 Enthalpic Heating

Figure 7.16 shows the Electronic enthalpic along the arc axis. As the ground domain get far from the arc axis or is eliminated, current density and plasma temperature increases. Figure 7.16 shows the electronic enthalpic along the arc axis. There is a noticeable change from positive to negative in electronic enthalpic flux at the highest temperature point (z=6.7 mm). The temperature gradient represents significant change at the highest temperature point is the reason for alteration in positive-negative. As shown in Figure 7.16, the enthalpic flux decreases along the arc axis from the cathode surface down to the z = 4.4 mm and then rebounds at z= 4.2 mm down to the anode surface. This can be concluded from assumption of NLTE layer near the cathode and

www.manaraa.com

anode that causes disturbance surface and the LTE condition in the plasma in which the enthalpic heating has a linear trend.

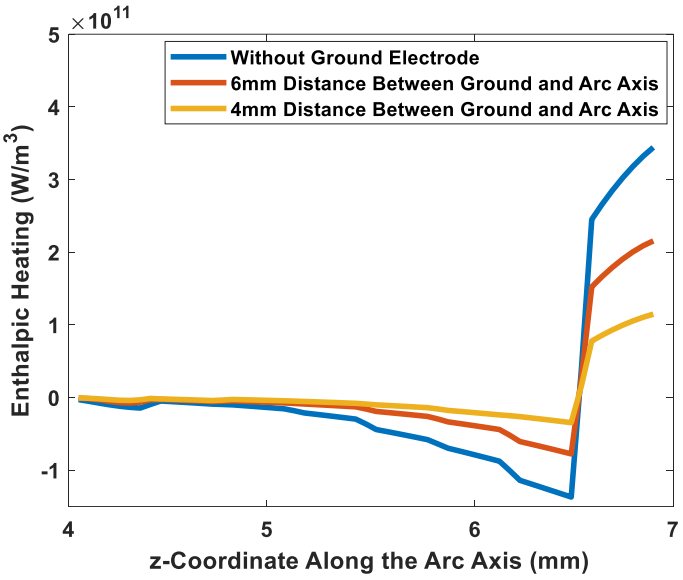

Figure 7.16 Electronic enthalpic along the arc axis at different distances of ground from the arc axis

7.4.2.4 Emission Heating

The emission heating is equals to the $4\pi\varepsilon_N$ in which ε_N is the net emission coefficient of the gas. Figure 7.17 represents the emission heat loss along the arc axis (between cathode ($r = 0$, $z = 7$ mm) and anode ($r = 0$, $z = 4$ mm). It can be seen that the value of emission heating is higher at close to the cathode and reduces along the arc axis down to the cathode. The emission heating peak is at the highest plasma temperature point that accelerate the electrons because of the strong field from the cathode. When the ground domain gets far from the arc axis or is eliminated, the emission heating increases significantly.

www.manaraa.com

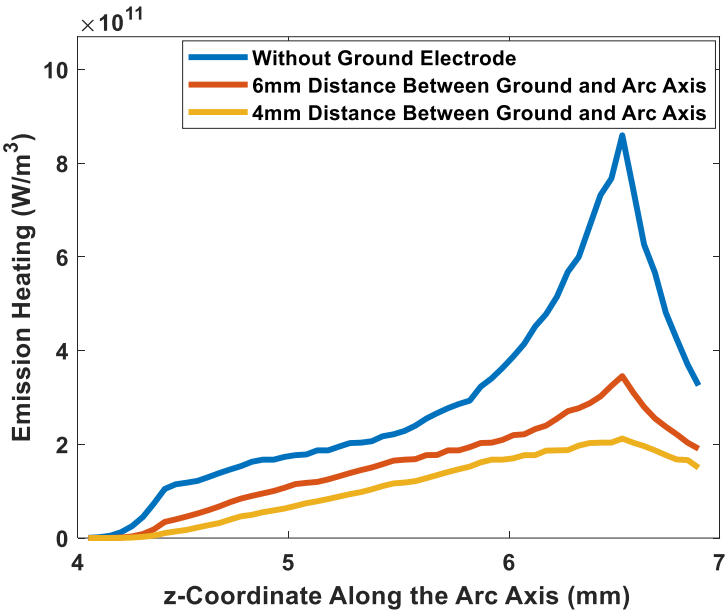

Figure 7.17 Emission heat loss along the arc axis at different distances of ground from the arc axis

7.4.2.5 Heat Flux

Figure 7.18 shows the heat flux along the anode's surface. An increasing trend in the peak of heat flux can be seen with different distances of ground from the arc axis. A significant change of heat flux along the radial distance from the arc center can be observed which can be described by similar behavior of energies' waveform. Also, it is observed that the heat flux shows a steeper increase for the model without ground domain. The sharper reduction of heat flux in cases without ground electrode or with the ground domain at far distance from the arc axis is due to higher emission loss at higher current densities because of reducing the effect of the ground.

www.manaraa.com

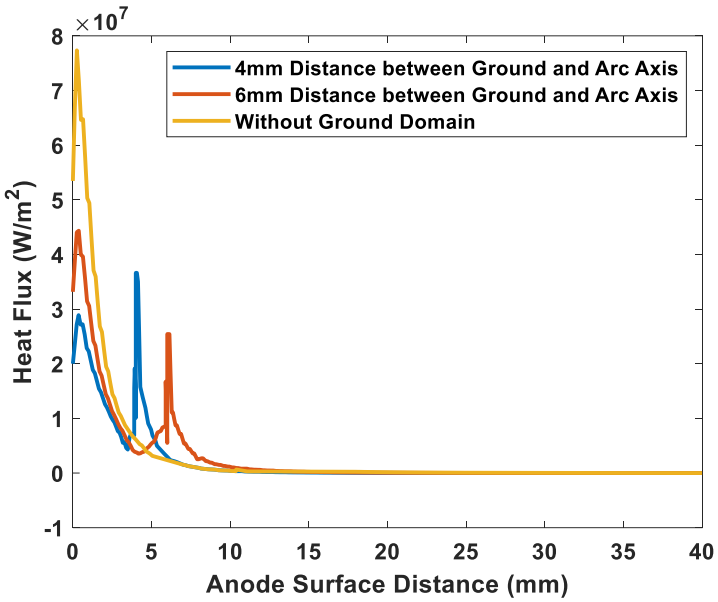

Figure 7.18 Heat Flux along the anode surface at different distances of ground from the arc axis

7.4.2.6 Current Density Along the Ground Domain

Figure 7.19 shows 1D plot for the current density along the ground domain axis for two different distances. As shown from the results, the current density along the ground distance increases as the ground is placed closer to the arc center. This confirms the effect of ground electrode configuration on the arc modeling.

www.manaraa.com

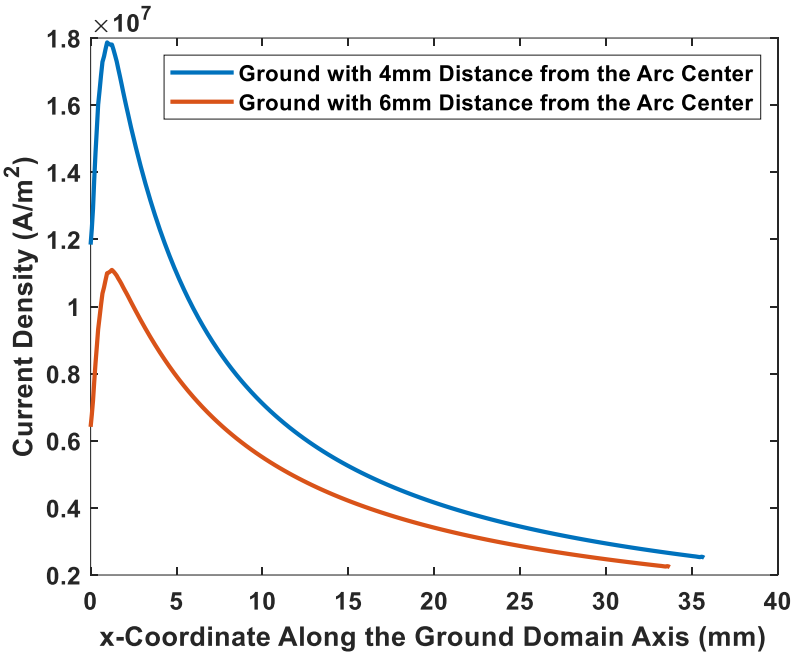

Figure 7.19 Current density along the ground domain at different distances of ground from the arc axis

7.5 Summary

The damage of CFRP composites clearly varies as a function of ground electrode configuration (i.e., insulating ground electrode edges). According to the results, the affected area increases with insulating the ground electrode edges. Electrical discharges, including lightning discharge, occur along the lowest resistance path. Hence, in lightning strike testbeds, lightning discharge can occur not only through the layers of the CFRP samples, but also over the surface of the CFRP samples to the ground electrode. If the electrical resistances of both paths are not significantly different, substantial amount of lightning discharge current will flow through both paths. The resistivity of the two paths are highly affected by the composite manufacture process (such as voids, resin and fiber non-uniformity). In this case, the division of the discharge current between the two paths depends on the conductivity (*i.e.,* 1/resistivity) ratio of the two paths.

www.manaraa.com

Although negligible, even in the cases, where one of the discharge paths has a substantially higher resistance than the other, current flowing through the high resistance path is not strictly zero. For example, if a sample has a particularly high electrical resistance, larger portion of lightning discharge may flow over the sample directly striking the ground electrode rather than flowing through the inner layers of the samples. Moreover, if the capacitors are charged to higher voltages to increase the energy of lightning discharge, enhanced electric field between the discharge electrode and the ground electrode increases the likelihood of a direct discharge between them instead of discharge current flowing through the sample. Therefore, ground electrode configuration must be designed carefully as it poses significant influence on the results of lightning strike experiments.

In addition to enabling the enhanced consistency of the lightning strike damage assessments, the electrically insulated ground electrode edges also enable the use of smaller composite samples. In the conventional testbeds, in which the ground electrode edges are exposed without any dielectric shielding, sufficiently large sizes of composite samples are required for lightning strike experiments. In contrast, with the electrically insulated ground electrode edges, smaller samples can be utilized virtually independent of electrode diameter as the entire lightning discharge current is ensured to fully interact with the samples without bypassing them. However, it is worth mentioning that there will be physical limits, to which the sample size can be reduced. For instance, the dielectric barriers surrounding the ground electrode edges should be sufficiently strong to withstand the high electric stress imposed on them during the experiments. Given that these physical limitations are not breached, the use of smaller samples provides more number of samples per cost and per the amount of constituent materials.

www.manaraa.com

CHAPTER VIII

LIGHTNING STRIKE DAMAGE TOLERANCE IMPROVEMENT OF CFRP COMPOSITES

8.1 Motivation

A lot of researchers are improving the electrical conductivity of resin by utilizing carbon nanofillers. There have been numerous studies that investigated the effect of adding conductive fillers on lightning strike damage mitigation, but the ideal nanofiller has not been developed yet. There is no specific material that is ideal for composite structures lightning strike damage mitigation and thus a thorough investigation on the additive material is essential for reducing the lightning strike damage of composite laminates, enhancing the protection of aircrafts, and reducing the manufacturing cost. The lightning damage mitigation method of CFRP composites is mainly based on increasing the electrical conductivity of the laminates. Carbon Black (CB), which is a cost-effective carbon filler material, is used to increase the electrical conductivity of CFRP composites. Also, the effect of various combinations of carbon nano-fillers including CB, CB/Carbon Nanotube (CNT), and CNT with identical volume ratio is investigated to find the best filler composition for CFRP composites. This chapter investigates the effect of CB on lightning strike damage mitigation and the results of the study will aid in the development of composite structures used in aerospace and wind energy industries. Nanofillers including CB, CB/CNT, and CNT are added to the CFRP composites during the fabrication process. Nine laminate samples

www.manaraa.com

were manufactured with 0.25%, 0.5%, and 0.75% of CB, CB/CNT, and CNT as explained in chapter 5.

8.2 Electrical Resistivity

In order to evaluate the difference in the electrical conductivity of the samples after adding the carbon nanofillers, four probe experiments were performed as shown in Figure 8.1. Four-probe test were employed using a Fluke 8846A Digital Precision Multimeter. For the resistivity test, we used three rows of nickel paint. In each row, the outer two painted locations were used to supply the current whereas the inner two senses the voltage, from which resistance is calculated. Three sets of values of resistance were calculated and averaged for each composite sample.

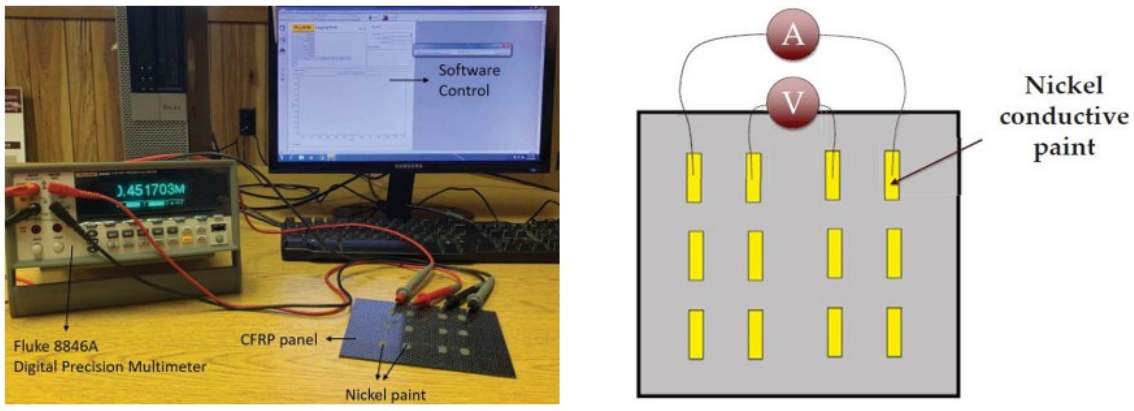

Figure 8.1 Four-probe resistance measurements for CFRP composite [30]

Figure 8.2 represents the electrical resistance data of CFRP composites with different amount of nano-filler measured via the four-probe method. It can be seen that adding CB decreases the electrical resistance and increasing the amount of the CB decreases the electrical resistivity significantly. While the electrical resistivity for the sample without additive nano-filler is 6.024 Ω,

www.manaraa.com

adding 0.25%, 0.5%, 0.75%, and 1% of CB decreases the electrical resistivity to 5.24 Ω, 4.81 Ω, 4.44 Ω, and 4.27 Ω, respectively. In addition, adding 0.25%, 0.5%, and 0.75% of CNT decreases the electrical resistivity to 4.13 Ω, 4.08 Ω, and 4.91 Ω, respectively. Furthermore, adding 0.25%, 0.5%, and 0.75% of CB+CNT decreases the electrical resistivity to 4.42 Ω, 4.81 Ω, and 5.53 Ω, respectively. While the electrical resistance of the CFRP composites reduces by adding CB up to 1%, adding combination of CB+CNT more than 0.25% or CNT more than 0.5% leads to increasement of the electrical resistivity. It was not possible to add CNT up to 1% because of the high viscosity of the resin after adding CNT. So, it is shown that adding CB has a linear trend in reducing the electrical resistance.

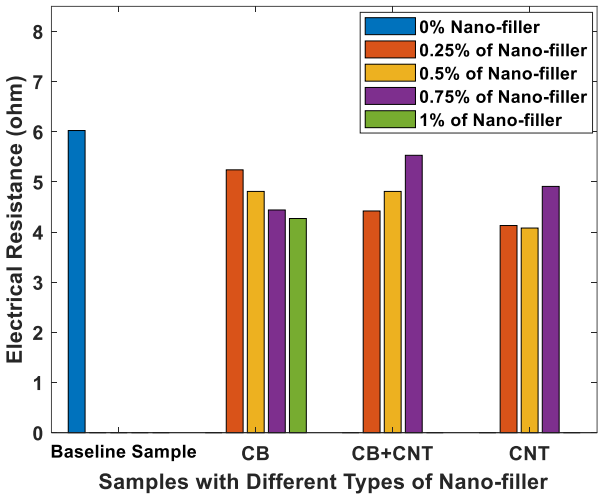

Figure 8.2 The electrical resistance results from the four-probe measurement

The trend in electrical resistivity of CB at different ratio is in agreement with results from reference [90]. By incorporating the CNT, the electrical resistivity increases for 0.75 % ratio of nano-fillers. It was not possible to add CNT up to 1% because of the high viscosity of the resin

www.manaraa.com

after adding CNT. It is expected that the electrical resistance decreases again by increasing the amount of nano-fillers. Such a behavior has been seen in some other studies and shown in Figure 8.3. As it can be seen in Figure 8.3, the reduction in electrical conductivity or increase in electrical resistance occur at nano-fillers with ratio 0.5% and 1%.

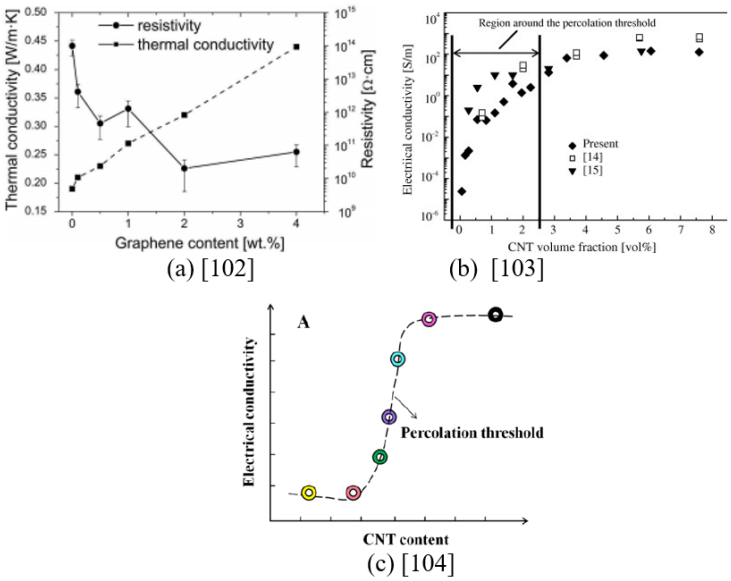

(a) [102] (b) [103]
(c) [104]

Figure 8.3 Electrical conductivity/resistance of composites with additive nanofillers: (a) Graphene; (b) CNT; (c) increase in concentration of nano-fillers

Beside the type and amount of the nanofillers, other factors such as dispersion quality, shape and hardness of nanofiller might affect the resistivity. Dalmas et al. [105] investigated the conductivity of carbon nanotube-filled polymer composites in two different processing methods including Evaporated and freeze - dried and pressed methods. He attributed the difference in electrical properties to the difference in tube-tube contact electrical properties. It is supposed that the part of the contact is adsorbed on the CNT surfaces and another part is dissolved in polymer, and that's why from the point that conductivity increases sharply, the volume fraction of the

www.manaraa.com

additive nano-filler has a lower effect on the conductivity. It is concluded that after at a threshold for contact surface (around 0.5% in this study), the effectiveness of the contact resistivity will deteriorate first and then increase with a lower steepness by adding more amount of additive nano-filler. To better understand the functionality of the additive nano-filler, Li et al. [104]has shown the trend in dispersion of the nano-fillers in the epoxy as it is represented in Figure 8.3 (c) and Figure 8.4.

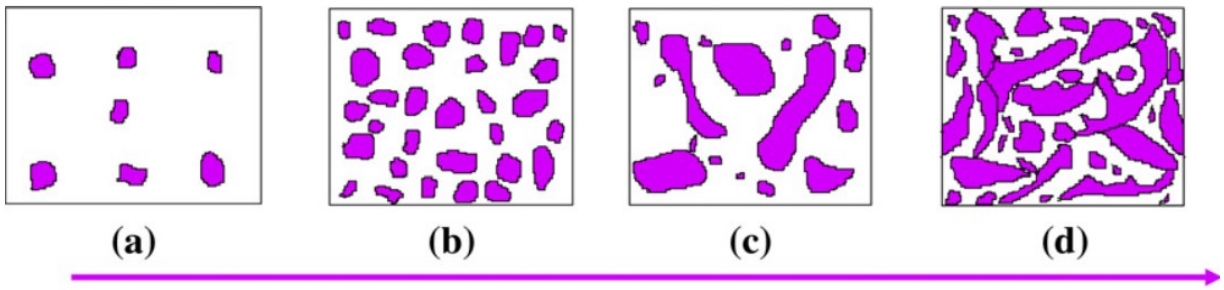

Figure 8.4 Increase in concentration of nano-fillers [104]

It is clearly shown that adding a small amount of the nano-fillers leads to the even distribution of the nano-fillers. But, adding more amount leads to attachment of the nano-fillers that decreases the filler distribution network first and then continuous networks are formed after adding more amount of the nano-fillers. Such a decrease and then increase threshold depends on several parameters including type of nano-fillers, size of nano-filler, and dispersion method.

8.3 Effect of Additive Nano-fillers on Surface Material Loss of CFRP Composites

For CFRP composites with different types and amount of conductive nano-fillers, the energy of lightning discharge was kept identical. CFRP composites with three different types and combinations of carbon nano-fillers were exposed to the lightning current impulse amplitude of

www.manaraa.com

120 kA using an identical size of discharge electrode. The impulse current waveform applied to the samples is shown in Figure 8.5.

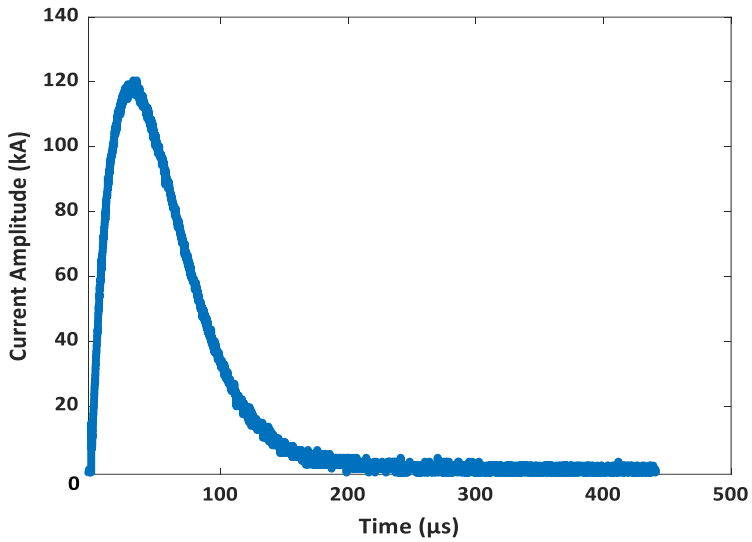

Figure 8.5 Simulated lightning strike waveform for testing CFRP composites with nano-filler

The damages of CFRP matrix composite laminates caused by the lightning strikes are shown in Figure 8.6. The results show that the surface material loss decreases considerably by adding conductive nano-fillers. Here, the surface material loss area refers to the area where the material experiences complete fiber and matrix vaporization, fiber breakage, and fiber pullout. The surface material loss area forms an approximate circular shape since the electrical and thermal conductivities in the longitudinal and transverse directions are identical for the woven carbon fiber composite. A clear trend of increasing CFRP damage is observed as a function of additive nano-fillers. While there is a noticeable carbon fiber surface material loss observed on the CFRP composites without nano-filler, there is no significant surface material loss by adding CB and CNT. Figure 8.6 (a) shows the big size of damage on the panel without any nano-filler. The surface

www.manaraa.com

material loss of panels with 0.25%, 0.5%, 1% of CNT is the same. In addition, a trend of lightning strike damage increasing can be seen where the amount of CB+CNT increases from 0.25% to 0.75%. Furthermore, a trend of lightning strike damage reduction can be seen where the amount of CB increases from 0.25% to 1%. This can be due to better squishable property of CB, splitting to smaller particles that leads to better spread of CB in epoxy, which improves the mixing result and prevents the agglomeration of the nano-particles. It is therefore evident that, for component D of lightning current waveform, the CB has a considerable influence on reducing the surface material loss of CFRP matrix composite laminates due to lightning strike.

www.manaraa.com

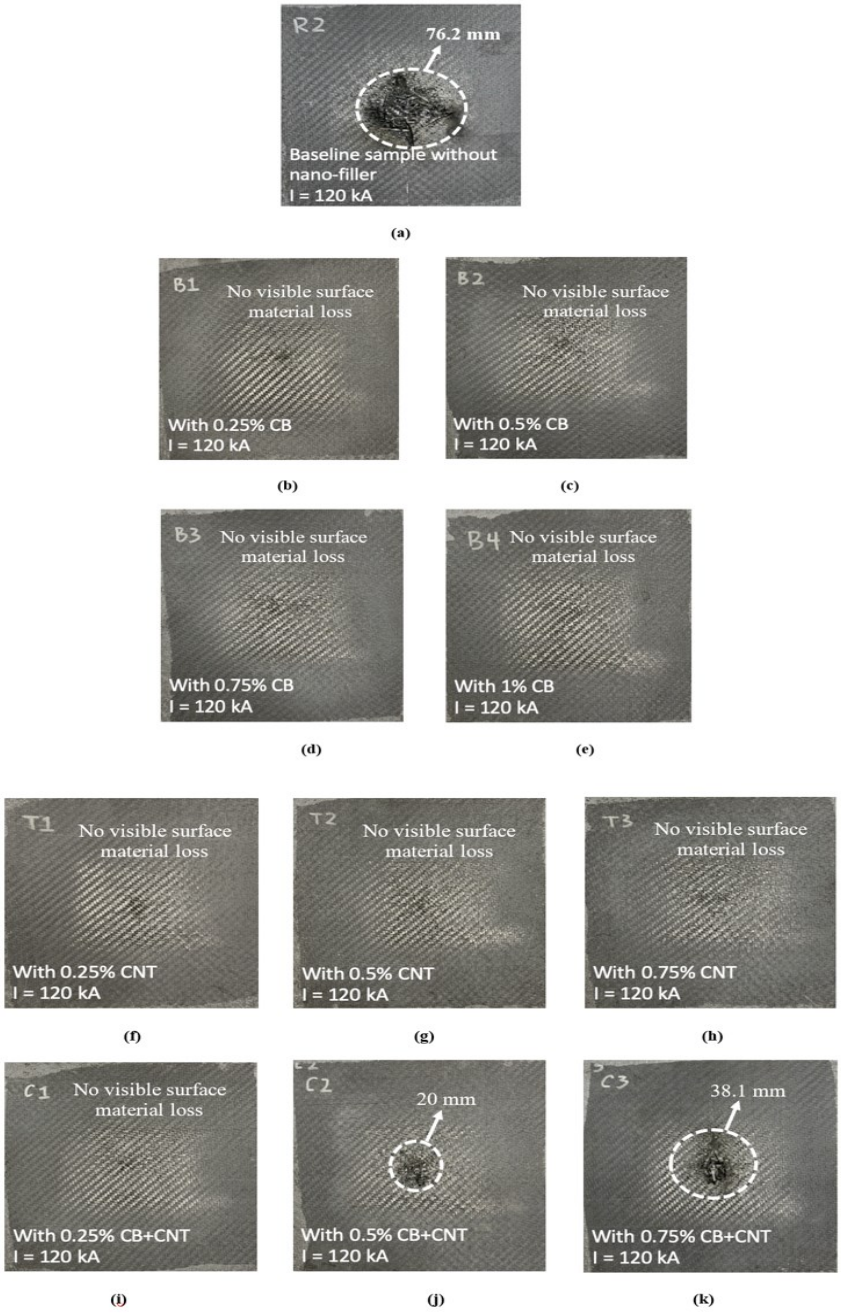

Figure 8.6 Lightning strike damage on CFRP matrix composite laminates by using ground insulation at 120 kA lightning current: (a) Baseline sample without nano-filler, (b) With 0.25% of CB (c) With 0.5% of CB, (d) With 0.75% of CB, (e) With 1% of CB, (f) With 0.25% of CNT, (g) With 0.5% of CNT, (h) With 0.75% of CNT, (i) With 0.25% of CB+CNT, (j) With 0.5% of CB+CNT, (k) With 0.75% of CB+CNT

www.manaraa.com

The influence of the additive nano-fillers on the severity of the surface material loss is clearly summarized in Figure 8.7. Here, the surface material loss area refers to the area where the material experiences complete fiber and matrix vaporization along with fiber breakage and fiber pullout. The surface material loss area forms an approximate circular shape since the electrical and thermal conductivities in the longitudinal and transverse directions are identical for the woven carbon fiber composite. The corresponding diameter of the surface material loss area is measured. A clear trend of the increasing CFRP damage is observed as a function of additive nano-fillers. All combinations reduce the surface material loss, but do not have identical effect. While there is no noticeable carbon fiber surface material loss area on samples with CB and CNT, the surface material loss area increases to 3.2 cm2 and 11.4 cm2 for the samples with 0.5% and 0.75% of CB+CNT.

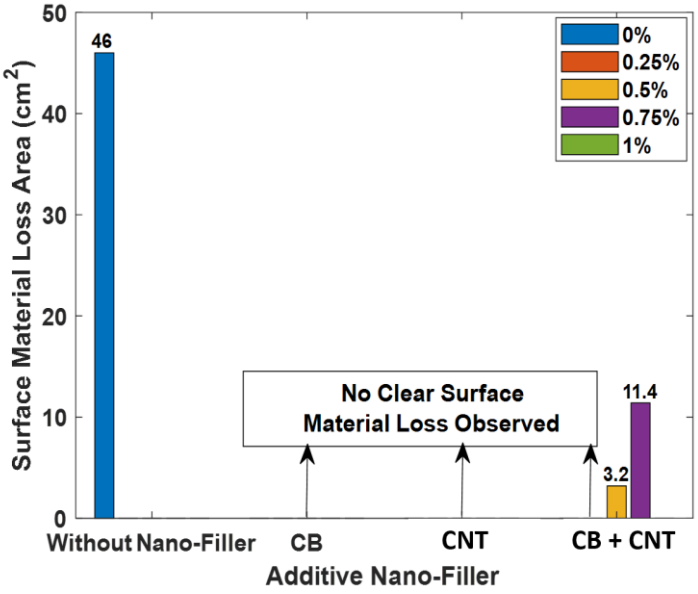

Figure 8.7 Effect of Additive nano-fillers on Lightning strike damage on CFRP composites

www.manaraa.com

8.4 Effect of Additive Nano-fillers on the Delamination of CFRP Composites

Figure 8.8 shows the C-Scan images of the corresponding lightning strike damaged CFRP composites shown in Figure 8.6. The more greenish color represents greater delamination of the composite sample. As one can see, the c-scan images are in close agreement with the visual observations shown in Figure 8.6. The delaminated area clearly decreases when adding carbon nano-fillers to the CFRP composites. A trend of delamination reduction can be seen where the amount of CB increases from 0.25% to 1%. Also, the delamination propagates into much deeper layers of the composite laminates in the cases where higher amount of CNT and combination of CNT+CB are used. The B-scan images of Figure 8.6 is represented in Figure 8.8 and show that delamination occurring in deeper CFRP layers with the use of carbon nano-fillers. Comparing the delamination images from C-scan and B-scan images represents lower lightning strike damage of CFRP composites with CB than the ones with CNT and combination of CB+CNT.

www.manaraa.com

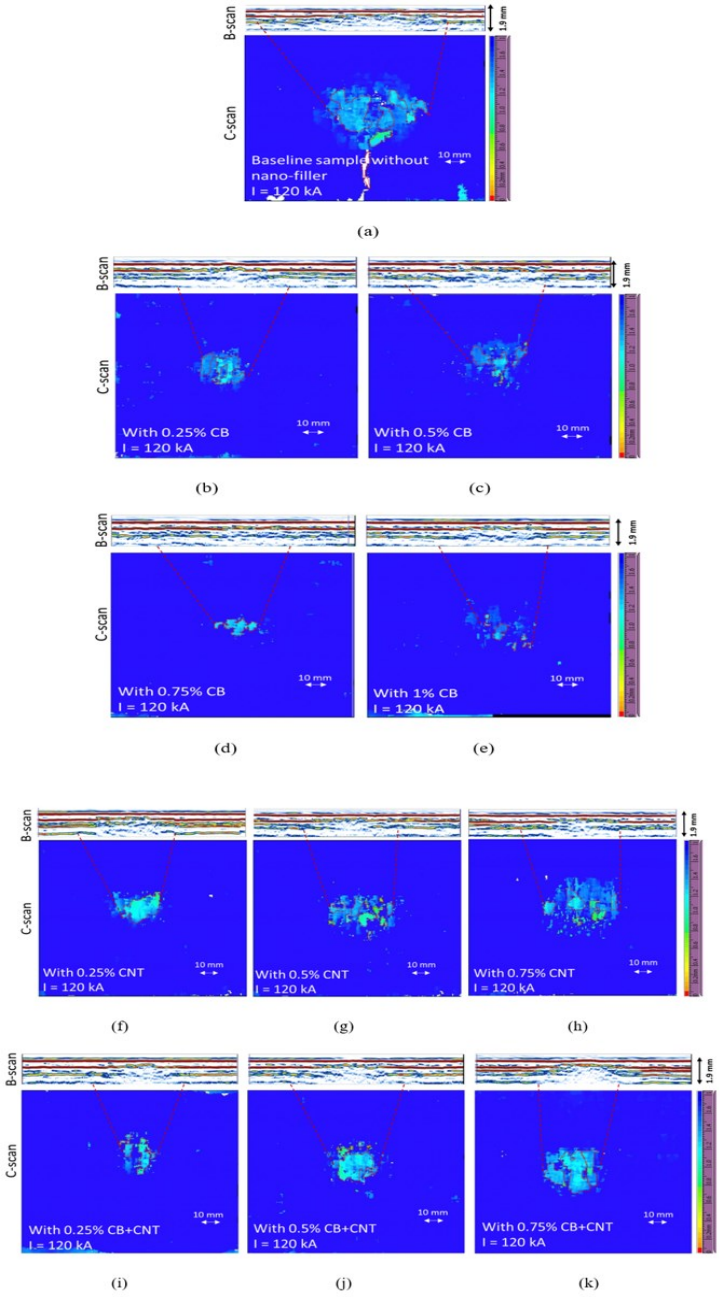

Figure 8.8 C-Scan and B-scan images showing the delamination of the CFRP composites after simulated lightning strike tests at 120 kA: (a) Baseline sample without nano-filler, (b) With 0.25% of CB (c) With 0.5% of CB, (d) With 0.75% of CB, (e) With 1% of CB, (f) With 0.25% of CNT, (g) With 0.5% of CNT, (h) With 0.75% of CNT, (i) With 0.25% of CB+CNT, (j) With 0.5% of CB+CNT, (k) With 0.75% of CB+CNT

www.manaraa.com

The trend in influence of the additive nano-fillers on the severity of the delamination is clearly shown in Figure 8.9. Here, severe delamination is defined as areas where delamination occurred on multiple layers. For all three cases using three different additive nano-fillers, the size of the delamination area reduced by 85 %, 75% and 60 % when CB, CB+CNT, and CNT were used in best scenarios, respectively, compared to the case without any nano-filler. In addition, while the lightning strike delamination damage area decreases as the amount of CB increases, the delamination area for the samples with CNT and CB+CNT do not show a linear trend and is similar to the trend of electrical resistivity. This also indicates that the delamination area of CFRP composites is a function of the electrical resistivity.

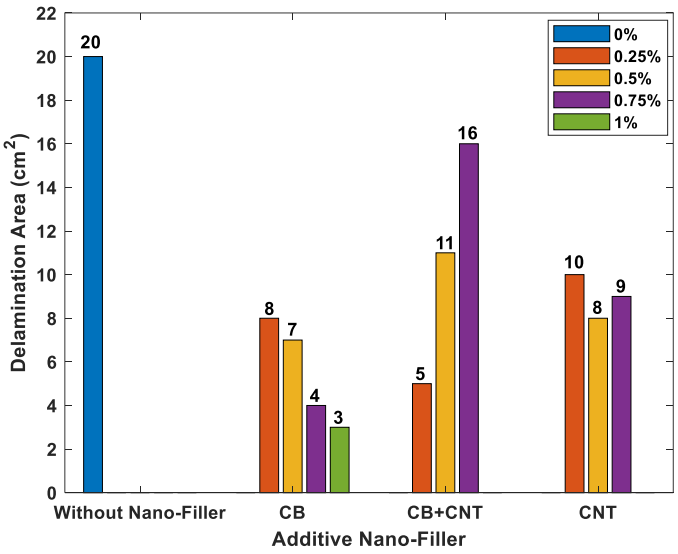

Figure 8.9 Delamination caused by 120 kA lightning current

www.manaraa.com

8.5 Summary

The damage of CFRP composites clearly varies as a function of electrical resistance (i.e., with additive conductive nano-filler). According to the results, the affected area decreases with adding conductive nano-fillers such as CB and CNT. Electrical discharges, including lightning discharge, occur along the lowest resistance path. For other nanofillers, it is not possible to increase the amount of the additive nano-fillers from a certain amount. CB has squash ability, that means the particles break, which enables the use of more amount of additive CB, in which the viscosity of the resin does not increase suddenly and helps to mix the nano-filler with resin properly.

In this chapter, the effect of conductive carbon nanofillers (i.e., CNT, CB, and CNT+CB) is investigated on the lightning strike damage mitigation of CFRP composites. Component A of lightning strike with amplitude of 120 kA was simulated to strike the CFRP composites. Different combinations of carbon nanofillers were used to premix with the epoxy to fabricate conductive CFRP composite laminates. The lightning strike damage of the CFRP composites with and without the nanofillers was compared while the lightning strike currents were kept identical for each test sample. The results suggest that the lightning strike damage of CFRP composites reduces incredibly by adding CB. The result of this study is expected to assist with the development of the protection of CFRP composites against lightning strike.

www.manaraa.com

CHAPTER IX

CONCLUSION

This dissertation is focused on understanding the requirements for lightning strike damage mitigation of CFRP composites through design, simulation, and experimental investigations. Lightning experiment testbed is improved by selecting a suitable discharge electrode and adding insulation layer to the ground electrode edges. Furthermore, a new method for improving the lightning strike damage tolerance of CFRP composites is introduced.

A unique testbed was designed and constructed in compliance with SAE standard to reduce the chance of data misinterpretation in lightning strike studies. The damage of CFRP matrix composite laminates significantly varies as a function of electrode size (i.e., lightning discharge diameter). According to the results, the affected area decreases with increasing electrode diameter. Such trend is likely contributed by the increasing discharge current density with decreasing cross section area of the discharge. Larger current density flowing through a smaller cross-sectional area of CFRP sample causes significantly larger Joule heating and greater damage. The size of the delaminated area increased by 192 % and 1,294 % when the 46 mm and the 16 mm diameter electrode were used, respectively, compared to the case of the 98 mm diameter electrode. So, the 46 mm electrode, which is close to the minimum size of electrode recommended by standard, was used to investigate the lightning strike damage mitigation study. In addition, the lightning strike damage of CFRP composites clearly varies as a function of ground electrode configuration (i.e.,

www.manaraa.com

insulating ground electrode edges). According to the results, the affected area increases if the ground electrode edges are insulated. Electrical discharges, including lightning discharge, occur along the lowest resistance path. Hence, in lightning strike testbeds, lightning discharge can occur not only through the layers of the CFRP samples, but also over the surface of the CFRP samples to the ground electrode. If the electrical resistances of both paths are not significantly different, substantial amount of lightning discharge current will flow through both paths. The decrease of lightning strike damage occurs if some portion of discharge energy hits the ground electrode directly without propagating through the CFRP composites. So, an insulation is introduced to the ground electrode to ensure the flow of whole lightning discharge through the CFRP composites.

The effect of conductive carbon nanofillers was investigated to mitigate the lightning strike damage of CFRP composites. The results suggest that the lightning strike damage of CFRP composites reduces substantially by adding CB which is a cost-effective and cheap nano-filler. A trend of lightning strike damage reduction is observed with the amount of CB increases from 0.25% to 1%.

It has been shown in this dissertation that the accurate investigation of lightning strike damage mitigation requires a reliable testbed to prevent misleading results. Also, the use of CB as a new conductive filler was shown to have a significant impact on reducing lightning strike damage. Consequently, the methods applied in this dissertation propose a new test setup and method for mitigating lightning strike damages.

www.manaraa.com

CHAPTER X

FUTURE WORK

As discussed in this dissertation, the lightning strike damage of materials depends on electrical conductivity of the material. Therefore, the CB which was used in this study can be used in the future works to be more applicable for mitigating the lightning strike damages of composite structures. The lightning strike damage mitigation effect of CB can be tested by applying other components of the lightning strike such as component C and component B to find a comprehensive understanding on effect of CB on reducing the lightning strike damages. For this purpose, it is needed to use an impulse generator that is capable of simulating those components of the lightning. In addition, the carbon nano-fillers are incorporated in multiple applications such as eliminating the electromagnetic issues in electronic devices and cables, microwave absorption, and improving the fire retardancy of structures. The application of CB in such studies that other carbon nano-fillers applicable can lead to promising results. Moreover, many researchers are studying the additive of combination of multiple nano-fillers in lightning strike mitigation applications to maintain the mechanical property of the materials. The combination of other nano-fillers such as PANI powders and MWCNT can be used for further studies. Furthermore, to better understanding the trend of additive nano-fillers effect in electrical resistivity of the CFRP composite materials, TEM and SEM methods can be approached for further investigation.

www.manaraa.com

REFERENCES

[1] M. A. Caminero, G. P. Rodríguez, and V. Muñoz, "Effect of stacking sequence on Charpy impact and flexural damage behavior of composite laminates," *Compos. Struct.*, vol. 136, pp. 345–357, Feb. 2016, doi: 10.1016/j.compstruct.2015.10.019.

[2] G. Sun, X. Xia, X. Liu, Q. Luo, and Q. Li, "On quasi-static behaviors of different joint methods for connecting carbon fiber reinforce plastic (CFRP) laminate and aluminum alloy," *Thin-Walled Struct.*, vol. 164, p. 107657, Jul. 2021, doi: 10.1016/j.tws.2021.107657.

[3] The Faculty of Operation and Economics of Transport The Air Transport Department Univerzitna 1, 010 26 Zilina, Slovak Republic, mraz.marie@gmail.com and M. Maria, "Advanced composite materials of the future in aerospace industry," *INCAS Bull.*, vol. 5, no. 3, pp. 139–150, Sep. 2013, doi: 10.13111/2066-8201.2013.5.3.14.

[4] B. Roeseler, B. Sarh, and M. Kismarton, "Composite Structures – The First 100 Years," p. 41.

[5] H. G. Willett, "Characterisation of composites for wind turbine blades," *Reinf. Plast.*, vol. 56, no. 5, pp. 34–36, Sep. 2012, doi: 10.1016/S0034-3617(12)70111-X.

[6] "Electric field magnitudes and lightning initiation in thunderstorms - Marshall - 1995 - Journal of Geophysical Research: Atmospheres - Wiley Online Library." https://agupubs.onlinelibrary.wiley.com/doi/abs/10.1029/95JD00020 (accessed May 28, 2021).

[7] R. Solomon, V. Schroeder, and M. B. Baker, "Lightning initiation–conventional and runaway-breakdown hypotheses," *Q. J. R. Meteorol. Soc.*, vol. 127, no. 578, pp. 2683–2704, 2001, doi: https://doi.org/10.1002/qj.49712757809.

[8] M. A. Uman, *Lightning*. Courier Corporation, 2012.

[9] V. A. Rakov and M. A. Uman, *Lightning: Physics and Effects*. Cambridge University Press, 2003.

[10] N. US Department of Commerce, "NWS JetStream - The Positive and Negative Side of Lightning." https://www.weather.gov/jetstream/positive (accessed May 28, 2021).

www.manaraa.com

[11] P. Gharghabi, “Experimental and Numerical Studies of Lightning Strike Induced Damage to Carbon Fiber Epoxy Composites,” Ph.D., Mississippi State University, United States -- Mississippi, 2018. Accessed: Apr. 26, 2020. [Online]. Available: https://search.proquest.com/docview/2161832856/abstract/1E2265339D9C439DPQ/1

[12] A. R. Taylor, “Diameter of lightning as indicated by tree scars,” *J. Geophys. Res. 1896-1977*, vol. 70, no. 22, pp. 5693–5694, 1965, doi: https://doi.org/10.1029/JZ070i022p05693.

[13] M. A. Uman, “The diameter of lightning,” *J. Geophys. Res. 1896-1977*, vol. 69, no. 4, pp. 583–585, 1964, doi: https://doi.org/10.1029/JZ069i004p00583.

[14] R. Morrow, “A new theory for the expansion of lightning channels from a diameter of centimetres to metres via ionizing waves,” *J. Atmospheric Sol.-Terr. Phys.*, vol. 189, pp. 18–26, Aug. 2019, doi: 10.1016/j.jastp.2019.04.003.

[15] F. A. Fisher and J. A. Plumer, *Lightning Protection of Aircraft*. National Aeronautics and Space Administration, Scientific and Technical Information Office, 1977.

[16] P. L. Rustan, “The lightning threat to aerospace vehicles,” *J. Aircr.*, vol. 23, no. 1, pp. 62–67, 1986, doi: 10.2514/3.45267.

[17] Y. Murooka, “A Survey of Lightning Interaction with Aircraft in Japan,” *J. Atmospheric Electr.*, vol. 12, no. 1, pp. 101–106, 1992, doi: 10.1541/jae.12.101.

[18] ARP, SAE. ‘5414 Revision A-Aircraft Lightning Zone.’ SAE Aerospace (2012).

[19] Aerospace Recommended Practice ARP 5412. Aircraft lightning environment and related test waveforms. SAE; 1999.

[20] K. Yousefpour, W. Lin, Y. Wang, and C. Park, “Discharge and ground electrode design considerations for the lightning strike damage tolerance assessment of CFRP matrix composite laminates,” *Compos. Part B Eng.*, vol. 198, p. 108226, Oct. 2020, doi: 10.1016/j.compositesb.2020.108226.

[21] T. Roberts, “Rapid growth forecast for carbon fibre market,” *Reinf. Plast.*, vol. 51, no. 2, pp. 10–13, Feb. 2007, doi: 10.1016/S0034-3617(07)70051-6.

[22] C. Chen, et al. ‘Simulation and analysis of EMP transient electromagnetic effect of aircraft.’ *The Journal of Engineering* 2019.16 (2019): 2464-2467.

[23] SAE ARP 5416: 2013. Aircraft Lightning Test Methods. SAE Aerospace. USA, 2013. − pp. 1-145.

[24] F. S. Wang, N. Ding, Z. Q. Liu, Y. Y. Ji, and Z. F. Yue, “Ablation damage characteristic and residual strength prediction of carbon fiber/epoxy composite suffered from lightning strike,” *Compos. Struct.*, vol. 117, pp. 222–233, Nov. 2014, doi: 10.1016/j.compstruct.2014.06.029.

www.manaraa.com

[25] P. Naghipour, E. J. Pineda, and S. M. Arnold, "Simulation of Lightning-Induced Delamination in Un-protected CFRP Laminates," *Appl. Compos. Mater.*, vol. 23, no. 4, pp. 523–535, Aug. 2016, doi: 10.1007/s10443-016-9472-9.

[26] J. Gou, Y. Tang, F. Liang, Z. Zhao, D. Firsich, and J. Fielding, "Carbon nanofiber paper for lightning strike protection of composite materials," *Compos. Part B Eng.*, vol. 41, no. 2, pp. 192–198, Mar. 2010, doi: 10.1016/j.compositesb.2009.06.009.

[27] G. Abdelal and A. Murphy, "Nonlinear numerical modelling of lightning strike effect on composite panels with temperature dependent material properties," *Compos. Struct.*, vol. 109, pp. 268–278, Mar. 2014, doi: 10.1016/j.compstruct.2013.11.007.

[28] Y. Wang and O. I. Zhupanska, "Thermal Ablation in Fiber-Reinforced Composite Laminates Subjected to Continuing Lightning Current," in *57th AIAA/ASCE/AHS/ASC Structures, Structural Dynamics, and Materials Conference*, American Institute of Aeronautics and Astronautics. doi: 10.2514/6.2016-0986.

[29] Y. Wang, "Multiphysics analysis of lightning strike damage in laminated carbon/glass fiber reinforced polymer matrix composite materials: A review of problem formulation and computational modeling," *Compos. Part Appl. Sci. Manuf.*, vol. 101, pp. 543–553, Oct. 2017, doi: 10.1016/j.compositesa.2017.07.010.

[30] S. Lampkin, W. Lin, M. Rostaghi, K. Yousefpour, Y. Wang, and J. Klüss, *Epoxy Resin with Carbon Nanotube Additives for Lightning Strike Damage Mitigation of Carbon Fiber Composite Laminates*. 2019. doi: 10.12783/asc34/31338.

[31] V. Kumar *et al.*, "Factors affecting direct lightning strike damage to fiber reinforced composites: A review," *Compos. Part B Eng.*, vol. 183, p. 107688, Feb. 2020, doi: 10.1016/j.compositesb.2019.107688.

[32] R. S. Martins, "Experimental and theoretical studies of lightning arcs and their interaction with aeronautical materials," Theses, UNIVERSITE PARIS-SACLAY, 2016. Accessed: May 29, 2021. [Online]. Available: https://hal.archives-ouvertes.fr/tel-01434026

[33] J. Lee *et al.*, "Artificial lightning strike tests on PRSEUS panels," *Compos. Part B Eng.*, vol. 154, pp. 467–477, Dec. 2018, doi: 10.1016/j.compositesb.2018.09.016.

[34] Y. Hirano, S. Katsumata, Y. Iwahori, and A. Todoroki, "Artificial lightning testing on graphite/epoxy composite laminate," *Compos. Part Appl. Sci. Manuf.*, vol. 41, no. 10, pp. 1461–1470, Oct. 2010, doi: 10.1016/j.compositesa.2010.06.008.

[35] T. Ogasawara, Y. Hirano, and A. Yoshimura, "Coupled thermal–electrical analysis for carbon fiber/epoxy composites exposed to simulated lightning current," *Compos. Part Appl. Sci. Manuf.*, vol. 41, no. 8, pp. 973–981, Aug. 2010, doi: 10.1016/j.compositesa.2010.04.001.

www.manaraa.com

[36] V. Kumar *et al.*, “Interleaved MWCNT buckypaper between CFRP laminates to improve through-thickness electrical conductivity and reducing lightning strike damage,” *Compos. Struct.*, vol. 210, pp. 581–589, Feb. 2019, doi: 10.1016/j.compstruct.2018.11.088.

[37] S. Yamashita, T. Sonehara, J. Takahashi, K. Kawabe, and T. Murakami, “Effect of thin-ply on damage behaviour of continuous and discontinuous carbon fibre reinforced thermoplastics subjected to simulated lightning strike,” *Compos. Part Appl. Sci. Manuf.*, vol. 95, pp. 132–140, Apr. 2017, doi: 10.1016/j.compositesa.2017.01.010.

[38] A. Katunin, K. Krukiewicz, R. Turczyn, P. Sul, A. Łasica, and M. Bilewicz, “Synthesis and characterization of the electrically conductive polymeric composite for lightning strike protection of aircraft structures,” *Compos. Struct.*, vol. 159, pp. 773–783, Jan. 2017, doi: 10.1016/j.compstruct.2016.10.028.

[39] P. Feraboli and M. Miller, “Damage resistance and tolerance of carbon/epoxy composite coupons subjected to simulated lightning strike,” *Compos. Part Appl. Sci. Manuf.*, vol. 40, no. 6, pp. 954–967, Jul. 2009, doi: 10.1016/j.compositesa.2009.04.025.

[40] Szatkowski, George N., et al. "Common practice lightning strike protection characterization technique to quantify damage mechanisms on composite substrates." *NASA report* (2013).

[41] Y. Guo, Y. Xu, Q. Wang, Q. Dong, X. Yi, and Y. Jia, “Enhanced lightning strike protection of carbon fiber composites using expanded foils with anisotropic electrical conductivity,” *Compos. Part Appl. Sci. Manuf.*, vol. 117, pp. 211–218, Feb. 2019, doi: 10.1016/j.compositesa.2018.11.022.

[42] Y. Li, R. Li, L. Lu, and X. Huang, “Experimental study of damage characteristics of carbon woven fabric/epoxy laminates subjected to lightning strike,” *Compos. Part Appl. Sci. Manuf.*, vol. 79, pp. 164–175, Dec. 2015, doi: 10.1016/j.compositesa.2015.09.019.

[43] T. Sonehara, H. Kusano, N. Tokuoka, and Y. Hirano, “Visualization of lightning impulse current discharge on CFRP laminate,” in *2014 International Conference on Lightning Protection (ICLP)*, Oct. 2014, pp. 835–839. doi: 10.1109/ICLP.2014.6973239.

[44] Kumar, Vipin, et al. "*3d printed layer of polyaniline-based conductive polymer for lightning strike protection of cfrps*." Oak Ridge National Lab. (ORNL), Oak Ridge, TN (United States), 2019.

[45] V. Kumar, T. Smith, J. Condon, P. S. Yeole, A. (ORCID:0000000328521222) Hassen, and V. Kunc, “Replacing Metal-Based Lightning Strike Protection Layer of CFRPS by 3D Printed Electronically Conductive Polymer Layer,” Oak Ridge National Lab. (ORNL), Oak Ridge, TN (United States), Sep. 2019. Accessed: May 29, 2021.

[46] Techniques—Part, High-Voltage Test. ‘1: General definitions and test requirements.’ IEC Standard (2010): 60060-1.

www.manaraa.com

[47] Electromagnetic Environmental Effects Requirements for Systems, MIL-STD-464, 18 March 1997.

[48] C. E. R. Bruce and E. V. Appleton, "The initiation of long electrical discharges," *Proc. R. Soc. Lond. Ser. Math. Phys. Sci.*, vol. 183, no. 993, pp. 228–242, Nov. 1944, doi: 10.1098/rspa.1944.0034.

[49] Y. Liu and Y. Wang, "Modeling the lightning continuing current electric arc discharge and material thermal damage: Effects of combinations of amplitude and duration," *Int. J. Therm. Sci.*, vol. 162, p. 106786, Apr. 2021, doi: 10.1016/j.ijthermalsci.2020.106786.

[50] Y. LIU, Z. FU, Q. LIU, B. LIU, and A. GUHA, "Experimental and analytical investigation on metal damage suffered from simulated lightning currents," *Plasma Sci. Technol.*, vol. 19, no. 12, p. 125301, Oct. 2017, doi: 10.1088/2058-6272/aa8aca.

[51] F. Lago, J. J. Gonzalez, P. Freton, and A. Gleizes, "A numerical modelling of an electric arc and its interaction with the anode: Part I. The two-dimensional model," *J. Phys. Appl. Phys.*, vol. 37, no. 6, pp. 883–897, Feb. 2004, doi: 10.1088/0022-3727/37/6/013.

[52] S. L. J. Millen, A. Murphy, G. Abdelal, and G. Catalanotti, "Sequential finite element modelling of lightning arc plasma and composite specimen thermal-electric damage," *Comput. Struct.*, vol. 222, pp. 48–62, Oct. 2019, doi: 10.1016/j.compstruc.2019.06.005.

[53] J. Haidar and A. J. D. Farmer, "Surface temperature measurements for tungsten-based cathodes of high-current free-burning arcs," *J. Phys. Appl. Phys.*, vol. 28, no. 10, pp. 2089–2094, Oct. 1995, doi: 10.1088/0022-3727/28/10/014.

[54] P. Freton, J. J. Gonzalez, and A. Gleizes, "Comparison between a two- and a three-dimensional arc plasma configuration," *J. Phys. Appl. Phys.*, vol. 33, no. 19, pp. 2442–2452, Sep. 2000, doi: 10.1088/0022-3727/33/19/315.

[55] G.F. Abdelal, A. Murphy, A multiphysics simulation approach for efficient modeling of lightning strike tests on aircraft structures, IEEE Trans. Plasma Sci. 45 (2017) 725–735.".

[56] G. F. Abdelal and A. Murphy, "A Multiphysics Simulation Approach for Efficient Modeling of Lightning Strike Tests on Aircraft Structures," *IEEE Trans. Plasma Sci.*, vol. 45, no. 4, pp. 725–735, Apr. 2017, doi: 10.1109/TPS.2017.2673543.

[57] J. J. Lowke, R. Morrow, and J. Haidar, "A simplified unified theory of arcs and their electrodes," *J. Phys. Appl. Phys.*, vol. 30, no. 14, pp. 2033–2042, Jul. 1997, doi: 10.1088/0022-3727/30/14/011.

[58] J. P. Trelles, "Electrode patterns in arc discharge simulations: effect of anode cooling," *Plasma Sources Sci. Technol.*, vol. 23, no. 5, p. 054002, Sep. 2014, doi: 10.1088/0963-0252/23/5/054002.

www.manaraa.com

[59] L. Michael, S. T. Millmore, and N. Nikiforakis, “A Multi-physics Methodology for Four States of Matter,” *Commun. Appl. Math. Comput.*, vol. 2, no. 3, pp. 487–514, Sep. 2020, doi: 10.1007/s42967-019-00047-4.

[60] Y. Aider, “A unified plasma-materials finite element model of lightning strike interaction with carbon fiber composite materials,” *Miss. State Univ.*, Jul. 2019, Accessed: May 29, 2021. [Online]. Available: https://ir.library.msstate.edu/handle/11668/14594

[61] M. S. Benilov, M. D. Cunha, and G. V. Naidis, “Modelling interaction of multispecies plasmas with thermionic cathodes,” *Plasma Sources Sci. Technol.*, vol. 14, no. 3, pp. 517–524, Jun. 2005, doi: 10.1088/0963-0252/14/3/014.

[62] K. C. Hsu, K. Etemadi, and E. Pfender, “Study of the free-burning high-intensity argon arc,” *J. Appl. Phys.*, vol. 54, no. 3, pp. 1293–1301, Mar. 1983, doi: 10.1063/1.332195.

[63] J. J. Lowke and M. Tanaka, “`LTE-diffusion approximation’ for arc calculations,” *J. Phys. Appl. Phys.*, vol. 39, no. 16, pp. 3634–3643, Aug. 2006, doi: 10.1088/0022-3727/39/16/017.

[64] L. Chemartin, P. Lalande, E. Montreuil, C. Delalondre, B. G. Chéron, and F. Lago, “Three dimensional simulation of a DC free burning arc. Application to lightning physics,” *Atmospheric Res.*, vol. 91, no. 2, pp. 371–380, Feb. 2009, doi: 10.1016/j.atmosres.2008.07.009.

[65] L. Chemartin, P. Lalande, C. Delalondre, B. Cheron, and F. Lago, “Modelling and simulation of unsteady dc electric arcs and their interactions with electrodes,” *J. Phys. Appl. Phys.*, vol. 44, no. 19, p. 194003, Apr. 2011, doi: 10.1088/0022-3727/44/19/194003.

[66] L. Tholin, P. Chemartin, and F. Lalande, “Numerical investigation of the surface effects on the dwell time during the sweeping of lightning arcs,” *undefined*, 2013, Accessed: May 29, 2021. [Online]. Available: /paper/Numerical-investigation-of-the-surface-effects-on-Tholin-Chemartin/2806f007a42614eb4562b07f0744c0916a0845ed

[67] Fusheng, W. A. N. G., et al. "Evolution simulation of lightning discharge based on a magnetohydrodynamics method." *Plasma Science and Technology* 20.7 (2018): 075301.

[68] C. Christopoulos, *Principles and Techniques of Electromagnetic Compatibility*. CRC Press, 2018.

[69] V. Kumar *et al.*, “Low Cost Carbon Fiber as Potential Lightning Strike Protection for Wind Turbine Blades,” *Proc. Am. Soc. Compos. — Thirty-Fifth Tech. Conf.*, vol. 0, no. 0, Art. no. 0, 2020, doi: 10.12783/asc35/34880.

[70] J. C. Abry, S. Bochard, A. Chateauminois, M. Salvia, and G. Giraud, “In situ detection of damage in CFRP laminates by electrical resistance measurements,” *Compos. Sci. Technol.*, vol. 59, no. 6, pp. 925–935, May 1999, doi: 10.1016/S0266-3538(98)00132-8.

المنارة للاستشارات
www.manaraa.com

[71] M. Louis, S. P. Joshi, and W. Brockmann, “An experimental investigation of through-thickness electrical resistivity of CFRP laminates,” *Compos. Sci. Technol.*, vol. 61, no. 6, pp. 911–919, May 2001, doi: 10.1016/S0266-3538(00)00177-9.

[72] H. Che *et al.*, “Metallization of Carbon Fiber Reinforced Polymers for Lightning Strike Protection,” *J. Mater. Eng. Perform.*, vol. 27, no. 10, pp. 5205–5211, Oct. 2018, doi: 10.1007/s11665-018-3609-y.

[73] D. M. Lombetti and A. A. Skordos, “Lightning strike and delamination performance of metal tufted carbon composites,” *Compos. Struct.*, vol. 209, pp. 694–699, Feb. 2019, doi: 10.1016/j.compstruct.2018.11.005.

[74] J. Han *et al.*, “The combination of carbon nanotube buckypaper and insulating adhesive for lightning strike protection of the carbon fiber/epoxy laminates,” *Carbon*, vol. 94, pp. 101–113, Nov. 2015, doi: 10.1016/j.carbon.2015.06.026.

[75] A. Duongthipthewa, M. Lu, K. Du, L. Ye, and L. Zhou, “Experimental and numerical simulation of lightning damage development on composites with/without a carbon-based protection layer,” *Compos. Struct.*, vol. 260, p. 113452, Mar. 2021, doi: 10.1016/j.compstruct.2020.113452.

[76] Polyaniline/phenol-divinylbenzene resin for CFRP composite with enhanced electrical and mechanical properties | ICCM22 2019.” https://search.informit.org/doi/abs/10.3316/INFORMIT.864147012392467 (accessed May 29, 2021).

[77] A. Katunin, K. Krukiewicz, R. Turczyn, P. Sul, and M. Bilewicz, “Electrically conductive carbon fibre-reinforced composite for aircraft lightning strike protection,” *IOP Conf. Ser. Mater. Sci. Eng.*, vol. 201, p. 012008, May 2017, doi: 10.1088/1757-899X/201/1/012008.

[78] T. Kashiwagi, F. Du, J. F. Douglas, K. I. Winey, R. H. Harris, and J. R. Shields, “Nanoparticle networks reduce the flammability of polymer nanocomposites,” *Nat. Mater.*, vol. 4, no. 12, Art. no. 12, Dec. 2005, doi: 10.1038/nmat1502.

[79] T. Kashiwagi, E. Grulke, J. Hilding, R. Harris, W. Awad, and J. Douglas, “Thermal Degradation and Flammability Properties of Poly(propylene)/Carbon Nanotube Composites,” *Macromol. Rapid Commun.*, vol. 23, no. 13, pp. 761–765, 2002, doi: https://doi.org/10.1002/1521-3927(20020901)23:13<761::AID-MARC761>3.0.CO;2-K.

[80] Z. Zhao, J. Gou, S. Bietto, C. Ibeh, and D. Hui, “Fire retardancy of clay/carbon nanofiber hybrid sheet in fiber reinforced polymer composites,” *Compos. Sci. Technol.*, vol. 69, no. 13, pp. 2081–2087, Oct. 2009, doi: 10.1016/j.compscitech.2008.11.004.

[81] J. W. Gilman *et al.*, “Flammability Properties of Polymer−Layered-Silicate Nanocomposites. Polypropylene and Polystyrene Nanocomposites,” *Chem. Mater.*, vol. 12, no. 7, pp. 1866–1873, Jul. 2000, doi: 10.1021/cm0001760.

www.manaraa.com

[82] F. Du, R. C. Scogna, W. Zhou, S. Brand, J. E. Fischer, and K. I. Winey, "Nanotube Networks in Polymer Nanocomposites: Rheology and Electrical Conductivity," *Macromolecules*, vol. 37, no. 24, pp. 9048–9055, Nov. 2004, doi: 10.1021/ma049164g.

[83] V. Kumar *et al.*, "Scavenging phenomenon and improved electrical and mechanical properties of polyaniline–divinylbenzene composite in presence of MWCNT," *Int. J. Mech. Mater. Des.*, vol. 14, no. 4, pp. 697–708, Dec. 2018, doi: 10.1007/s10999-017-9397-y.

[84] J. Zhang, X. Zhang, X. Cheng, Y. Hei, L. Xing, and Z. Li, "Lightning strike damage on the composite laminates with carbon nanotube films: Protection effect and damage mechanism," *Compos. Part B Eng.*, vol. 168, pp. 342–352, Jul. 2019, doi: 10.1016/j.compositesb.2019.03.054.

[85] B. P. Singh, V. Choudhary, P. Saini, and R. B. Mathur, "Designing of epoxy composites reinforced with carbon nanotubes grown carbon fiber fabric for improved electromagnetic interference shielding," *AIP Adv.*, vol. 2, no. 2, p. 022151, Jun. 2012, doi: 10.1063/1.4730043.

[86] E. Kandare *et al.*, "Improving the through-thickness thermal and electrical conductivity of carbon fibre/epoxy laminates by exploiting synergy between graphene and silver nano-inclusions," *Compos. Part Appl. Sci. Manuf.*, vol. 69, pp. 72–82, Feb. 2015, doi: 10.1016/j.compositesa.2014.10.024.

[87] S.-Y. Yang *et al.*, "Synergetic effects of graphene platelets and carbon nanotubes on the mechanical and thermal properties of epoxy composites," *Carbon*, vol. 49, no. 3, pp. 793–803, Mar. 2011, doi: 10.1016/j.carbon.2010.10.014.

[88] Katunin, A., et al. 'Concept of a conducting composite material for lightning strike protection.' *Advances in Materials Science*16.2 (2016): 32-46.

[89] S. Han, J. T. Lin, Y. Yamada, and D. D. L. Chung, "Enhancing the thermal conductivity and compressive modulus of carbon fiber polymer–matrix composites in the through-thickness direction by nanostructuring the interlaminar interface with carbon black," *Carbon*, vol. 46, no. 7, pp. 1060–1071, Jun. 2008, doi: 10.1016/j.carbon.2008.03.023.

[90] D. Zhang, L. Ye, S. Deng, J. Zhang, Y. Tang, and Y. Chen, "CF/EP composite laminates with carbon black and copper chloride for improved electrical conductivity and interlaminar fracture toughness," *Compos. Sci. Technol.*, vol. 72, no. 3, pp. 412–420, Feb. 2012, doi: 10.1016/j.compscitech.2011.12.002.

[91] H. Yang *et al.*, "Effect of carbon black on improving thermal stability, flame retardancy and electrical conductivity of polypropylene/carbon fiber composites," *Compos. Sci. Technol.*, vol. 113, pp. 31–37, Jun. 2015, doi: 10.1016/j.compscitech.2015.03.013.

www.manaraa.com

[92] T. Haryono, K. T. Sirait, Tumiran, and H. Berahim, "The Design of A High Amplitude Impulse Current Generator," in *2008 International Conference on High Voltage Engineering and Application*, Nov. 2008, pp. 339–343. doi: 10.1109/ICHVE.2008.4773942.

[93] O. Diaz and F. Roman, "Design and Construction of a Compact Electrostatic Fast Impulse Current Generator," in *2005 IEEE Pulsed Power Conference*, Jun. 2005, pp. 771–774. doi: 10.1109/PPC.2005.300775.

[94] I. F. Gonos, N. Leontides, F. V. Topalis, and I. A. Stathopulos, "Analysis and design of an impulse current generator," p. 7.

[95] N. Wang and C. Cho, "Effect of compressive loading speed and stacking sequence on mechanical characteristics of satin weave E-glass/epoxy composites," *Polym. Compos.*, vol. 33, no. 9, pp. 1603–1612, 2012, doi: https://doi.org/10.1002/pc.22296.

[96] K. Yousefpour, M. R. Chalaki, W. Lin, F. Haque, Y. Wang, and C. Park, "The Impact of Lightning Channel Diameter on the Damage of Carbon Fiber Reinforced Polymer Matrix (CFRP) Composite Laminates," in *2020 IEEE Electrical Insulation Conference (EIC)*, Jun. 2020, pp. 128–131. doi: 10.1109/EIC47619.2020.9158586.

[97] Y. Naghizadeh-Kashani, Y. Cressault, and A. Gleizes, "Net emission coefficient of air thermal plasmas," *J. Phys. Appl. Phys.*, vol. 35, no. 22, pp. 2925–2934, Nov. 2002, doi: 10.1088/0022-3727/35/22/306.

[98] Liu, Yakun, and Yeqing Wang. 'Modeling the lightning continuing current electric arc discharge and material thermal damage: Effects of combinations of amplitude and duration.' International Journal of Thermal Sciences 162 (2021): 106786.".

[99] P. Fauchais and A. Vardelle, "Thermal plasmas," *IEEE Trans. Plasma Sci.*, vol. 25, no. 6, pp. 1258–1280, Dec. 1997, doi: 10.1109/27.650901.

[100] C. Wang *et al.*, "Thermodynamic and Transport Properties of Real Air Plasma in Wide Range of Temperature and Pressure," *Plasma Sci. Technol.*, vol. 18, no. 7, pp. 732–739, Jun. 2016, doi: 10.1088/1009-0630/18/7/06.

[101] L. Chemartin *et al.*, "Direct Effects of Lightning on Aircraft Structure: Analysis of the Thermal, Electrical and Mechanical Constraints," *AerospaceLab*, no. 5, pp. 1–15, Dec. 2012.

[102] L. Jarosinski, A. Rybak, K. Gaska, G. Kmita, R. Porebska, and C. Kapusta, "Enhanced thermal conductivity of graphene nanoplatelets epoxy composites," *Mater. Sci.-Pol.*, vol. 35, no. 2, pp. 382–389, Jul. 2017, doi: 10.1515/msp-2017-0028.

www.manaraa.com

[103] N. Hu, Z. Masuda, G. Yamamoto, H. Fukunaga, T. Hashida, and J. Qiu, "Effect of fabrication process on electrical properties of polymer/multi-wall carbon nanotube nanocomposites," *Compos. Part Appl. Sci. Manuf.*, vol. 39, no. 5, pp. 893–903, May 2008, doi: 10.1016/j.compositesa.2008.01.002.

[104] W. Li, "The self-sensing, electrical and mechanical properties of the epoxy composites reinforced with carbon nanotubes-micro reinforcement nano/micro hybrids," phdthesis, Ecole Centrale Paris, 2013. Accessed: May 29, 2021. [Online]. Available: https://tel.archives-ouvertes.fr/tel-00997409

[105] F. Dalmas, R. Dendievel, L. Chazeau, J.-Y. Cavaillé, and C. Gauthier, "Carbon nanotube-filled polymer composites. Numerical simulation of electrical conductivity in three-dimensional entangled fibrous networks," *Acta Mater.*, vol. 54, no. 11, pp. 2923–2931, Jun. 2006, doi: 10.1016/j.actamat.2006.02.028.

www.manaraa.com